Saule Tulebekova

Dynamic response of tall timber buildings under service load

Modal analysis-based experimental investigations and modelling

☐ **NTNU**
Norwegian University of
Science and Technology

Saule Tulebekova

Dynamic response of tall timber buildings under service load

Modal analysis-based experimental investigations and modelling

Thesis for the Degree of Philosophiae Doctor

Trondheim, September 2023

Norwegian University of Science and Technology
Faculty of Engineering
Department of Structural Engineering

NTNU
Norwegian University of
Science and Technology

Preface

This doctoral thesis is submitted in partial fulfilment of the requirements for the degree of Philosophiae Doctor (Ph.D.) at the Faculty of Engineering of the Norwegian University of Science and Technology (NTNU). The research was conducted at the Department of Structural Engineering at NTNU in Trondheim, Norway.

This doctoral dissertation is a collection of scientific papers, published or submitted for publication in peer-reviewed scientific journals. It also contains an introductory part that gives the summary of the research questions, provides the context and binds all the papers together.

Abstract

The rising awareness of sustainability importance has led to wider adoption of timber in structural design. While there is a growing number of multi-storey timber buildings, there is still a lack of confidence by designers in the use of timber for tall building constructions due to limited knowledge of their dynamic response under serviceability level loading. Generally tall timber buildings are able to resist ultimate state loads but are naturally susceptible to wind-induced excitation due to intrinsically low density and low stiffness. While wind-induced vibrations do not usually threaten the structural integrity of the building, the comfort criteria might become a significant issue. A lack of reliable data for modelling is considered as one of the main barriers to a wider application of timber in tall buildings. Therefore, this thesis aims to contribute to a better understanding of tall timber building dynamic response under serviceability level loading. The objectives of the thesis include experimental full-scale dynamic identification of tall timber buildings using ambient and forced vibration tests and the development of representative finite element models which are able to predict the vibration response of tall timber buildings.

Firstly, an ambient vibration testing campaign was conducted on seven multi-storey CLT buildings ranging between 9-13 storeys. Using the output-only stochastic subspace identification technique, accurate estimations of the natural frequencies and mode shapes were obtained from the ambient vibration measurements and the identified damping ratios were in the range between 1%-2%.

Secondly, long-term ambient vibration testing and forced vibration testing campaigns were conducted on an 18-storey glulam frame building. The output-only techniques were combined with the modal decomposition tool to process non-stationary data from ambient vibration measurements. The identified natural frequencies were quite stable and similar to their counterparts from forced vibration tests. An amplitude-dependent behaviour of damping ratios was observed based

on forced vibration tests, which has significant implications on the design of tall timber building response under wind-induced loading, where damping plays an important role. The range of damping variation was between 0.5%-3.0% for the first two modes of vibration.

Thirdly, finite element models of the instrumented buildings were developed. A focus on the stiffness of connections and non-structural elements and their impact on global modal response was made. The effect of stiffness of connections in tall timber buildings is usually omitted by the designers and simplified assumptions of rigid or pinned connections are made. It was demonstrated that the stiffness of connections can have a significant impact on the global modal response of tall timber buildings. Moreover, the non-structural elements in tall glulam frame buildings have a partial stiffness contribution to the building modal response.

The results of the extensive tall timber buildings measurement campaign contribute significantly to the limited database of existing tall timber buildings' dynamic properties. Moreover, the knowledge of damping properties in CLT and glulam frame buildings has been significantly extended. The proposed modelling approach is able to accurately predict the modal properties of tall timber buildings and can serve as a useful guideline for practising engineers in the development of their prediction models of tall timber buildings under serviceability level loading.

Acknowledgements

First, I would like to acknowledge my main supervisor Professor Kjell Arne Malo for giving me an opportunity to work as a PhD student on a great international project and providing constant guidance and support throughout the entire process. I would also like to thank my co-supervisor Professor Anders Rønnquist for the guidance in the field of structural dynamics and for providing access to the expertise of the Structural Dynamics group.

The Structural Dynamics group and Professors Petter Nåvik and Gunnstein Frøseth in particular are gratefully acknowledged for their invaluable assistance with experimental setups and data processing.

Special thanks to Professor Alex Pavic and Professor Wai Kei Ao for opening up an entirely new world of forced vibration tests of buildings for me. Your expertise, guidance and readiness to help despite the difference in time zones are very important to me.

Very sincere gratitude to my senior colleagues from the Timber Structures group, and in particular to Katarzyna, Mirko and Haris. It would have been a much more difficult and lonely journey without their constant support and encouragement. My friends from the department, Trondheim and abroad are also gratefully acknowledged for their warm presence and numerous discussions about everything.

I came to Norway alone but gained so many new friends here and met my love Stian, to whom I also express my sincere gratitude for his love and support.

Finally, I would like to express my heartful gratitude to my biggest fans - my family. To my parents, Bibigul and Kanat, for their unconditional love and support. To my younger siblings, Meruyert and Damir, whose presence in my life made it so much more joyful.

Contents

List of Publications

Included publications

The following papers are included in this thesis:

I. Tulebekova, S., Malo, K.A., and Rønnquist, A. (2023). *Dynamic identification and model calibration of connection stiffness in multi-storey cross-laminated timber buildings.* Journal of Building Engineering 72(2023). https://doi.org/10.1016/j.jobe.2023.106607

II. Tulebekova, S., Malo, K.A., Rønnquist, A., and Nåvik, P. (2022). *Modeling stiffness of connections and non-structural elements for dynamic response of taller glulam frame buildings.* Engineering Structures 261(2022). https://doi.org/10.1016/j.engstruct.2022.114209.

III. Tulebekova, S., Ao, W.K., Pavic, A., Malo, K.A., and Rønnquist, A. (2023). *Identification of modal properties of a tall glue-laminated timber frame building under long-term ambient vibrations and forced vibrations.* Submitted for publication to a peer-reviewed journal.

IV. Tulebekova, S., Malo, K.A., Rønnquist A., Nåvik, P. (2023). *Investigation of long-term modal properties of a tall glue-laminated timber frame building under environmental variations.* Accepted to the World Conference on Timber Engineering (WCTE2023), Oslo, Norway.

Declaration of authorship

The author, Saule Tulebekova, is responsible for conducting the numerical work, implementation of the theory, data processing, analyses and writing all the manuscripts. The experimental work was organized and conducted together with the co-authors. The co-authors have also contributed with valuable constructive discussions, planning of the experimental work, suggestions and reviews to improve the presented research work.

1. Introduction

1.1 Motivation

1.1.1 Tall timber buildings

The use of timber as a structural material in tall buildings has gained popularity in recent years due to its renewability and ecological friendliness compared to traditional steel and reinforced concrete materials [1]. Treet building was constructed in Norway in 2014 and was the tallest all-timber building in the world at a time [2] until 2019 when Mjøstårnet was constructed (Figs.1.1(b) and 1.1(a)). As of April 2023, an 18-storey (85.4 m) glue-laminated timber frame building Mjøstårnet still holds the title of the tallest all-timber building in the world [3]. Apart from them, a large number of hybrid buildings, incorporating timber in the structural design have been constructed. Among them, a 25-storey mass timber-concrete hybrid tower Ascent in the United States holds the record for height at 86.6 m [4]. In Europe, the tallest hybrid buildings with timber include an 84 m tall HoHo building in Austria (timber-concrete hybrid), a 73 m tall Haut in the Netherlands (timber-concrete hybrid), and a 72.8 m tall Sara Kulturhus (Fig.1.1(c)) in Sweden (timber-steel hybrid) [5].

Generally, tall timber buildings have sufficient capacity to fulfil the ultimate limit state requirements for strength [6]. However, despite being relatively short in height compared to high-rise reinforced concrete and steel buildings, the existing tall timber buildings are prone to excessive vibration under wind load [7]. This issue arises due to the inherently low density and stiffness of timber, which leads to wind-induced excitation being the governing design criterion for tall timber buildings. While the wind-induced vibrations generally do not compromise the structural integrity of the building, the comfort criteria can become a significant issue [8].

(a) Mjøstårnet, Norway   (b) Treet, Norway   (c) Sara Kulturhus, Sweden
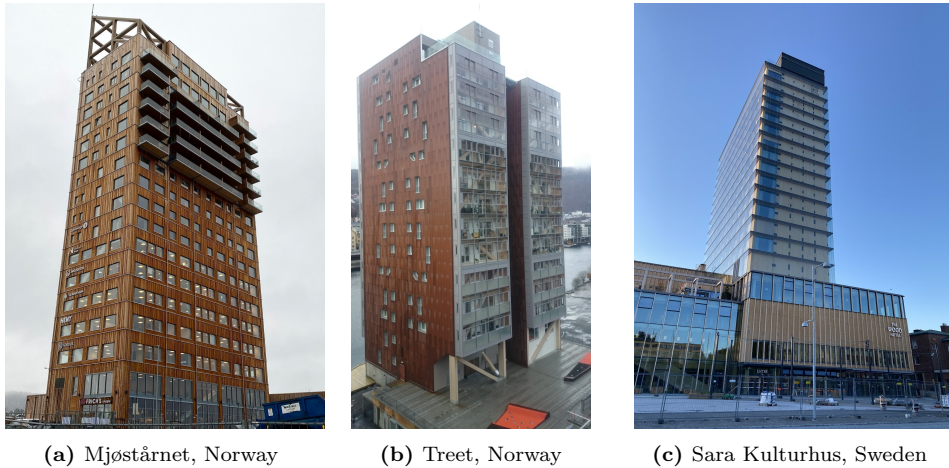
Figure 1.1: Tall buildings with timber

1.1.2   Comfort criteria

The comfort criteria for tall buildings were introduced due to human's sensitivity to building motions. The adverse effects on the inhabitants include nausea or motion sickness, and tiredness. Both sudden short strong motions and low-level motions can have a physiological and psychological impact on inhabitants [9, 10]. Exposure to steady low-level accelerations can cause tiredness and sleepiness in the occupants, even though they are not perceptible. Sudden strong motions over a short period can lead to motion sickness/nausea and if the motion is observable and/or audible, it can lead to fear of the building being unsafe and prone to collapse.

The ISO 10137 standard [11] is used for evaluating the comfort criteria of buildings due to wind-induced vibrations (Fig.1.2). The standard uses the 1-year return period for wind velocity and sets the acceleration limit for the low-frequency horizontal motion of buildings subjected to wind loading. The computations involve the peak acceleration and the first natural frequency of the building within a range of 0.06 Hz-5.0 Hz, where curve 1 is for residential buildings, and curve 2 is for offices.

1.1.3   Wind-induced acceleration estimation

The Eurocode 1-4 standard [12] presents two methods (Annex B and C) for calculating the along-wind acceleration. Both Eurocode methods, as well as other international standards, utilise the simplified SDOF model of a cantilever beam
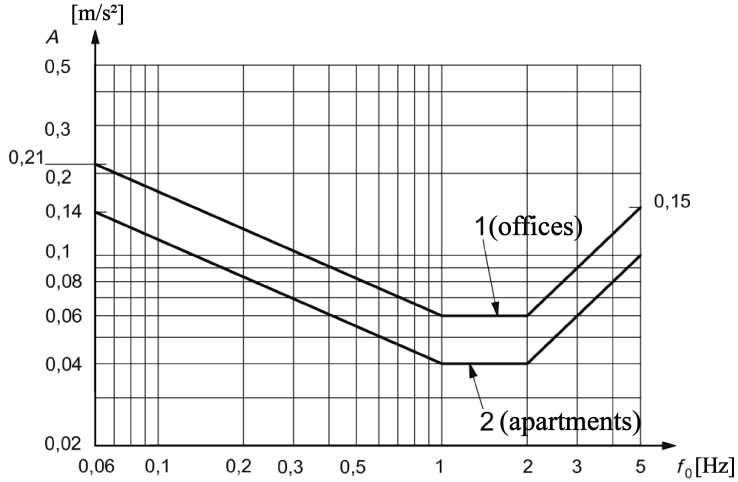
Figure 1.2: ISO 10137 comfort criteria

with only the first eigenmode considered. The inputs required for the calculation of the peak acceleration include the wind data specific to the location, building geometry, and modal properties from the modal analysis. The general equation for the along-wind peak acceleration can be expressed as follows [13]:

$$a_{peak} = b \cdot h \cdot q_{z_{ref}} \cdot C_f \cdot K_p \cdot K \cdot \phi_{1,x}(z) \cdot \frac{1}{M_1} \cdot R \qquad (1.1)$$

where a_{peak} is a peak acceleration in m/s^2, $b \cdot h$ is the building area normal to wind direction in m^2, $q_{z_{ref}}$ is the wind pressure in N/m^2, C_f is the force factor, K_p is the global peak factor, K is the modal factor, $\phi_{1,x}(z)$ is the first mode shape, M_1 is the modal mass in kg, and R is the resonance response factor.

1.1.4   Challenges of wind-induced response prediction

The performance of buildings under wind loading depends on their dynamic properties, which include natural frequencies, damping ratios and mode shapes. These properties are governed by the distribution of mass, stiffness, and damping in the building. However, in tall timber buildings, the vibration behaviour is difficult to predict during the design stage [14]. In particular, the knowledge of the stiffness and damping properties in tall timber buildings is limited and more knowledge is required in this field for accurate prediction of dynamic properties. Stiffness properties from connections and non-structural elements are subject to uncertainty and

their contribution is generally omitted in the current practice. Moreover, the live load values from Eurocode 1-1 [15] prescribed for the serviceability limit state are not usually representative of the actual live load distribution, which is important for assessing the dynamic behaviour of in-service buildings. Additionally, the damping ratio values used for serviceability limit state calculations of timber buildings in Eurocode 1-4 [12] do not have a scientific and tall timber buildings-related basis.

1.2   Objectives and limitations

1.2.1   Objectives and scope of work

The main objective of this thesis is to experimentally identify the modal properties of tall timber buildings under service load and to develop the corresponding representative finite element models for predicting the vibration response of tall timber buildings.

To accomplish the research objectives, the following scope of work was established:

- **Acquire full-scale measurement data from tall timber buildings**

  Conduct full-scale dynamic tests using ambient vibration tests and forced vibration tests to identify modal properties of in-service tall timber buildings.

- **Quantify natural frequency and damping of in-service tall timber buildings**

  Quantify and evaluate the natural frequencies and damping ratios of in-service tall timber buildings and investigate the amplitude-dependent behaviour of damping ratios.

- **Develop representative finite element models of tall timber buildings**

  A representative finite element model is important in the dynamic identification of in-service tall timber buildings. The impact of connections and non-structural elements on the dynamic response of tall timber buildings under service-level loading is unknown. Therefore, a proper approach for modelling the stiffness of connections between the timber elements as well as the non-structural elements of in-service tall timber buildings should be developed.

- **Validate the predicted response with experimental measurements**

  Once the representative finite element model is established, develop and implement an effective finite element model updating strategy using realistic parameter values to validate the finite element model of in-service tall timber buildings.

1.2.2 Limitations and assumptions

The following assumptions and limitations were made in this thesis:

- Only the vibration-based dynamic response using ambient and forced vibration tests was considered in this thesis. The underlying assumption of vibration-based testing is that the distribution of mass, stiffness, and energy dissipation properties of the building govern the dynamic response of the building.

- The thesis focuses on the dynamic identification of tall timber buildings (i.e. natural frequencies, mode shapes and damping ratios), which are crucial for the wind-induced behaviour evaluation based on the standards.

- Timber buildings with only two types of structural systems are considered in this thesis: truss system with glue-laminated timber beams columns and diagonals and platform system with cross-laminated timber panels. While there exist other types of structural systems for tall timber buildings, the two covered systems are representative of the majority of the existing tall timber buildings.

- The focus of this thesis is on the serviceability limit state under wind-induced loading (elastic behaviour) and does not include the ultimate limit state or seismic-induced loading.

- Finite element model with linear material properties is considered and modal and steady-state dynamic analyses are performed.

1.3   Structure of the thesis

This thesis is composed of an introductory part followed by the included papers. The introductory part is comprised of six chapters. The first chapter presents the motivation and the objectives of the thesis. The second chapter presents a brief summary of structural timber and tall timber systems. The third chapter is a theoretical background on the methodologies for system identification and modal analysis. The experimental and numerical frameworks are presented in Chapter 4. A summary of the included papers is presented in Chapter 5. Finally, the main findings and future work suggestions are outlined in Chapter 6.

2. Structural timber and tall timber systems

2.1 Structural timber

2.1.1 Material model for timber

Timber is a natural composite material with highly anisotropic behaviour. The stiffness of timber varies significantly between the different directions, and from one wood sample to another. The mathematical models for structural timber are constituted from various small and large-scale tests. Over the last century, the constitutive relationships for the elastic mechanical behaviour of timber have been developed and are generally used nowadays for modelling timber structures [16, 17, 18].

Fig.2.1 shows a cylindrical orthotropic timber material model, where the longitudinal (L) direction is the direction along the wood fibres, and R and T are radial and tangential directions to the wood annual rings respectively.
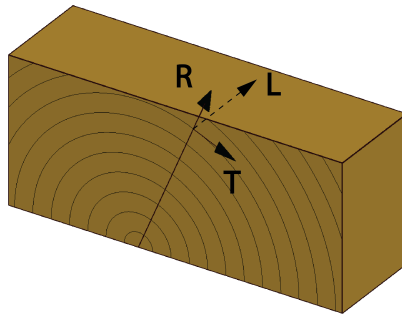

Figure 2.1: Principal directions for wood material model

For orthotropic material the elastic compliance matrix is expressed as follows:

$$\mathbf{S}_e = \begin{bmatrix} \dfrac{1}{E_R} & -\dfrac{\nu_{TR}}{E_T} & -\dfrac{\nu_{LR}}{E_L} & 0 & 0 & 0 \\[2ex] -\dfrac{\nu_{RT}}{E_R} & \dfrac{1}{E_T} & -\dfrac{\nu_{LT}}{E_L} & 0 & 0 & 0 \\[2ex] -\dfrac{\nu_{RL}}{E_R} & -\dfrac{\nu_{TL}}{E_T} & \dfrac{1}{E_L} & 0 & 0 & 0 \\[2ex] 0 & 0 & 0 & \dfrac{1}{G_{TL}} & 0 & 0 \\[2ex] 0 & 0 & 0 & 0 & \dfrac{1}{G_{RL}} & 0 \\[2ex] 0 & 0 & 0 & 0 & 0 & \dfrac{1}{G_{RT}} \end{bmatrix} \tag{2.1}$$

where E, G, and ν are elastic modulus, shear modulus and Poisson's ratio respectively. A total of nine engineering constants are needed for the timber model.

For large engineering products, such as glue-laminated timber and cross-laminated timber, further simplifications are made since the difference between the stiffness properties in the perpendicular (R and T) to the grain direction is quite small compared to the stiffness properties in parallel to the grain direction (L). In this case, the wood is considered a pseudo-transversely isotropic material with the plane of isotropy being plane R-T. Thus, the number of independent engineering constants was reduced to five: E_0, E_{90}, G_0, G_{90}, and ν, where 0 and 90 indicate parallel and perpendicular to wood fibres direction respectively.

2.1.2 Engineering timber products

Glue-laminated timber (glulam) and cross-laminated timber (CLT) are some of the most common structural timber products used in engineering.

Glulam is made by glueing together multiple layers of timber to create a strong and dimensionally stable structural material. Each layer is called lamella and is made of solid timber boards, which are glued together with high-strength adhesive. The grain direction in each lamella is parallel to the structural member direction. The glulam beams are shaped into various shapes, lengths and dimensions, and can be applied in a variety of construction and architectural applications. Fig.2.2(a) shows an example of glulam application in structural columns and diagonals.

CLT is different from the glulam in a way that it is made by layering timber boards

in alternating directions. These boards are glued to each other with strong adhesives to create a solid structural panel. It has versatile applications, including walls, floors, and ceilings. CLT is a relatively new material, that is gaining popularity in some regions of Europe and North America. An example of CLT application in a building is shown in Fig.2.2(b), where CLT is used as a wall and a ceiling panel.

(a) Glulam element   **(b)** CLT element

Figure 2.2: Examples of engineering timber products in buildings

2.2   Structural systems for tall timber buildings

According to Foster et al., the definition of tallness in buildings is subjective and depends on the context which can be provided by the historical use of particular structural material or by the structural system [19]. They further remark that the definition of tallness with respect to the use of new structural materials, such as engineering timber, is especially interesting due to its inherent material properties. In comparison to traditional structural materials such as concrete and steel, structural timber has relatively low mass and stiffness, but quite a high stiffness-to-mass ratio. Therefore, the buildings made of structural timber become susceptible to lateral loading, such as wind and seismic actions, at significantly lower slenderness ratios. Subsequently, this will lead to the use of tall structural systems at much smaller heights for timber buildings, than it would be required for concrete or steel buildings [19].

The most common structural systems for tall timber buildings include platform systems (plate elements) [20], truss systems (columns, beams and diagonals) [2], moment-resisting frame systems (frames with fixed joints) [21], and hybrid structures (timber combined with concrete/steel) [22]. The following sections will describe the truss systems and platform systems and their connections.

2.2.1   Truss systems

In the truss systems, the diagonal elements are used to stabilise the buildings against lateral loadings, such as wind and earthquake loading. In tall timber buildings truss systems are implemented with glulam elements. The glulam trusses can extend over several floors as shown in Fig.2.3 and are placed at the outer layer to maximise the internal space. Glulam columns and beams are used for supporting vertical load transferred from the floor elements.

The two tallest all-timber buildings in the world, Mjøstårnet and Treet (Figs.1.1(a) and 1.1(b)) are made with the glulam truss structural system. The glulam truss members in such tall buildings can reach quite large dimensions. For example, the cross-sectional area of the diagonal elements in Mjøstårnet is on average 600 mm by 750 mm, while the cross-sectional area of the columns can reach 600 mm by 1500 mm. Having such large diagonal elements can create architectural challenges, such as obstruction of the window view.
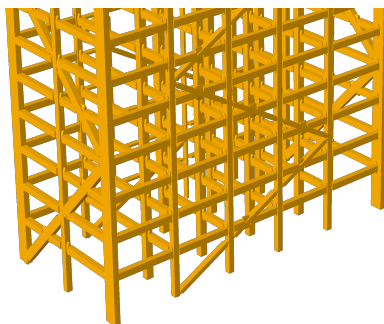
Figure 2.3: Truss building example

2.2.2   Platform systems

In a platform-type system, the planar elements are assembled together with mechanical connections to create a box-like structure. In tall timber buildings, the platform-type system can be implemented with CLT panels. Fig.2.4 shows an ex-

ample of a CLT platform system, where floors, walls and ceilings are made with CLT panels. The CLT panels have a high capacity to resist lateral and compressive loading and they are often used in multi-storey and long-span diaphragm applications. Sara Kulturhus in Sweden (Fig.1.1(c)) is an example of a hybrid building which utilises CLT panels in the structural system.

(a) Platform type construction   **(b)** CLT building example
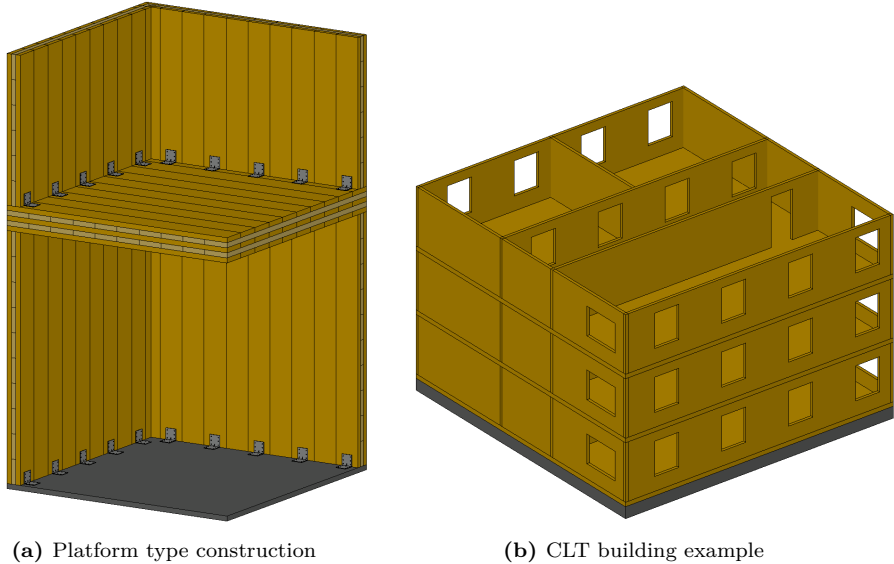
Figure 2.4: Platform type CLT building

2.2.3   Connections in timber buildings

Mechanical connections in timber buildings play a critical role in transferring loads and stresses between different parts of the structure. Connections in the glulam truss buildings and in CLT platform-type buildings are described further.

Connections in glulam truss buildings

Glulam frame members in tall timber buildings are usually connected to each other with a combination of slotted-in plates and dowels made of steel as shown in Fig.2.5. In Mjøstårnet the diameter of steel dowels was 12 mm and the steel plate thickness was 10 mm. The 13 mm cuts were sawn in the glulam to insert steel plates and a large number of dowels is used to connect the steel plates to the glulam frame. An example of the installation process of the slotted-in steel plates and dowels is shown in Figs.2.5(a) and 2.5(b): here the glulam specimen with connection is prepared in the lab for testing.

(a) Slotted-in steel plate   **(b)** Glulam connection specimen
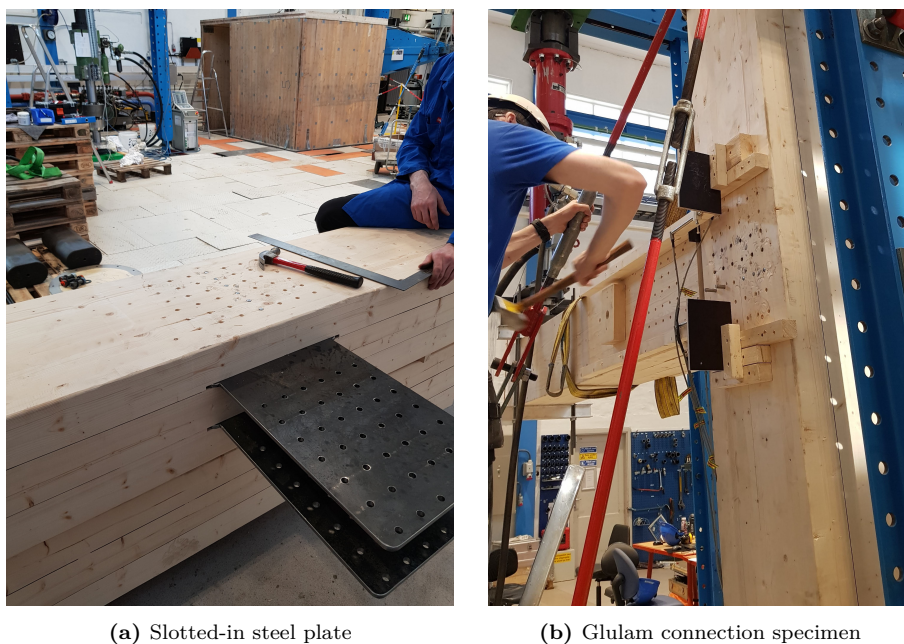
Figure 2.5: Slotted-in steel plate connection

Fig.2.6 shows an example of the connections between the column and the diagonal in Mjøstårnet. The holes that were used for installing steel dowels were covered with timber plugs, which serve two purposes: for the protection of steel dowels from the heat in case of fire and for the aesthetics of the glulam members.

While the stiffness of glulam connections with slotted-in steel plates and dowels can be estimated according to the design code (Eurocode 5 in Europe [23]), the calculated values might not be representative of an actual connection stiffness behaviour in tall timber buildings [2].

Connections in CLT buildings

CLT panels in the CLT building are usually connected to each other with a series of hold-down brackets and steel angle brackets as shown in Fig.2.7. Hold-downs (Fig.2.7(b)) are typically used for connecting the CLT superstructure to the reinforced concrete foundation or to transfer loads from the roof or upper floors to the foundation. Angle brackets (Fig.2.7(a)) are used for connecting the CLT plates together at a corner or other angle and are designed to resist lateral forces. Both angle brackets and hold-downs are usually made with steel and connected to the

Figure 2.6: Connections in glulam truss

panels with a set of screws (or bolts).

The CLT panels are rigid in comparison to their connections, and therefore the stiffness of CLT buildings depends mostly on the stiffness of these connections. The previous studies showed that the stiffness of the connections could have a significant impact on the dynamic properties of multi-storey CLT buildings [24, 25]. Since the stiffness of these connections is subject to uncertainty, their behaviour in timber buildings needs to be studied in more detail.

(a) Steel angle bracket

(b) Hold down bracket

Figure 2.7: Connections in CLT buildings

3. Theoretical background on system identification and modal analysis

In civil engineering structures, and in timber structures in particular, the gap between the predictive models and the real systems can be significant due to a lack of data for modelling and uncertainties related to the various properties of the structure. The system identification and modal analysis aim to bridge this gap between the model and the real system by allowing for experimental verification of the modal parameters. The evaluation of the vibration data of the structure can be divided into two main parts: development of the predictive mathematical models (known as system identification) and estimation of the modal properties of the system (known as modal analysis). Numerous system identification techniques and modal analysis methods exist and the following sections will describe the most common ones. Additionally, the corresponding model updating schemes and existing applications to timber buildings are presented.

3.1 Structural dynamic models

3.1.1 Finite element model

The dynamic behaviour of the structure is described by the following second-order linear differential equation of motion:

$$\mathbf{M}\ddot{\mathbf{q}}(t) + \mathbf{C}\dot{\mathbf{q}}(t) + \mathbf{K}\mathbf{q}(t) = \mathbf{F}(t) \tag{3.1}$$

where $\mathbf{M}$ is the mass matrix, $\mathbf{C}$ is the damping matrix, $\mathbf{K}$ is the stiffness matrix, all with dimensions $[n \times n]$. The vector $\mathbf{q}$ contains the displacements of the system, and $\mathbf{F}$ is external excitation, both with dimensions $[n \times 1]$. n designates the number of degrees of freedom.

A closed-form solution to the one-degree-of-freedom linear system with free vibration (no external excitation) can be obtained and has the following form:

$$q(t) = e^{(-\xi\omega t)}\left(\frac{v_0 + \xi\omega u_0}{\omega_d}\sin\omega_d t + u_0\cos\omega_d t\right) \tag{3.2}$$

where ω, ξ are the natural frequency and damping ratio of the mode, ω_d is the damped natural frequency, which is equal to $\omega\sqrt{1 - \xi^2}$. The solution of the forced vibrations of the linear system subjected to $f(t)$ involves using Duhamel's integral and can be expressed as follows:

$$q(t) = \frac{1}{m\omega_d}\int_0^t e^{-\xi\omega(t-\tau)}f(\tau)\sin\omega_d(t - \tau)d\tau \tag{3.3}$$

While an analytical solution is possible only for simple force-time relationships, the use of numerical integration is required for most systems. The use of numerical integration schemes such as Newmark can be used to obtain a numerical solution to the equations of motion.

3.1.2   State-space model

In many system identification techniques, the state-space formulation of the system is used.

Eqn.(3.1) can be rewritten in the following way:

$$\ddot{\mathbf{q}}(t) = -\mathbf{M}^{-1}\mathbf{K}\mathbf{q}(t) - \mathbf{M}^{-1}\mathbf{C}\dot{\mathbf{q}}(t) + \mathbf{M}^{-1}\mathbf{B_u}\mathbf{u}(t) \tag{3.4}$$

where $\mathbf{u}(t)$ is a vector containing the loads applied to the system with dimensions $[u \times 1]$, $\mathbf{B_u}$ is a matrix for the control forces with dimensions $[u \times n]$ such that $\mathbf{f}(t) = \mathbf{B_u}\mathbf{u}(t)$, where u is the number of system inputs.

The definition of the state vector:

$$\mathbf{x}(t) = \begin{bmatrix}\mathbf{q}(t)\\\dot{\mathbf{q}}(t)\end{bmatrix} \tag{3.5}$$

The state vector is of dimension $[2 \times n]$.

Substituting Eqn.(3.5) into Eqn.(3.4) and using the identity $\mathbf{M}\dot{\mathbf{u}}(t) = \mathbf{M}\dot{\mathbf{u}}(t)$ yields:

$$\begin{bmatrix} \ddot{\mathbf{q}}(t) \\ \dot{\mathbf{q}}(t) \end{bmatrix} = \begin{bmatrix} \mathbf{0} & \mathbf{I} \\ -\mathbf{M}^{-1}\mathbf{K} & -\mathbf{M}^{-1}\mathbf{C} \end{bmatrix} \begin{bmatrix} \mathbf{q}(t) \\ \dot{\mathbf{q}}(t) \end{bmatrix} + \begin{bmatrix} \mathbf{0} \\ \mathbf{M}^{-1}\mathbf{B_u} \end{bmatrix} \mathbf{u}(t) \qquad (3.6)$$

From Eqn.(3.6) the state matrix $\mathbf{A_c}$ with dimensions $[2n \times 2n]$ and the input matrix $\mathbf{B_c}$ with dimensions $[2n \times u]$ can be defined as follows:

$$\mathbf{A_c} = \begin{bmatrix} \mathbf{0} & \mathbf{I} \\ -\mathbf{M}^{-1}\mathbf{K} & -\mathbf{M}^{-1}\mathbf{C} \end{bmatrix} \qquad (3.7)$$

$$\mathbf{B_c} = \begin{bmatrix} \mathbf{0} \\ \mathbf{M}^{-1}\mathbf{B_u} \end{bmatrix} \qquad (3.8)$$

The state equation in continuous time is then written as:

$$\dot{\mathbf{x}}(t) = \mathbf{A_c}\mathbf{x}(t) + \mathbf{B_c}\mathbf{u}(t) \qquad (3.9)$$

The observation equation, which provides the vector of measured outputs as a function of input is written as follows:

$$\mathbf{y}(t) = \mathbf{C_a}(t)\ddot{\mathbf{q}}(t) + \mathbf{C_v}(t)\dot{\mathbf{q}}(t) + \mathbf{C_d}(t)\mathbf{q}(t) \qquad (3.10)$$

where $\mathbf{y}(t)$ is the $[l \times 1]$ system output, $\mathbf{C_a}$, $\mathbf{C_v}$, and $\mathbf{C_d}$ with dimensions $[l \times 2n]$ are the output location matrices for acceleration, velocity, and displacement with the assumption that the measurements of the structural response are taken at l locations.

The observation equation in continuous time is:

$$\mathbf{y}(t) = \mathbf{C_c}\mathbf{x}(t) + \mathbf{D_c}\mathbf{u}(t) \qquad (3.11)$$

In Eqn.(3.11), the $\mathbf{C_c}$ with dimensions $[l \times 2n]$ and $\mathbf{D_c}$ with dimensions $[l \times u]$ are the output matrix and the direct transmission matrix, which are expressed as

follows:

$$\mathbf{C_c} = \begin{bmatrix} \mathbf{C_d} & \mathbf{0} \\ \mathbf{0} & \mathbf{C_v} \\ -\mathbf{C_a M^{-1} K} & -\mathbf{C_a M^{-1} C} \end{bmatrix} \tag{3.12}$$

$$\mathbf{D_c} = \begin{bmatrix} \mathbf{0} \\ \mathbf{0} \\ \mathbf{C_a M^{-1} B_u} \end{bmatrix} \tag{3.13}$$

The continuous state space model for the structural system in Eqs.(3.9) and (3.11) is not practical for real-life application. In practice, the vibration signals are measured at discrete time instants, so the conversion of the state space model to discrete time is necessary. Using the Zero Order Hold (ZOH) assumption, which states that the input is piecewise constant over the sampling period Δt, the continuous time state-space model is converted to the discrete-time state-space model:

$$\begin{aligned} \mathbf{x}_{k+1} &= \mathbf{A}\mathbf{x}_k + \mathbf{B}\mathbf{u}_k \\ \mathbf{y}_k &= \mathbf{C}\mathbf{x}_k + \mathbf{D}\mathbf{u}_k \end{aligned} \tag{3.14}$$

where the relationship between the discrete and continuous parameters is as follows:

$$\mathbf{A} = e^{\mathbf{A_c} \Delta t}, \quad \mathbf{B} = (\mathbf{A} - \mathbf{I})\mathbf{A_c}^{-1}\mathbf{B_c}, \quad \mathbf{C} = \mathbf{C_c}, \quad \mathbf{D} = \mathbf{D_c} \tag{3.15}$$

3.1.3   Transfer function model

Transfer function models are used primarily for describing the relationship between the system measured inputs and the measured outputs. The following equation describes the basic transfer function model [26]:

$$\mathbf{y}(t) = \mathbf{G}(q)\mathbf{u}(t) + \mathbf{H}(q)\mathbf{e}(t) \tag{3.16}$$

where $\mathbf{y}(t)$ is the system outputs vector, $\mathbf{u}(t)$ is the system inputs vector, $\mathbf{e}(t)$ is the stochastic input from noise and prediction errors, $\mathbf{G}(q)$ is the transfer function of the system and $\mathbf{H}(q)$ is the transfer function of the disturbances.

The transfer function corresponds to the Laplace transform of the impulse response, while the frequency response function corresponds to the Fourier transform of the same impulse response function [27].

3.2   Classification of system identification methods

A large number of system identification methods exist and various classification methods are employed [28]. The most general classification of the system identification methods is according to the analysis domain: time domain and frequency domain. Time domain methods refer to the estimation methods applied to the time histories of the output signals and include such methods as the Kalman filter, recursive least squares, Bayesian inference, and stochastic modelling. Frequency domain methods include the Fourier transform-based parameter estimation methods.

System identification can be applied in the time domain directly on the output signal, or the data transformation to the frequency domain can be conducted first before applying the system identification. Selecting domain for system identification depends on the problem at hand. For example, the time domain methods might be suitable for output-only identification as they are optimal for dealing with noise in the data and are not exposed to signal processing errors, such as leakage. The frequency domain methods, on the other hand, are more suitable for averaging out the noise from the signals with harmonic excitation [29].

Another type of classification is regarding the nature of system input and separates the system identification into three different classes: experimental modal analysis (EMA), operational modal analysis (OMA), and combined experimental-operational modal analysis (OMAX) [30]. The first type, EMA, involves evaluating the data from the forced vibration tests (FVT). In EMA the structure is excited by the measured dynamic forces and the corresponding response of the structure is recorded, the modal parameters are then extracted from these input/output measurements. The EMA approach can also be called a deterministic method since the input force to the system is known. The second type is OMA, where the input force is unknown and the assumption that the unmeasured loads are realisations of a stationary stochastic process is made. The OMA method is also known as the output-only method since only output is analysed. The OMA method is suitable for large structures, such as buildings and bridges, where EMA is difficult to apply. In OMA the environmental forces are also called ambient forces, which gave the

name to the ambient vibration testing (AVT) method. A common assumption in the OMA method is that stochastic input is a white noise process with zero mean and finite variance. While the assumption is not always true, the OMA method still can give valid results, provided the input forces are not drastically different from the stationary white noise assumption. The third type is OMAX, where both artificial and operational forces are included in the system identification model.

Based on the nature of the data extraction methods, the classification into the parametric and non-parametric methods can be made [31]. In non-parametric methods, the modal extraction is done directly from the data, without any specific model fitting, while in parametric methods, a model is defined with an underlying mathematical structure and model parameters are fitted into the model.

Furthermore, the following classifications can be made: (1) linear and nonlinear models; (2) univariate model (single input-single output (SISO)) and multivariable models (single input-multiple outputs (SIMO), multiple inputs-multiple outputs (MIMO)); (3) deterministic and stochastic models; (4) discrete and continuous time models, etc. [32, 33, 34].

The following sections describe the most common system identification and modal analysis techniques as well as the corresponding damping estimation and model updating. Finally, a summary of some existing applications of system identification and modal analysis on tall timber buildings is presented.

3.3   Spectral estimation

Non-parametric methods can be used when little information about the signal is available in advance [35]. Spectral estimation methods are non-parametric methods based on the Fast Fourier Transform (FFT). Spectral estimation methods describe the way the power of the signal is distributed over each frequency bin, known as power spectral density (PSD). For a random zero-mean process, the power spectral density $S_{xx}(f)$ can be expressed using the Wiener-Khintchine relation as the Fourier transform of the auto-correlation function $R_{xx}(f)$ [36] at time instances t and $t + \tau$, where τ is the time lag:

$$S_{xx}(f) = \int_{-\infty}^{+\infty} R_{xx}(f)e^{-i2\pi f\tau}d\tau$$

$$\text{where} \quad R_{xx}(\tau) = \lim_{T\to\infty} \frac{1}{T}\int_0^T x(t)x(t+\tau)d\tau \tag{3.17}$$

The spectral estimation methods have some disadvantages including resolution and statistical stability. Welch's method is the modified periodogram where the original data is split into overlapping n data segments of length $T = N\Delta t$, where N is the block size for each FFT computation, with an overlap of D points and windowing is applied to each segment. The smoothed PSD spectrum using Welch's method is expressed as follows [37]:

$$S_{xx,wlc}(f) = \frac{2}{nN\Delta t} \sum_{i=1}^{n} \left| X_i(f) \right|^2 \tag{3.18}$$

3.4 Complex mode indicator function (CMIF)

The frequency response function (FRF) matrix describes the input/output relationship of the structure at each spectral line. In modal analysis, the FRF, $\mathbf{H}(\omega)$, for linear time-invariant multi-degree-of-freedom system can be expressed as [38]:

$$\mathbf{H}(\omega) = \mathbf{\Phi}(\lambda_r^2 - \omega^2)^{-1}\mathbf{\Phi}^{\mathrm{T}} \tag{3.19}$$

where $\mathbf{\Phi}$ is the mass-normalised eigenvector matrix, λ_r is the eigenvalue matrix.

Complex mode indicator is based on singular value decomposition (SVD) of the FRF functions for identification of the modes of the structure [39]. The singular value decomposition of the FRF at each spectral line is defined as:

$$\mathbf{H}(\omega) = \mathbf{U}(\omega)\mathbf{\Sigma}(\omega)\mathbf{V}(\omega)^{\mathrm{H}} \tag{3.20}$$

where $\mathbf{U}(\omega)$ is the $[N_o \times N_r]$ left side of the unitary matrix, $\mathbf{V}(\omega)$ is the $[N_r \times N_i]$ right side of the unitary matrix, $\mathbf{\Sigma}(\omega)$ is the $[N_r \times N_r]$ singular matrix, which is a diagonal matrix, $\{.\}^{\mathrm{H}}$ is the Hermitian transpose (or complex conjugate transpose), and $\mathbf{H}(\omega)$ is the $[N_o \times N_i]$ frequency response function. N_i is the number of input (reference) points, N_o is the number of response points.

The peaks of singular values on the CMIF plot indicate the existence of modes and the corresponding frequency locations give damped frequency values for these modes.

3.5 Peak picking

Peak picking is one of the common methods for the estimation of modal properties from collected response data. This method assumes that at the vicinity of the resonance peak of the FRF, the structural response is governed by a single vibration mode and the contribution from other modes is negligible. In this case, the multi-degree-of-freedom (MDOF) FRF of the structure can be treated as a single-degree-of-freedom (SDOF) FRF. The SDOF dynamic model can then be used with curve fitting for the extraction of modal parameters. This method can be applied together with the CMIF method. Disadvantages of this method are that it cannot be applied to closely-spaced modes, it requires good quality FRF data to produce accurate results, and its damping estimates are not reliable [40].

3.6 Stochastic Subspace Identification

3.6.1 Stochastic state space model

In operational modal analysis, the structure is excited by immeasurable force. The input $\mathbf{u}_k$ in Eqn.(3.14) is not known and the measured output of the system $\mathbf{y}_k$ is generated only by the stochastic processes. Thus, the discrete-time stochastic state-space model becomes as follows:

$$\begin{aligned} \mathbf{x}_{k+1} &= \mathbf{A}\mathbf{x}_k + \mathbf{w}_k \\ \mathbf{y}_k &= \mathbf{C}\mathbf{x}_k + \mathbf{v}_k \end{aligned}$$

(3.21)

where $\mathbf{w}_k$ is the process noise of dimension $[2n \times 1]$ due to disturbances and inaccuracies in the model and $\mathbf{v}_k$ is the measurement noise of dimension $[l \times 1]$ due to sensor inaccuracies.

Since the input force is unknown, $\mathbf{w}_k$ becomes the input in determination of the order $2n$ of the unknown system and realisation of the state matrix $[\mathbf{A}]$ and observation matrix $[\mathbf{C}]$ from a large amount of the output measurements $\mathbf{y}_k$. Both $\mathbf{w}_k$ and $\mathbf{v}_k$ are immeasurable and assumed to be zero mean Gaussian white noise

processes with covariance matrices given by:

$$E\left[\begin{pmatrix}\mathbf{w}_p \\ \mathbf{v}_p\end{pmatrix}\begin{pmatrix}\mathbf{w}_q^{\mathrm{T}} & \mathbf{v}_q^{\mathrm{T}}\end{pmatrix}\right] = \begin{bmatrix}\mathbf{Q} & \mathbf{S} \\ \mathbf{S}^T & \mathbf{R}\end{bmatrix}\delta_{pq} \qquad (3.22)$$

where E is the expected value operator, δ_{pq} is the Kronecker delta operator, p and q are two arbitrary time instants. Estimating the matrices $\mathbf{Q}$, $\mathbf{R}$, and $\mathbf{S}$ is part of the identification process.

3.6.2   Data-driven stochastic subspace identification

Stochastic subspace identification techniques are considered to be a powerful class of identification methods for natural input modal analysis in the time domain [41]. This section describes the data-driven stochastic subspace identification method (SSI-DATA).

The algorithm starts by sifting the original output data into a sequence of multi-dimensional vectors. The system response is represented by the data matrix:

$$\mathbf{Y} = \begin{bmatrix}y_0, y_1, ..., y_{N-1}\end{bmatrix}^{\mathrm{T}} \qquad (3.23)$$

where N is the number of data points. If $2i$ is the total number of block rows, where i is a prescribed time lag, then $j = N - 2i + 1$ multi-dimensional vectors from the data matrix can be obtained:

$$\mathbf{Y}_r = \begin{bmatrix}y_{r-1}, y_r, ..., y_{r+2i-2}\end{bmatrix}^{\mathrm{T}}, \quad r = 1, 2, ..., j \qquad (3.24)$$

The data is then organised in a Block Hankel matrix of dimension $[2li \times j]$ with $\mathbf{Y}_r$ as column vectors:

$$\mathbf{H} = \frac{1}{\sqrt{j}}\begin{bmatrix} y_0 & y_1 & \cdots & y_{j-1} \\ y_1 & y_2 & \cdots & y_j \\ \cdots & \cdots & \cdots & \cdots \\ y_{2i-1} & y_{2i} & \cdots & y_{j+2i-2} \end{bmatrix} \qquad (3.25)$$

where $\frac{1}{\sqrt{j}}$ is the scale factor [42]. The Hankel matrix can be divided into the "past" (the block Hankel matrix of the past outputs with the last i samples removed) and the "future" (the block Hankel matrix of the future outputs with the first i samples removed) parts with dimensions $[li \times j]$:

$$\mathbf{H} = \begin{bmatrix} \mathbf{H}_p \\ \mathbf{H}_f \end{bmatrix} \tag{3.26}$$

The block Toeplitz $[li \times li]$ matrix is defined as follows:

$$\mathbf{T} = \mathbf{H}_f \mathbf{H}_p^{\mathrm{T}} \tag{3.27}$$

The block Toeplitz can be decomposed as a product of the extended observability matrix $\mathbf{O}_i$ with dimensions $[li \times n_0]$ and the reversed extended controllability matrix $\mathbf{\Gamma}_i$ with dimensions $[n_0 \times li]$, where n_0 is the selected model order:

$$\mathbf{T} = \mathbf{O}_i \mathbf{\Gamma}_i = \begin{bmatrix} \mathbf{C} \\ \mathbf{CA} \\ ... \\ \mathbf{CA}^{i-1} \end{bmatrix} \begin{bmatrix} \mathbf{A}^{i-1}\mathbf{G} & \mathbf{A}^{i-1}\mathbf{G} & ... & \mathbf{G} \end{bmatrix} \tag{3.28}$$

By applying the singular value decomposition (SVD) to the block Toeplitz matrix its rank, which is equal to the number of nonzero singular values, can be obtained:

$$\mathbf{T} = \mathbf{U}\mathbf{\Sigma}\mathbf{V}^T = \begin{bmatrix} \mathbf{U}_1 & \mathbf{U}_2 \end{bmatrix} \begin{bmatrix} \mathbf{\Sigma}_1 & \mathbf{0} \\ \mathbf{0} & \mathbf{0} \end{bmatrix} \begin{bmatrix} \mathbf{V}_1^{\mathrm{T}} \\ \mathbf{V}_2^{\mathrm{T}} \end{bmatrix} \tag{3.29}$$

If zero singular values and corresponding singular vectors are omitted, Eqn.(3.29) becomes:

$$\mathbf{T} = \mathbf{O}_i \mathbf{\Gamma}_i = \mathbf{U}_1 \mathbf{\Sigma}_1 \mathbf{V}_1^{\mathrm{T}} \tag{3.30}$$

where $\mathbf{U}_1$ of dimension $[li \times n_0]$ contains the left singular vectors as columns and $\mathbf{V}_1$ of dimension $[n_0 \times li]$ contains the right singular vectors as rows, $\mathbf{\Sigma}_1$ of dimension $[n_0 \times n_0]$ is the diagonal matrix containing singular values in decreasing order. The matrices $\mathbf{O}_i$ and $\mathbf{\Gamma}_i$ are obtained as follows:

$$\mathbf{O}_i = \mathbf{U}_1 \mathbf{\Sigma}_1^{1/2} \mathbf{I}$$
$$\mathbf{\Gamma}_i = \mathbf{T}^{-1} \mathbf{\Sigma}_1^{1/2} \mathbf{V}_1^{\mathrm{T}}$$

$$(3.31)$$

Matrix $\mathbf{I}$ plays the role of a similarity transformation applied to the state space model.

The system matrices $\mathbf{A}$ and $\mathbf{C}$ can be obtained from Eqn.(3.31):

$$\mathbf{C} = \mathbf{O}_i(1:l;1:n)$$
$$\mathbf{A} = \underline{\mathbf{O}}_i^+ \overline{\mathbf{O}}_i$$

$$(3.32)$$

where $\mathbf{O}_i(1:l;1:n)$ is the first l rows and n columns of $\mathbf{O}_i$, $\underline{\mathbf{O}}_i$ is $\mathbf{O}_i$ without the last l rows, and $\overline{\mathbf{O}}_i$ is $\mathbf{O}_i$ without the first l rows, $+$ denotes the pseudo-inverse of a matrix.

Once the system matrices $\mathbf{A}$ and $\mathbf{C}$ are estimated, the modal characteristics of the system can be easily calculated by solving for eigenvalues and eigenvectors as shown in Eqs.(3.33-3.38).

The eigenvalue decomposition of the system matrix A can be performed as follows:

$$\mathbf{A} = \mathbf{\Psi} \mathbf{\Lambda} \mathbf{\Psi}^{-1}$$

$$(3.33)$$

where Λ is the diagonal matrix with eigenvalues λ_k. The relationship between the discrete and continuous time eigenvalues is as follows:

$$\lambda_{c,i} = \frac{ln(\lambda_k)}{\Delta t}$$

$$(3.34)$$

where $\lambda_{c,i}$ is the continuous time eigenvalue for mode i.

The modal properties, fundamental frequency and damping ratio, of the system, can be derived as follows:

$$\omega_i = |\lambda_{c,i}|$$

$$(3.35)$$

$$f_i = \frac{|\lambda_{c,i}|}{2\pi} \tag{3.36}$$

$$\xi_i = \frac{-\text{Re}(\lambda_{c,i})}{|\lambda_{c,i}|} \tag{3.37}$$

where Re denotes the real part of the complex eigenvalue. The mode shape vectors are obtained as follows:

$$\phi_i = \mathbf{C} \cdot \psi_i \tag{3.38}$$

where ψ_i is the vector corresponding to the columns of $\mathbf{\Psi}$.

One of the important parameters for the quantitative comparison of modal vectors is the Modal Assurance Criterion (MAC) [43]. MAC is calculated as the normalised scalar product of two sets of mode shape vectors ϕ_i and ϕ_j:

$$\text{MAC}(\phi_i, \phi_j) = \frac{|\phi_i^{\text{T}} \phi_j|^2}{(\phi_i^{\text{T}} \phi_i)(\phi_j^{\text{T}} \phi_j)} \tag{3.39}$$

The MAC is used to evaluate the similarity between the two mode shapes. The MAC values range between 0 (no consistent correspondence) and 1 (consistent correspondence). It can also be used to assess the orthogonality of the modes in the mode shape matrix.

The calculated poles ($\lambda_{c,i}$) from the SSI need to be evaluated through stabilisation criteria, which allows distinguishing between the physical and spurious poles. In practice, it is better to over-estimate the model order and then eliminate the spurious modes through the stabilisation criteria [44]. The common stability requirements are as follows:

$$\frac{f_p - f_{p+1}}{f_p} * 100 < 1\%$$

$$\frac{\xi_p - \xi_{p+1}}{\xi_p} * 100 < 5\% \tag{3.40}$$

$$\text{MAC}(\phi_p, \phi_{p+1}) > 95\%$$

For a more detailed description of the underlying theory on stochastic state-space model and subspace identification, the reader should refer to Rainieri and Fabbrocino [45], Van Overschee and De Moor [42].

3.7   Random Decrement Technique

The random decrement technique (RDT) is based on the assumption that the total response of the structure due to the random input consists of two parts: deterministic part and random part [46]. Using the trigger value (threshold amplitude), the signal is decomposed into a series of time segments. By averaging these time segments, the random part is cancelled out and only the deterministic part is left. This deterministic part is called the random decrement signature (RDS) and it contains the free response of the structure. A brief theory is outlined here with more detailed information found in the literature [47]. The random decrement function can be expressed as follows:

$$\alpha_{RDT}(\tau) = \mathrm{E}\big\{\mathrm{sgn}[x(t)]x(t+\tau)|\dot{x}(t) = 0\big\} \tag{3.41}$$

where $\alpha_{RDT}(\tau)$ is the extracted random decrement function, $\mathrm{E}\{x|C\}$ is the expectation of x given the triggering condition C, $\mathrm{sgn}[.]$ is the signum function, $x(t)$ is the measured response time series, τ is the length of the selected time series, and $\dot{x}(t)$ is the derivative of $x(t)$.

It was demonstrated that the random decrement signature $\alpha_{RDT}(\tau)$ is proportional to the autocorrelation function R_{xx} of the response $x(t)$ provided stationary and zero mean stochastic process:

$$\alpha_{RDT} = \frac{R_{xx}(\tau)}{R_{xx}(0)}x0 \tag{3.42}$$

where $R_{xx}(\tau)$ is the autocorrelation function of $x(t)$ and $R_{xx}(0)$ is the variance of $x(t)$.

Assuming that $x(t)$ is ergodic, the expectation can be replaced with arithmetic mean values of a sufficiently large number N of the response segments with peak values i, and expressed as follows:

$$\alpha_{RDT}(\tau) = \frac{1}{N}\sum_{i=1}^{N}\mathrm{sgn}[x(t)]x_i(t+\tau)\big|_{\dot{x}(t_i)=0} \tag{3.43}$$

Once the random decrement signature is obtained, the natural frequency and damping ratio can be obtained by approximating the RDS curve by free decay of oscil-

lations as follows [48]:

$$\alpha_{RDT}(\tau) = \alpha(\tau) + m(\tau) = \frac{x_0}{\sqrt{1 - \xi^2}} e^{-\omega_0 \xi \tau} \cos(\sqrt{1 - \xi^2} \omega_0 \tau - \varphi) + m(\tau) \quad (3.44)$$

where $\alpha(\tau)$ is the free damped oscillation function, ω_0 is a natural frequency, ξ is a damping ratio, φ is phase angle, $m(\tau)$ is the correction function of the approximation, which represents the filtered noise contribution after band-pass filtering [49].

3.8   Variational mode decomposition

Variational mode decomposition is a signal-processing tool, which decomposes the acceleration signal into a series of intrinsic mode functions (IMFs)- distinct modal responses and the corresponding centre frequencies [50]. The VMD technique can be used to extract the modes of interest from the non-stationary signals.

The response of the structure $x(t)$ can be expressed as a sum of amplitude-modulated and frequency-modulated components (IMFs) with a narrow frequency bandwidth:

$$x(t) = \sum_{k=1}^{K} u_k(t) \quad (3.45)$$

where $u_k(t)$ is the k-th IMF, K is the number of IMFs.

The bandwidth of each mode is then assessed by computing the analytic signal using the Hilbert transform, shifting the frequency spectrum to the estimated centre frequency, and calculating the square of the L^2 norm of the signal gradient. Based on the estimated bandwidth of each mode, the constrained variational problem is constructed:

$$\min_{\{u_k\}, \{\omega_k\}} = \left\{ \sum_k \left\| \partial_t \left[\left(\delta(t) + \frac{j}{\pi t} \right) * u_k(t) \right] e^{-j\omega_k t} \right\|_2^2 \right\}$$
$$s.t. \ x(t) = \sum_{k=1}^{K} u_k(t) \quad (3.46)$$

where $u_k(t)$ are the different modes, ω_k are the corresponding center frequencies, $\|.\|_2$ is the L^2 norm, ∂_t is the derivative with respect to time t, $\delta(t)$ is the Dirac function. This minimisation problem is then solved through Lagrangian multipliers using the alternate direction method of multipliers as described in [50].

3.9 Model updating

Model updating can be implemented to validate the developed finite element model based on the experimentally derived modal properties [51]. The process of model updating is usually conducted as follows:

- Collecting the experimental data on structural behaviour.

- Developing the base model using the best engineering judgement.

- Comparing the prediction model and the actual data.

- Conducting sensitivity analysis to investigate and rank the impact of input parameters of choice on the output properties of interest.

- Adjusting the model to better represent the behaviour by using realistic ranges of parameters in the previous step.

- Validate the final model by re-analysing that the updated model accurately reflects the actual behaviour of the structure.

A large number of model updating techniques can be found in the literature, and in general, can be divided into deterministic and stochastic model updating. Deterministic model updating involves making adjustments based on the deterministic comparison between the model and the measured behaviour. An example of deterministic model updating is the gradient method, where the search direction is defined by the gradient of the function. The genetic algorithm is an example of stochastic model updating. The genetic algorithm starts with a set of potential solutions to a problem and each of those sets is evaluated using a fitness function. Solutions with the highest fitness function are selected for the next set of solutions by combining the different sets. The process is repeated until a satisfactory solution is found.

3.10   Damping ratios estimation

In structural dynamics, damping refers to the ability of a structure to dissipate energy and reduce the amplitude of vibrations in response to an external loading or disturbance. Different damping models exist, such as viscous damping, structural damping, and hysteretic damping. The most common damping model used in the dynamic analysis is the viscous damping model due to its mathematical simplicity [52]. In the viscous damping model, the damping force is proportional to the velocity of motion and is in the opposite direction of motion. Viscous damping is typically represented by a dashpot element.

While the viscous damping ratio is most commonly used in the modelling of structural systems, such as bridges and buildings, the real damping behaviour in buildings is actually amplitude-dependent [53, 48]. Unlike traditional velocity-proportional viscous damping, amplitude-dependent damping is nonlinear and depends on the amplitude of displacement or velocity.

3.10.1   Damping in wind-induced calculations

For calculation of the wind-induced response of the buildings, the standard proposes the following equation for damping estimation [12]:

$$\delta = \delta_s + \delta_a + \delta_d \tag{3.47}$$

where δ is the logarithmic decrement of total damping, δ_s is the logarithmic decrement of structural damping, δ_a is the logarithmic decrement of aerodynamic damping, and δ_d is the logarithmic decrement of damping due to special devices, such as tuned-mass dampers. The logarithmic decrement of damping is related to the viscous damping ratio through the following expression:

$$\delta = 2\pi\xi \tag{3.48}$$

Structural damping value for the tall timber buildings is not provided in the standard, therefore structural damping for timber bridges ($\delta = 0.06 - 0.12$) is usually used for the design of timber buildings, which corresponds to 1.0%-1.9%.

3.10.2   Damping modelling

In the modal dynamic analysis using finite element software, damping can be introduced both at the material/element level and at the building level. Damping can be applied to a modal dynamic system in two forms: velocity-proportional viscous damping or displacement-proportional structural damping.

Velocity proportional viscous damping can be applied to the model in two options: Rayleigh damping and Modal damping. Rayleigh damping matrix $\mathbf{C}$ is defined by a linear combination of the mass and stiffness matrices:

$$\mathbf{C} = \alpha\mathbf{M} + \beta\mathbf{K} \tag{3.49}$$

where α and β are real scalars. For a single-degree-of-freedom system, the Rayleigh damping is given as follows:

$$\xi = \frac{\alpha\omega}{2} + \frac{\beta}{2\omega} \tag{3.50}$$

Instead of providing the α and β coefficients, which govern the modal damping ratio, it is possible to manually assign damping ratios for each mode. This approach is called the Modal damping approach, which has no physical basis and is a purely mathematical concept. This approach is convenient for comparison with the experimentally identified modal frequencies and damping ratios. For each mode n damping matrix C_n is defined as follows:

$$C_n = 2\xi_n\omega_n M_n \tag{3.51}$$

Structural damping in the modal dynamic analysis is applied as viscous-equivalent damping. Application of structural damping can lead to non-linear equations of motion due to dependence on displacement amplitude [54].

3.10.3   Experimental estimation of damping

The estimation of damping ratios from ambient vibration tests is subject to significant uncertainty due to the stochastic nature of output-only methods. The quality of the estimated damping ratios depends significantly on the quality of measurement data, and thus, the measurement noise and the processing techniques can impact the quality of the damping estimates.

The FRF-based damping ratios from forced vibration tests using the half-power bandwidth are also not reliable, since the method depends strongly on the resolu-

tion of data.

The most reliable estimates of the damping ratio and its amplitude dependency can be obtained through the free vibration test. In this test, the building is subjected to forced vibration at a specified natural frequency until a steady-state response is achieved and is followed by an abrupt stop to obtain a free decay response of the structure. By curve fitting the entire response curve or using a cycle-by-cycle curve fitting with a sinusoidal exponential decay function, the damping ratios and the corresponding acceleration levels can be obtained.

For good estimates of damping based on the ambient vibrations, considerably long measurement data is required. By using output-only techniques, the damping ratios and their amplitude dependency can be investigated from long-term measurements. The Random Decrement technique is a popular option for extracting amplitude-dependent damping ratios.

3.11   Existing studies on dynamic identification and modelling of tall timber buildings

This section aims to provide an overview of some studies on dynamic identification and the corresponding numerical modelling of tall timber buildings.

Multiple studies on dynamic identification using ambient vibration tests were conducted on timber buildings. An ambient vibration testing campaign of a set of seven to eight-storey CLT buildings was conducted [55, 56]. An amplitude-dependent behaviour of damping ratios was demonstrated for all buildings. Additionally, the lateral stiffness of the building was governed by the stiffness properties of the connections and non-structural elements had a significant impact on the modal properties of the building. Reynolds et al. conducted an ambient vibration testing of two types of five-storey timber-concrete buildings: a timber frame building and a CLT building [57]. Both buildings exhibited similar dynamic responses, which could be attributed to the concrete core. Aloisio et al. investigated the dynamic properties of an 8-storey CLT building using ambient vibrations and conducted model updating using a simplified analytical model of the building [58]. Mugabo et al. conducted ambient vibration testing of a four-storey CLT building and performed a multi-stage FE model calibration which indicated that non-structural elements impact the modal response of the building considerably [59]. Edskär conducted a parametric FE modelling for comparison against the ambient vibration

measurements of CLT and glulam frame buildings and assessed the acceleration and comfort criteria of the buildings in accordance with ISO 10137 and Euroode 1-4 [60]. It was demonstrated that the Eurocode underestimated the acceleration levels due to wind loading. Landel conducted vibration tests and modelling of glulam connections with simple spring models [61].

Several modal identification studies using forced vibration tests were conducted on multi-story timber buildings. One of the first full-scale studies on a multi-story timber building was conducted by Ellis and Bourgard [62]. In this study, the dynamic identification of a 6-storey timber framed building using ambient vibration tests and forced vibration was conducted. The results showed that adding non-structural elements, such as external cladding, staircases and plasterboards added to the stiffness of the building under service-level vibrations. Similarly, a later study by Steiger et al. on a 3-story light frame timber building indicated that adding non-structural elements, such as internal and external walls to the structure increases the natural frequencies of the building [63]. Additionally, this study demonstrated an amplitude-dependent behaviour of damping ratios using forced vibration tests. More lately, an FRF-based modal testing of a seven-storey CLT building was conducted by Ao et al. [64]. Based on this experimental study, FE model updating was performed by Kurent et al., which indicated the influence of connections on modal properties of the building [25].

4. Experimental and numerical framework

4.1 Experimental methods

Modal vibration testing is a common tool employed to obtain the dynamic properties of the structure. Various modal testing methods exist and the choice depends on the type of structure, the required level of accuracy, and the testing environment. In this thesis, the ambient vibration tests and the forced vibration tests were conducted.

4.1.1 Ambient vibration testing

Modal vibration test through ambient vibration measurements is a relatively easy and convenient way of obtaining the modal properties of the building. While there are certain limitations and drawbacks to this method, such as the requirement of stationarity and uncertainties in the estimated dynamic properties, especially in the damping ratios, it is still quite popular and successful in the field of civil engineering structures.

The ambient vibrations measurement setup for instrumenting the timber buildings in this thesis consisted of a set of high-sensitivity triaxial accelerometers, which were wired to the data acquisition system. Accelerometers were attached to the structural elements using metal plates and small screws, which were drilled directly into the structure. In the glulam frame building, accelerometers were mounted on the glulam beams as shown in Fig.4.1(a), and in the CLT buildings, accelerometers were mounted on the CLT elements as shown in Fig.4.1(b).

Accelerometers were placed throughout the building to capture the global behaviour and at the locations with the highest response amplitudes expected. However, due to the buildings being fully operational and occupied by the residents, the placements of the accelerometers were not always the most optimal ones. Nevertheless, the response of the building was successfully captured with the available

ambient measurement setups.

<div align="center">

(a) Accelerometer mounting on a glulam beam   **(b)** Accelerometer mounting on a CLT plate

Figure 4.1: Accelerometer mounting on timber elements

</div>

The obtained raw data from the field vibration tests were filtered with the Butterworth filter and downsampled to remove high-frequency components. The stochastic subspace identification (SSI) technique was then applied to obtain the modal properties. The nonparametric PSD technique was applied to verify the results of the SSI technique. Fig.4.2 shows an example of the stabilisation diagram obtained from the SSI technique co-plotted with the PSD diagram for a signal. For the investigation of amplitude dependency of damping from ambient vibration data, the random decrement technique (RDT) was applied. For modal extraction from long-term ambient vibration data, the variational mode decomposition (VMD) was applied using the MATLAB Signal Processing Toolbox [65] in combination with the output-only analysis techniques.

4.1.2   Forced vibration testing

The forced vibration tests (FVTs) were conducted using two methods: the electrodynamic shaker and the human-induced excitation.

Electrodynamic shaker-based tests

The electrodynamic shaker-based FVTs consisted of two synchronised electrodynamic shakers with a horizontal mass reaction system of 1000 kg placed at the top floor of the building (Fig.4.3). High-sensitivity accelerometers were distributed along
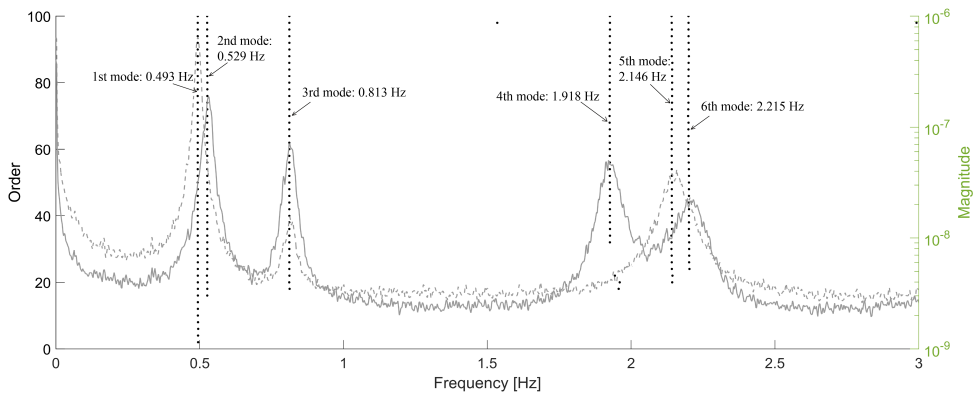
Figure 4.2: Stabilisation diagram and power spectral density of a signal

the building and the data were acquired simultaneously from all accelerometers by using precisely synchronised wireless data loggers (yellow boxes) as shown in Fig.4.4.
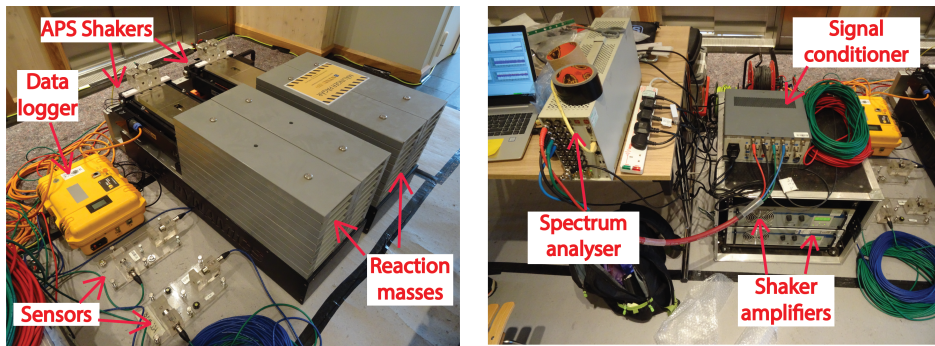

Figure 4.3: Electrodynamic shaker-based FVT setup

Two tests were conducted using the electrodynamic shaker FVTs: the random excitation test to obtain the frequency response functions (FRFs) and the shaker shut down test to obtain the free decay response of the building. Both tests were conducted in the x- and y-directions as shown in Fig.4.4. FRF averaging was conducted with 100 blocks, 75% overlap Hanning windowing. The complex mode indicator function (CMIF) was computed with the singular values of the estimated FRFs to guide the choice of peaks. From the selected peaks the modal extraction using polynomial function fitting was then conducted. The example FRF curves from the top floor response of the building in the two directions are shown in
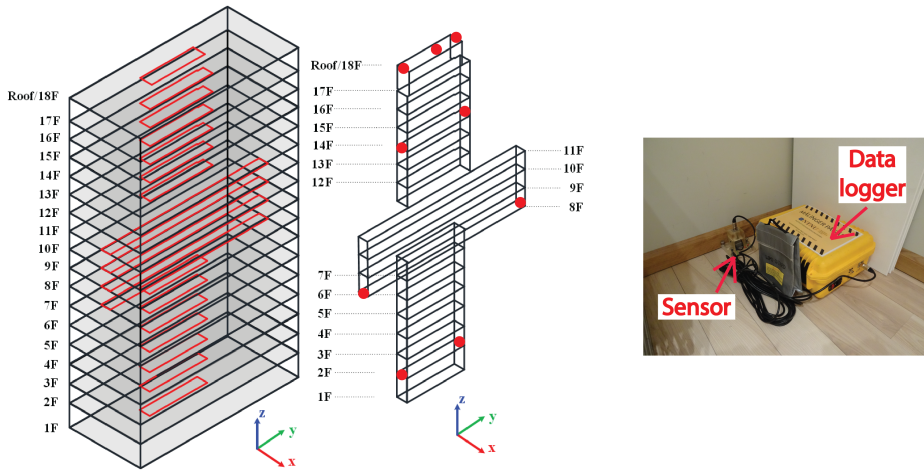
Figure 4.4: Accelerometers placement in the building

Fig.4.5(a).

Curve fitting of the free decay response from the shaker shut down test was conducted using the exponential sinusoidal decay function to obtain the modal properties. An example of free decay response and the corresponding curve fitting is shown in Fig.4.5(b). Additionally, a cycle-by-cycle fitting of the free decay response was conducted to investigate the amplitude-dependent behaviour of modal properties.
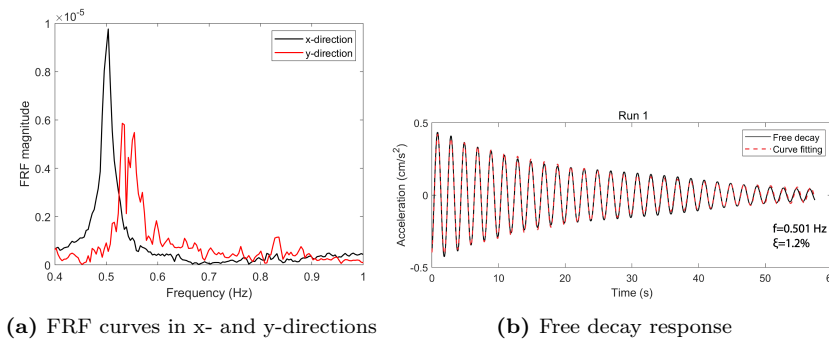
**(a)** FRF curves in x- and y-directions

(b) Free decay response

Figure 4.5: Sample results from the electrodynamic shaker-based FVTs

Human-induced excitation tests

Human-induced excitation tests were conducted to obtain the free decay response of the building. The tests were conducted in both x- and y-direction using the synchronised swaying of 4 people at the first two fundamental frequencies of the building as shown in Fig.4.6(a). The synchronised swaying of only 4 people was able to achieve levels of acceleration comparable to the electrodynamic shaker-based FVTs indicating that the human-induced excitation tests can be a cheap and easy alternative to the traditional FVTs requiring large equipment. Sample free decay response and the corresponding curve fitting are shown in Fig.4.6(b).

(a) Test setup with 4 people
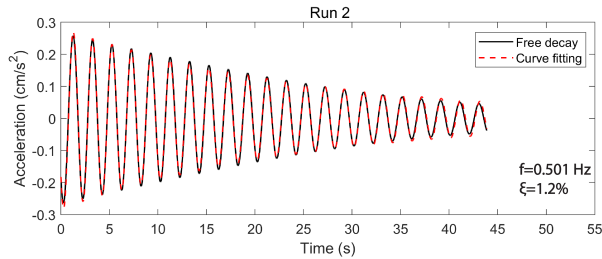
(b) Sample free decay response

Figure 4.6: Human-induced excitation tests

4.2   Numerical methods

Finite element modelling and analysis of the buildings was conducted in Abaqus CAE [66]. The modelling of the buildings was conducted based on the best engineering judgement. The actual mass and stiffness properties of the prefabricated timber elements were used and relevant linear material models were applied. The live loads in the buildings were calculated manually based on the site visits to replicate the as-built mass properties. The stiffness of connections and non-structural

elements were included in the model as well through several modelling approaches.

The analysis of the finite element model included the modal analysis to obtain the natural frequencies and mode shapes of the buildings. Additionally, the steady-state modal analysis was conducted to obtain the frequency response functions (FRFs), when the comparison with the experimental FRFs was performed. Steady-state modal analysis is the linear dynamic analysis using modal superposition.

The FE model updating and sensitivity analysis were conducted using the ISight tool [67], which can be integrated with the Abaqus CAE.

5. Summary of the included papers

The work presented in this thesis is a collection of scientific papers which have been published or submitted to international journals or conferences. The summary and main findings of each paper are presented below.

5.1 Paper I

Tulebekova, S., Malo, K.A., and Rønnquist, A. (2023). *Dynamic identification and model calibration of connection stiffness in multi-storey cross-laminated timber buildings.* Journal of Building Engineering 72(2023) 106607. https://doi.org/10.1016/j.jobe.2023.106607.

Paper I presents the dynamic identification of multi-storey CLT buildings and the corresponding finite element model updating. First, full-scale ambient vibration measurements were conducted on a total of 7 multi-storey CLT buildings ranging from 9- to 13-storeys. The stochastic subspace identification technique was used to identify the modal properties of the buildings. Second, two finite element modelling approaches for modelling connections in multi-storey CLT buildings under service-level ambient vibrations were proposed. In the first modelling approach, which is also called a "detailed" approach, the stiffness of connections between the CLT panels was modelled as a set of discrete connectors with specified stiffness properties. In the second approach, which is called a "simplified" approach, the stiffness of connections between the CLT panels was modelled with generalised 2D shell elements, which stiffness properties are directly dependent on the connected main elements through the reduction factors. To validate the proposed modelling approaches, the finite element model updating was conducted based on the experimental modal properties. A close match was achieved for both modelling approaches, indicating that the "simplified" modelling approach can be applied for modelling multi-storey CLT buildings under service-level loading. Suggestions were given regarding the prescribed stiffness values for each modelling approach.

5.2   Paper II

Paper II presents the finite element modelling approach for connections in tall glulam frame buildings under service-level vibrations. In real life, the connections between the glulam frame members consist of a combination of dowels and slotted-in steel plates. The stiffness of such connections in buildings is subject to uncertainty since it is difficult to accurately quantify their value. To this end, the modelling of connections using "connection-zones" was introduced in this paper. The "connection-zones" are beam and shell elements with generalised linear section behaviour, whose geometry properties are directly dependent on the connected main elements. By assuming that the axial and rotational stiffnesses are linearly dependent on the cross-sectional area and the second moment of inertia respectively, the reduction factors to the geometrical properties of the "connection-zones" can be introduced. Additionally, "connection-zones" were introduced at the ends of non-structural elements (partitions and external walls) to evaluate the stiffness contribution from non-structural elements to the global structure response. The length of the "connection-zone" element is equal to either the height of the connected beam element or the thickness of the connected non-structural element.

To validate the proposed finite element model, the ambient vibration measurements of an 18-story glue-laminated timber frame building Mjøstårnet were conducted. Based on sensitivity analysis of the "connection-zones" the axial stiffness of the glulam diagonals was shown to be the governing parameter, while the rotational stiffness of the beams did not have a considerable impact on the modal response of the timber building. Model updating of the finite element model on the experimental modal properties (natural frequencies and mode shapes) indicated a semi-rigid behaviour with partial contributions from both axial diagonal stiffness and rotational beam stiffness. The partial contribution of non-structural elements stiffness was observed as well.

5.3   Paper III

Tulebekova, S., Ao, W.K., Pavic, A., Malo, K.A., and Rønnquist, A. (2023). *Identification of modal properties of a tall glue-laminated timber frame building under long-term ambient vibrations and forced vibrations.* Submitted for publication to a peer-reviewed journal.

In Paper III, the modal identification in a tall glulam frame building Mjøstårnet using long-term ambient vibrations and forced vibrations is presented. Firstly, a combined operational modal analysis scheme for the modal identification of acceleration data from long-term ambient vibration tests (AVTs) was introduced. In this scheme, the two modal identification techniques, Stochastic Subspace Identification (SSI) and Random Decrement Technique (RDT) were combined with the variational mode decomposition (VMD) technique to decompose non-stationary signals into underlying oscillatory components. Secondly, the forced vibration tests (FVTs) using measured electrodynamic shakers excitation and unmeasured human excitation were conducted. In the first part of the FVTs, two electrodynamic shakers with 1-tonne reaction mass were used to conduct random excitation tests to obtain the frequency response functions (FRFs) and shaker shut down tests to obtain the free decay response of the building. In the second part of the FVTs, the human-induced excitations were conducted using the synchronised movement of 4 people to obtain free decay response of the building. Successful implementation of the human-induced vibrations with few people indicates that these tests can be an efficient alternative to the traditional shaker-based tests.

Good agreement between the natural frequencies obtained from the long-term ambient vibration measurements and the forced vibration measurements was observed. The amplitude-dependent behaviour of the damping ratios was observed in both AVTs and FVTs, with a larger variation in the FVT-based results (0.5%-2.0% for the first mode and 0.5%-3.0% for the second mode). Moreover, the two-stage model updating of a linear FE model based on FRF curve measurements was conducted and a good match of frequencies and damping ratios was achieved.

5.4   Paper IV

Tulebekova, S., Malo, K.A., Rønnquist A., Nåvik, P. (2023). *Investigation of long-term modal properties of a tall glue-laminated timber frame building under environmental variations.* Accepted to the World Conference on Timber Engineering (WCTE2023), Oslo, Norway.

Paper IV investigates the long-term modal properties of an 18-storey glulam frame building Mjøstårnet under environmental variations. The combined operational modal analysis scheme based on the variational mode decomposition (VMD) and Stochastic Subspace Identification (SSI) was used for modal identification. A total of 18 months of full-scale ambient vibration measurements were recorded and analyzed with the proposed combined scheme. The corresponding mean outdoor temperature and relative humidity data were obtained from the nearby weather station and co-plotted with the identified natural frequencies and damping ratios. Based on observation, the seasonal behaviour of natural frequencies was observed with an average variation of ± 0.02 Hz. Damping ratios did not exhibit seasonal variations as opposed to natural frequencies and had relatively stable values. From co-plotted figures, the natural frequencies had an inverse relationship with the mean temperature, indicating the high delay of response to temperature variation (6 months). On the other hand, a positive relationship between the natural frequency and mean relative humidity was observed, where natural frequencies increased with an increase of the relative humidity with a delay of approximately 1-2 months.

6. Conclusions and future work

6.1 Concluding remarks

Based on the results of the research the following conclusions were made to answer the objectives of the thesis:

- **Acquire full-scale measurement data from tall timber buildings**

  An extensive measurement campaign was conducted on multiple timber buildings. All of the buildings were in fully operational condition and were fully occupied. This testing condition was desirable since it represented the actually designed conditions, which could not be captured if the measurements were conducted in an empty building. On the other hand, these testing conditions posed some challenges, such as limited space available for placement of the accelerometers and equipment, rigorous planning and constant communication with the building manager, and flexibility to modify the testing conditions in unforeseeable events. Nevertheless, the testing campaigns were conducted successfully and good-quality measurement data was obtained.

  Seven multi-storey CLT buildings were instrumented with ambient vibrations measurements equipment to obtain modal properties. The buildings were located in two different cities: Trondheim and Tromsø. The same ambient vibration measurement setup was used on all buildings: a set of four accelerometers, cables and a data acquisition box. The measurements were conducted at several elevation points and two accelerometers were placed at the top level to capture any in-plane movement. For each building, a minimum of 10-h measurements were recorded and the modal properties were successfully extracted.

  A long-term ambient vibration measurement campaign was conducted on an 18-storey glulam frame building. Three accelerometers were placed at different elevations inside the evacuation staircase shaft, which was the only

available place for the instrumentation. The acceleration measurement data were continuously acquired and modal properties were successfully obtained.

A unique forced vibration testing campaign was conducted on an 18-storey glulam frame building Mjøstårnet. The FRF-based tests were conducted and good-quality FRFs were obtained, which demonstrates the feasibility of the exercise. Additionally, the free vibration tests were conducted using an elec-trodynamic shaker and human-induced excitation. The synchronised swaying of only four people was able to achieve acceleration levels, comparable to the electrodynamic shaker-based tests, which indicates that human-induced ex-citation tests are an efficient alternative to the traditional shaker-based tests.

- **Quantify natural frequency and damping of in-service tall timber buildings**

  Modal properties were obtained from ambient vibration measurements using output-only techniques.

  For the 5 identical CLT buildings, the natural frequencies were within the 2% variation range, which indicates the repeatability of the measurements. The natural frequencies for the two CLT buildings in Tromsø were quite stable. The identified damping ratios for the seven CLT buildings were in the 1%-2% range.

  The combined technique was used to process the long-term ambient vibration data from Mjøstårnet. The SSI and RDT techniques were combined with the VMD technique to overcome the non-stationarity of the data. The identified modal properties from the combined technique were quite stable. Based on the comparison of the results from the long-term AVTs and FVTs, the natural frequencies were quite similar, demonstrating that AVTs can be used for accurate estimation of natural frequencies. The damping ratios from the free vibration tests exhibited amplitude-dependent behaviour, where damping ratios varied in the range between 0.5%-3%. This finding has implications for the serviceability design of tall timber buildings, where damping ratios play an important role.

  A study on the impact of environmental variations on the modal properties of the Mjøstårnet was conducted. The study showed that damping ratios are not affected by changes in outdoor temperature and relative humidity. An inverse relationship between the identified natural frequencies and mean outdoor temperature was observed, which indicates a high delay (approx.6

months) between the variation of temperature and the corresponding variation of the natural frequencies. A positive trend between the natural frequencies and the mean outdoor relative humidity was observed, where natural frequencies increased with an increase of the relative humidity with a short delay (approx.1-2 months).

- **Develop and validate the representative finite element models of tall timber buildings**

  Finite element models for the instrumented tall timber buildings were developed. A focus of the FE modelling was on the aspects with high uncertainty based on the previous studies: the stiffness of connections and the impact of non-structural elements. Additionally, the live load was manually calculated instead of using the Eurocode-prescribed values, which were overestimating the actual live load in the building.

  Two approaches for modelling CLT buildings were presented: the "detailed" approach and the "simplified" approach. In the "detailed" approach, the connections between the CLT panels were modelled with discrete connectors with specified stiffness properties. Additionally, the building geometry was modelled as detailed as possible: openings and secondary structural elements were placed at their exact locations. In the "simplified" approach, the connections between the CLT panels were modelled with 2D shell elements with material properties of the CLT material and varying thickness, which is directly related to the thickness of the connected panel through the reduction factor. Additionally, the building geometry was generalised: a similar layout and openings were used for all levels.

  The glulam frame building Mjøstårnet was modelled with "connection-zone" elements, which represented the stiffness of connections and non-structural elements. "Connection-zones" are generalised elements with geometrical properties directly related to the connected main elements through the reduction factors. This generalised approach allows for an efficient analysis of stiffness contribution from the connections between the glulam elements without manually assigning stiffness to each connection.

- **Validate the predicted response with experimental measurements**
  The model updating was conducted on the FE models to validate the predicted response based on the experimental results.

  The model updating of the two FE modelling approaches of the CLT build-

ings resulted in a close match of natural frequencies and mode shapes. The recommended stiffness values for both modelling approaches were given. This indicated that the "simplified" approach can give accurate results and can be a good alternative to the "detailed" modelling approach for developing the prediction models of the CLT buildings under service level loading.

The results of the model updating of the FE model of the glulam frame building showed that the stiffness of connections has a significant impact on the dynamic response of the building under service-level loading. In particular, the axial stiffness of diagonals was the governing parameter, while the rotational stiffness of the beams played a minor role in comparison. A semi-rigid behaviour of connections was observed based on the results of the model updating. The stiffness of non-structural elements, such as external walls and internal partitions, had a partial contribution to the global modal response.

The conducted extensive experimental campaign contributes to the existing database of the modal properties of tall timber buildings. Moreover, the findings of the research significantly expand the limited knowledge of the damping properties of tall timber buildings. The proposed finite element modelling approaches serve as a useful guideline for practising engineers in the development of their prediction models of tall timber building dynamic response under service loads.

6.2   Suggestions for future work

Future work on the dynamic identification and modelling of tall timber buildings includes, but is not limited to, the following:

- Conducting forced vibration measurements using mechanical shakers or human-induced excitations on a larger number of glulam frame buildings to investigate the amplitude-dependent damping and extend the existing database of the damping ratios in tall timber buildings.

- Instrument tall timber buildings with the anemometers together with the ambient vibration measurement setup to evaluate the response of the building based on the wind direction.

- Investigate the possible approaches for incorporating amplitude-dependent damping into the FE models of tall timber buildings.

- Conduct laboratory tests on stiffness and damping properties of connections and incorporate the results into the global timber building models to evaluate the modal response.

- Instrument the buildings with the indoor and outdoor climate sensors together with the accelerometers to further investigate the impact of environmental variations on the modal properties of tall timber buildings.

Bibliography

[1] J. Skullestad, R. Bohne, J. Lohne, High-rise timber buildings as a climate change mitigation measure - a comparative LCA of structural system alternatives, Energy Procedia 96 (2016) 112–123.

[2] K. Malo, R. Abrahamsen, M. Bjertnæs, Some structural design issues of the 14-storey timber framed building Treet in Norway, Eur.J.Wood.Prod. 74 (2016) 407–424.

[3] Council on Tall Buildings and Urban Habitat, Tallest all-timber building in the world, `https://www.ctbuh.org/buildings-of-distinction/mjostarnet` (2019).

[4] Council on Tall Buildings and Urban Habitat, High-rise in Milwaukee takes title of world's tallest mass timber hybrid, `https://www.skyscrapercenter.com/building/ascent/34292` (2022).

[5] Council on Tall Buildings and Urban Habitat, Tallest mass timber buildings, `https://www.ctbuh.org/mass-timber-buildings` (2022).

[6] B. Ellingwood, Probability-based LRFD for engineered wood construction, Structural Safety 19 (1997) 53–65.

[7] B. K. Fryer, Wind dynamics of the next generation of tall timber builidngs, Ph.D. thesis, University of Cambridge (2021).

[8] I. Smith, A. Frangi, Overview of design issues for tall timber buildings, Structural Engineering International 2 (2008) 141–147.

[9] K. Kwok, P. Hitchcock, M. Burton, Perception of vibration and occupant comfort in wind-excited tall buildings, Journal of Wind Engineering and Industrial Aerodynamics 97 (2009) 368–380.

[10] M. Burton, K. Kwok, A. Abdelrazaq, Wind-induced motion of tall buildings: designing for occupant comfort, International Journal of High-Rise Buildings 4 (2015) 1–8.

[11] International Organization for Standardization, ISO 10137: Bases for design of structures — Serviceability of buildings and walkways against vibrations, Switzerland (2007).

[12] European Committee for Standardization, Brussels, Belgium, CEN1991-1-4: Eurocode 1: Actions on structures. Part 1-4: Wind actions (2002).

[13] P. Landel, M. Johansson, A. Linderholt, Comparative study of wind-induced accelerations in tall timber buildings according to four methods, in: World Conference on Timber Engineering WCTE 20021, Santiago, Chile, 2021.

[14] S. Tesfamariam, Performance-based design of tall timber buildings under earthquake and wind multi-hazard loads: past, present, and future, Frontiers in Built Environment 8 (2022).

[15] European Committee for Standardization, Brussels, Belgium, CEN1991-1-1: Eurocode 1: Actions on structures. Part 1-1: General actions (2002).

[16] R. Hearmon, The elastic constants of anisotropic materials, Reviews of Modern Physics 18 (1946) 409–440.

[17] F. Kollmann, W. Côté, Principles of Wood Science and Technology I: Solid Wood, Springer-Verlag, New York, US, 1968.

[18] J. Dinwoodie, Timber: Its nature and behaviour, EFN SPON, London,UK, 2000.

[19] R. Foster, T. Reynolds, M. Ramage, Proposal for defining a tall timber building, Journal of Structural Engineering 142 (2016).

[20] V. Bolvardi, S. Pei, J. van de Lindt, J. Dolan, Direct displacement design of tall cross-laminated timber platform buildings with inter-story isolation, Engineering Structures 167 (2018) 740–749.

[21] A. Vilguts, H. Stamatopoulos, K. Malo, Parametric analyses and feasibility study of moment-resisting frames under service loads, Engineering Structures 228 (2021).

[22] X. Zhang, L. Xuan, W. Huang, L. Yuan, Li.P., Structural design and analysis for a timber-concrete hybrid building, Frontiers in Materials 9 (2022).

[23] European Committee for Standardization, Brussels, Belgium, EN 1995-1-1:2004: Design of timber structures - Part 1-1: General- Common rules and rules for buildings (2004).

[24] X. Zhang, Y. Pan, T. Tannert, The influence of connection stiffness on the dynamic properties and seismic performance of tall cross-laminated timber buildings, Engineering Structures 238 (2021).

[25] B. Kurent, B. Brank, W. Ao, Mode updating of seven-storey cross-laminated timber building designed on frequency-response-functions-based modal testing, Structure and Infrastructure Engineering (2021).

[26] L. Ljung, System Identification: Theory for the User, Prentice Hall, NJ, USA, 1999.

[27] C. De Silva, Vibration and Shock Handbook, Taylor and Francis, FL, USA, 2005.

[28] E. Reynders, System identification methods for (operational modal analysis): Review and comparison, Archives of Computational Methods in Engineering 19 (2012).

[29] C. Rainieri, Operational modal analysis for seismic protection of structures, Ph.D. thesis, University of Naples 'Federico II' (2008).

[30] J. Cara, Computing the modal mass from the state space model in combined experimental-operational modal analysis, Journal of Sound and Vibration 370 (2016).

[31] R. Isermann, M. Münchhof, Identification of Dynamic Systems: An Introduction with Applications, Springer, Heidelberg, Germany, 2011.

[32] T. Söderström, P. Stoica, System Identification, Prentice Hall, UK, 1989.

[33] R. Brincker, C. Ventura, Introduction to Operational Modal Analysis, Wiley, 2015.

[34] L. Ljung, System identification and simple process models (2003).

[35] T. E. Saaed, Structural control and identification of civil engineering structures, Ph.D. thesis, Lulea University of Technology (2015).

[36] I. Araujo, J. Laier, Operational modal analysis using SVD of power spectral density transmissibility matrices, Mechanical Systems and Signal Processing 46 (2014) 129–145.

[37] P. Welch, The use of fast fourier transform for the estimation of power spectra: a method based on time averaging over short, modified periodograms, IEEE Transactions on Audio and Electroacoustics 15 (1967) 70–73.

[38] D. Ewins, Model testing: Theory and Practice, Wiley, 1984.

[39] C. Shih, Y. Tsuei, R. Allemang, D. Brown, Complex mode indication function and its applications to spatial domain parameter estimation, Mechanical Systems and Signal Processing 2 (1988) 367–377.

[40] W. Ren, Z. Zong, Output-only modal identification of civil engineering structures, Structural Engineering and Mechanics 17 (2004).

[41] R. Brincker, P. Andersen, Understanding stochastic subspace identification, in: Proceedings of the 24th IMAC, St.Louis, MO, USA, 2021.

[42] P. Van Overschee, B. De Moor, Subspace Identification for Linear Systems: Theory, Implementation, Applications, Kluwer Academic Publishers, Leuven, Belgium, 1996.

[43] M. Pastor, M. Binda, T. Harcarik, Modal assurance criterion, Procedia Engineering 48 (2012) 543–548.

[44] D. P. Pasca, Ambient vibration testing of civil engineering structures: development of a python module and applications to case studies, Ph.D. thesis, Norwegian University of Life Sciences (2008).

[45] C. Rainieri, G. Fabbrocino, Operational Modal Analysis of Civil Engineering Structures: An Introduction and Guide for Applications, Springer, New York, USA, 2014.

[46] H. Cole, On-line failure detection and damping measurement of aerospace structures by random decrement signatures, NASA, VA (1973).

[47] J. Vandiver, C. R. Dunwoody, A.B., M. Cook, A mathematical basis for the random decrement vibration signature analysis technique, Journal of Mechanical Design 104 (1982) 307–313.

[48] Y. Tamura, L. Zhang, A. Yoshida, S. Nakata, T. Itoh, Ambient vibration tests and modal identification of structures by FDD and 2DOF-RD Technique, in: Structural Engineers World Congress (SEWC2002), Yokohama, Japan, 2002.

[49] P. Gorski, Identification of dynamic characteristics of tall industrial chimney based on GPS measurements using Random Decrement Method, Engineering Structures 83 (2015).

[50] K. Dragomiretskiy, D. Zosso, Variational mode decomposition, IEEE Transactions on signal processing 62 (2014).

[51] J. Mottershead, Model updating in structural dynamics: a survey, Journal of Sound and Vibration 167 (1993) 347–375.

[52] A. Chopra, Dynamics of Structures: Theory and Applications to Earthquake Engineering, 5th Edition, Pearson, United Kingdom, 2020.

[53] T. Kijewski-Correa, D. Pirnia, Dynamic behavior of tall buildings under wind: Insights from full-scale monitoring, The Structural Design of Tall and Special Buildings 16 (2007) 471–486.

[54] N. Labonnote, Damping in timber structures, Ph.D. thesis, NTNU (2012).

[55] B. A. V. J. Reynolds, T., W. Chang, R. Harris, J. Bawcombe, J. Bregulla, Ambient vibration testing and modal analysis of multi-storey cross-laminated timber buildings, in: World Conference on Timber Engineering (WCTE) 2014, Quebec, Canada, 2014.

[56] T. Reynolds, R. Harris, W. Chang, J. Bregulla, J. Bawcombe, Ambient vibration tests of a cross-laminated timber building, Construction Materials 168 (2015).

[57] T. Reynolds, D. Casagrande, R. Tomasi, Comparison of multi-story cross-laminated timber and timber frame buildings by in situ modal analysis, Construction and Building Materials 102 (2016) 1009–1017.

[58] A. Aloisio, D. Pasca, R. Tomasi, M. Fragiacomo, Dynamic identification and model updating of an eight-story CLT building, Eng.Struct. 213 (2020).

[59] I. Mugabo, A. Barbosa, M. Riggio, Dynamic characterization and vibration analysis of a four-story mass timber building, Frontiers in Built Environment 5 (2019).

[60] I. Edskär, Modal analysis, dynamic properties and horizontal stabilisation of timber buildings, Ph.D. thesis, Luleå University of Technology (2019).

[61] P. Landel, Wind-induced vibrations in tall timber buildings. design standards, experimental and numerical modal analyses, Ph.D. thesis, Linnaeus University (2022).

[62] B. Ellis, A. Bougard, Dynamic testing and stiffness evaluation of a six-storey timber framed building during construction, Engineering Structures 23 (2001) 1232–1242.

[63] R. Steiger, G. Feltrin, F. Weber, S. Nerbano, M. Motavalli, Experimental modal analysis of a multi-storey light-frame timber building, Bulletin of Earthquake Engineering 15 (2017) 3265–3291.

[64] W. Ao, A. Pavic, B. Kurent, F. Perez, Novel FRF-based fast modal testing of multi-storey CLT building in operation using wirelessly synchronised data loggers, Journal of Sound and Vibration 548 (2023).

[65] The MathWorks, Inc., Matlab and statistics toolbox release 2022b, `https://www.mathworks.com/products/signal.html` (2022).

[66] Simulia, Abaqus FEA Software (2017).

[67] DassaultSystemes, Isight. automated design exploration and optimization, `https://www.3ds.com/fileadmin/PRODUCTS-SERVICES/SIMULIA` (2014).

Appended Papers

Paper I

Full length article

Dynamic identification and model calibration of connection stiffness in multi-storey cross-laminated timber buildings

Saule Tulebekova *, Kjell Arne Malo, Anders Rønnquist

Department of Structural Engineering, Norwegian University of Science and Technology (NTNU), Richard Birkelands vei 1A, 7491, Trondheim, Norway

ABSTRACT

This study presents the dynamic identification of cross-laminated timber (CLT) residential buildings and the corresponding finite element model calibration of connection stiffness in CLT buildings. A total of 7 CLT buildings, ranging from 9-storeys to 13-storeys, were instrumented with accelerometers and their dynamic properties (natural frequencies, mode shapes, and damping ratios) were identified. For CLT buildings the resistance to lateral loads is concentrated at the connections (screws, angles, brackets, etc.); thus, understanding the stiffness properties of these connections is important. Therefore, the two modeling approaches for connection stiffness in multi-storey cross-laminated timber buildings were studied: the discrete connector approach and the distributed stiffness approach. Connection stiffness properties in the two models were then calibrated against the identified dynamic properties from ambient vibrations, and a close match to experimental results was achieved. Based on this study the recommended values for connection stiffness parameters using both modeling approaches were proposed for developing prediction models of multi-storey CLT buildings under serviceability level response.

1. Introduction

The use of timber as a structural material has been growing steadily in the field of residential construction [1]. In particular, cross-laminated timber (CLT) has been one of the fast-growing structural systems [2]. Most of the completed multi-storey CLT buildings are constructed in the low-seismic regions [3]. While CLT buildings have sufficient capacity to resist vertical and horizontal loads, there is an issue of wind-induced vibrations which can cause excessive accelerations leading to discomfort for occupants [4–7]. The amount of acceleration in the building is governed by mass, stiffness, and damping properties intrinsic to the structure, however, the values and distributions of the last two in CLT buildings are still not well known [6,8]. In service-level vibrations, the proper identification of dynamic properties, such as frequencies, mode shapes, and damping ratios, is an important first step for assessing building response. However, the amount of research on ambient level dynamics of CLT buildings is still significantly smaller compared to the research on response under seismic loading [9–13].

Since the introduction of CLT as an engineering material in the early 1990s, it has spread over Europe and started gaining popularity in other parts of the world, such as the UK and North America [14]. The most common type of construction of CLT buildings is called platform-type construction. Multi-storey CLT buildings with a platform-type of construction in the 6–12 storey range can be found across Europe and in North America [9,11,12,14]. In platform type of construction, the walls, floor and roof assemblies are usually made with CLT panels. Fig. 1(a) illustrates the platform-type construction: where the CLT panels are 'stacked'

(a) Platform-type system
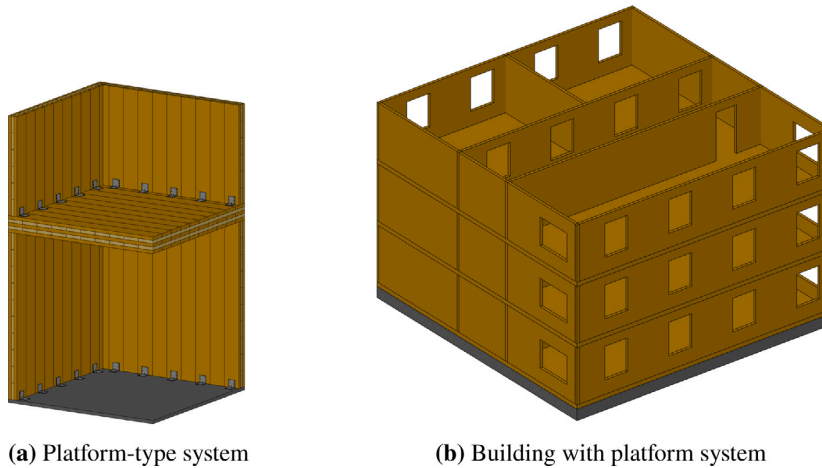
(b) Building with platform system

Fig. 1. CLT platform-type system and its application in the multi-storey building.

on top of each other and connected to each other with steel brackets and screws. Fig. 1(b) shows an example multi-storey platform-type CLT building with openings for doors and windows. In the platform-type CLT building, CLT panels are the main load-carrying structural elements. In order to resist lateral loading, the hold-down brackets are utilized at the outer walls of the building to resist the lateral loading. The CLT panels are pre-fabricated and are brought to the construction site in the ready form.

The fundamental importance of connections in the dynamic properties of CLT buildings has been shown in the previous studies, however, there is still limited knowledge of their behavior in the buildings [7,13,15,16]. In the building the prefabricated CLT panels are used for floors, walls, and roofing. These CLT panels exhibit stiff plate behavior and most of the deformations due to lateral loading take place in connections. Previous studies at both component and building levels showed that connections have a lower capacity compared to the CLT members themselves [12,17,18]. CLT connections are usually made of a combination of steel brackets and angles, and various types of screws and nails. These steel connections resist loading in both axial and shear directions, and therefore it is important to investigate both [19]. The number of these steel elements can be quite large and for example, the number of screws in a CLT building can reach hundreds of thousands. A large amount of these connecting elements makes it challenging to develop accurate prediction models for their behavior. When developing prediction finite element (FE) models, it is common to neglect the effect of connections between the CLT panels and assume either rigid or pinned connection under low-level vibrations [11–13]. Connections in CLT panels are, however, extensively analyzed under seismic loading [17,20,21]. The common approach to model CLT connections under seismic/collapse loading is by using discrete connector elements with specified stiffness properties [22–25]. Alternatively, the 2D models representing the connections between the CLT panels have been applied for seismic analysis [26,27].

Within this context, the main objectives of this paper are: (i) to identify modal properties of multi-storey CLT buildings using ambient vibration measurements due to wind loading and provide statistical estimates of the natural frequencies and modal damping values (Buildings set I & II); (ii) to present two different approaches to modeling connections in CLT buildings under ambient vibrations, validate their results by conducting model calibrating to the experimental modal parameters, and estimate the common values for connection stiffness parameters for modeling of CLT buildings (Buildings set II).

2. Building set I: 9-storey CLT buildings in Trondheim

2.1. Buildings description

Five nominally identical CLT buildings were constructed as part of Moholt student village in Trondheim, Norway (Fig. 2). The buildings are 9-storeys tall with Y-shape floor plan, where the first storey is made of reinforced concrete and the top 8 storeys are made entirely of CLT panels. The basement floor of the building is made of reinforced concrete as well. The buildings were built with platform construction, where walls are interrupted at each level. The total height of each building is 27.7 m and the total area of each floor is 403 m². The buildings serve as student housing and all floors have a typical plan view with 15 student rooms and a common area in the middle as shown in Fig. 5. The timber floors are loaded in perpendicular to grain direction and are made of 140-mm CLT panels, which are covered with 40-mm concrete screed and 30-mm insulation. The concrete screed is not designed as part of load carrying system and is assumed to act as an added mass on the CLT floor panels. An example of a detailed floor/wall composition description can be found in Appendix A. The timber walls, which act as shear walls, are made of five different types of CLT panels with thickness varying from 80-mm (3 layers) to 160-mm (5 layers). Additionally, a few glue-laminated timber beams (glulam) were used in the common area to maximize the space. The glulam beams of strength grade GL30c (30 MPa bending

Fig. 2. Building layout at Moholt Student Village (right) and the view of Building 1 (left).

Table 1
Material properties for CLT [30].

ρ [kg/m3]	E_1 [MPa]	E_2 [MPa]	E_3 [MPa]	G_{12} [MPa]	G_{13} [MPa]	G_{23} [MPa]
420	11 000	370	370	690	690	50

Table 2
Characteristic strength values for CLT [30].

$f_{m,k}$ [MPa]	$f_{c,0,k}$ [MPa]	$f_{c,90,k}$ [MPa]	$f_{t,0,k}$ [MPa]	$f_{t,90,k}$ [MPa]	$f_{v,k}$ [MPa]
24	21	2.5	14.5	0.12	4

strength) with width of 200 mm and height of 500 mm were used [28]. More detailed information on the layout of CLT wall panels and glulam beams in the building can be found in Appendix B. C24 grade timber boards in accordance with EN 338 [29] were used for manufacturing CLT panels. Tables 1 and 2 show the properties for CLT panels as specified by Stora Enso [30]. Indices 1, 2, and 3 in Table 1 indicated longitudinal (primary) direction, transverse (secondary) direction, and perpendicular to panel (normal) direction respectively. In Table 2 $f_{m,k}$ indicates characteristic bending strength, $f_{c,0,k}$ and $f_{c,90,k}$ indicate compressive strength parallel and perpendicular to grain respectively, $f_{t,0,k}$ and $f_{t,90,k}$ indicate tensile strength parallel and perpendicular to strength respectively, $f_{v,k}$ indicate the characteristic shear strength. Angle steel brackets are used for connection between the CLT floors and walls as shown in Fig. 3. The steel grade of S355 is used in angle brackets, corresponding to 355 MPa yield strength [31]. The average dimensions for steel brackets (one side) are 110 mm in width (W), 70 mm in length (L), and 3 mm in thickness. The screws of 5 mm in diameter and 60 mm in length are used to attach the angle brackets to the CLT panels (Fig. 3(c)). Steel angle brackets are installed with 400 mm spacing.

2.2. Field measurements

A field measurement campaign was conducted on all five buildings from Fig. 2. The ambient vibration testing setup consisted of 4 triaxial accelerometers, a data acquisition center, and connecting cables. Triaxial accelerometers in the setup had high sensitivity (2000 mV/g), a frequency range between 0 Hz and 1000 Hz, and a sampling rate of 400 Hz. At the time of testing, all buildings have been in fully operational condition, therefore certain limitations were imposed on the testing to minimize the obstruction of the occupants' activities.

The staircase shaft was used for each building instrumentation and accelerometers were placed at three different levels: 4th, 7th and 10th (Fig. 4(a)). Two accelerometers were installed at 10th level to detect any in-plane movement. Accelerometers were attached directly to CLT panels using small screws (Fig. 4(b)). For each building, continuous acceleration time series of minimum 12 h were recorded. The recorded data was filtered using an anti-aliasing filter to 20 Hz.

While the accelerometer setups inside the staircase were able to capture fundamental frequencies and damping ratios for all five buildings, the in-plane (plane x-y) mode shapes were more difficult to visualize due to the irregular shape of the buildings. Therefore, in addition to the staircase accelerometer setup, the in-plane acceleration measurements were recorded in the common living area as shown in Fig. 5. This setup was installed solely for the purpose of visualization of the in-plane mode shapes corresponding to the natural frequencies and damping ratios, which were already identified using the staircase shaft setup. As shown in Fig. 5, the accelerometers were installed in the common living area of the 9th floor of the building at the farthest corners to obtain the largest possible response of the building. The acceleration measurements in the common living area required much more preparation and discussions with the building manager due to a significant disruption of the daily activities of the residents. Therefore, the acceleration setup in the common living area was performed in one building only (building 1 from Fig. 2) and the assumption that the other four buildings have similar mode shapes was made.
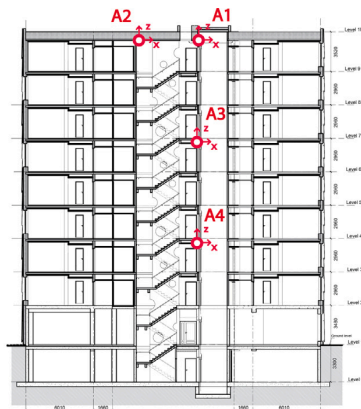
(a) Steel bracket with screws

(b) Steel bracket side view
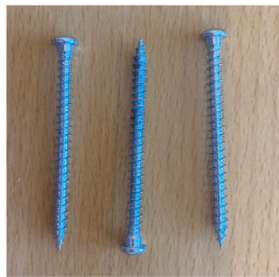
(c) Connecting screws

Fig. 3. Steel angle bracket for CLT panel connection.

(a) Elevation view of accelerometers at Moholt buildings

(b) Accelerometer attachment

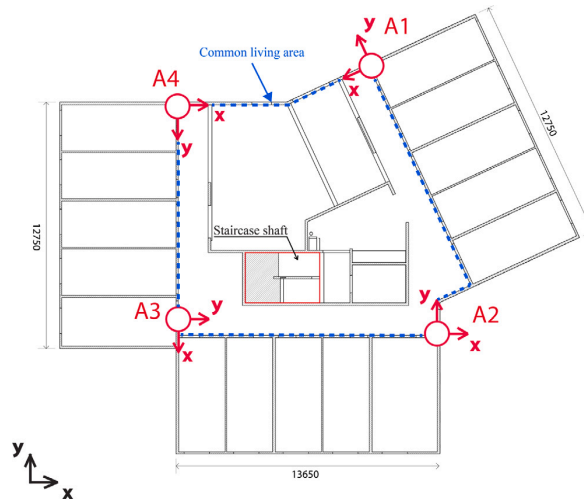**Fig. 4.** Acceleometer layout in Moholt buildings 1-5.

Fig. 5. Plan view of accelerometer setup in the common area (dashed blue line) for mode shapes visualization in Moholt building 1.

2.3. Theoretical background on system identification

Measured data were processed using output-only measurement Stochastic Subspace Identification (SSI) method. SSI is an operational modal analysis (OMA) method used for modal parameters estimation using output-only acceleration measurements [32]. The covariance-based stochastic subspace identification algorithm (Cov-SSI) was used in this study. A brief procedure of the method is presented below, whereas a more extensive description can be found in the literature [33,34].

Discrete-time stochastic state-space model of a dynamic system is written as follows:

$$\{x_{k+1}\} = [A]\{x_k\} + \{w_k\} \tag{1}$$

$$\{y_k\} = [C]\{x_k\} + \{v_k\} \tag{2}$$

where $\{x_k\}$ and $\{y_k\}$ are state vector and measured output vector correspondingly, and $\{w_k\}$ and $\{v_k\}$ are system noise and measurement noise, k is a discrete time step corresponding to a sampling frequency. $\{w_k\}$ and $\{v_k\}$ are assumed as spatially white noise with zero mean. **A** is a state matrix and **C** is an output matrix.

Through eigenvalue decomposition of the system matrices **A** and **C** in the identified state space model, the discrete system poles (λ_i) are obtained, and modal frequencies and damping ratios can be computed as follows:

$$f_i = \frac{|\lambda_i|}{2\pi} \qquad \zeta_i = \frac{-Re(\lambda_i)}{|\lambda_i|} \tag{3}$$

The SSI method requires the order of the model defined since the system order is not known. Thus, the stabilization matrix of the specified order is constructed, which allows for distinguishing the true poles from the spurious poles. The poles containing the physical system arise in the stabilization plot as aligned vertical dots by assigning the tolerance to frequency and damping values.

2.4. Field measurement results

Three stable frequencies were detected from the stabilization diagram for building 1 as shown in Fig. 6. The power spectral densities in both in-plane directions are plotted on top of the stabilization diagram to verify the results. The chosen stabilization criteria were 1% for frequency and 5% for damping values. The frequency values for the first three modes are 2.02 Hz, 2.33 Hz, and 2.57 Hz respectively. Due to the irregularity of the building shape, all modes are a combination of translational and torsional mode. Fig. 7 shows the mode shapes from the in-plane experimental setup (Fig. 5): mode 1 at 2.02 Hz is a translational mode in the y-direction with a small torsional component, mode 2 at 2.33 Hz is a translational mode in the x-direction with a small torsional component, and mode 3 at 2.57 Hz is the combination of torsional and translational modes.

Likewise, measurement data from the remaining four buildings was analyzed and standard deviation values were calculated.

Each building had a minimum of 12 h of measurement data recorded, and the SSI analysis was performed on 1-h increments for each building. Tables 3 and 4 show the summary of the mean fundamental frequencies and damping ratios obtained from measurement data as well as standard deviations. The difference between the identified natural frequencies for the five buildings ranges between 2%–5%. These variations in the identified natural frequencies for the five buildings show slight differences due to inevitable imperfections and variations in design and materials at the time of construction [35,36].
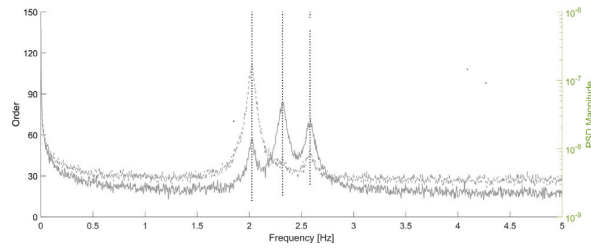
Fig. 6. Stabilization diagram (vertically aligned dots) and power spectral densities in two in-plane directions (curves) for Moholt-1 building.
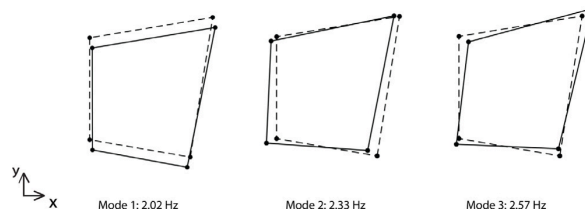

Fig. 7. In-plane mode shapes for the Moholt-1 building.

Table 3
Frequency summary for the Moholt buildings [Hz].

Building no.	f_1 [Hz]	COV_{f1} [%]	f_2 [Hz]	COV_{f2} [%]	f_3 [Hz]	COV_{f2} [%]
1	2.02	0.20	2.33	0.17	2.57	0.35
2	1.98	0.15	2.27	0.18	2.47	0.36
3	1.99	0.15	2.31	0.26	2.50	0.56
4	1.94	0.21	2.23	0.22	2.43	0.33
5	1.96	0.15	2.25	0.22	2.46	0.41
Mean	1.98	1.53	2.27	1.82	2.49	1.91

Table 4
Damping summary for Moholt buildings.

Building no.	ξ_1 [%]	$COV_{\xi1}$ [%]	ξ_2 [%]	$COV_{\xi2}$ [%]	ξ_3 [%]	$COV_{\xi3}$ [%]
1	1.35	8.89	1.54	11.04	1.79	11.17
2	1.52	9.21	1.55	12.26	1.84	14.13
3	1.42	11.27	1.65	15.76	1.86	13.44
4	1.53	11.76	1.72	11.05	1.81	12.15
5	1.37	10.22	1.41	9.93	1.70	12.94
Mean	1.44	5.8	1.57	6.7	1.80	3.08

2.5. Numerical modeling

A linear numerical model was developed and the modal analysis was conducted to compare against the experimental results. Since all of the buildings have modal results which are highly similar, only one numerical model was necessary. The numerical model was developed in Abaqus CAE 2017 [37] and the assembly of the model is shown in Fig. 8. All area elements (CLT panels and reinforced concrete base) were modeled with four-node shell elements with six degrees of freedom at each node (S4R element). The CLT floor panels are connected to each other using the overlap joints and self-tapping screws [38], which assures the rigid in-plane behavior of the floor diaphragms. Composite shell structure was used to model CLT panels with orthotropic material properties as shown in Table 1. The properties in the composite shells are assigned layer by layer, varying from 3 layers to 5 layers, which are perpendicular to the adjacent layer grain direction. Connections between the CLT panels were not taken into account and a rigid connection was assumed. Reinforced concrete floors and walls were modeled as shell elements with linear isotropic material properties. The normal strength reinforced concrete properties were used with an elastic modulus of 34 GPa, Poisson ratio of 0.2, and density of 2500 kg/m^3. The foundation of the building is solid rock, and thus, fixed boundary conditions were assigned to the model.
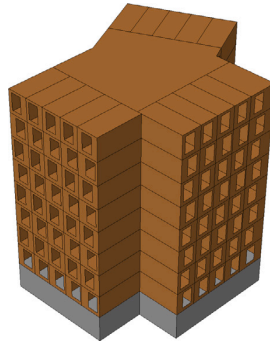
Fig. 8. FE Model Assembly of the Moholt building (gray color indicates reinforced concrete material, brown color indicates CLT material).
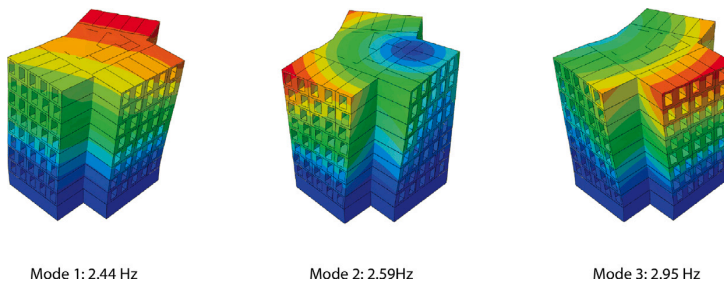

Mode 1: 2.44 Hz   Mode 2: 2.59Hz   Mode 3: 2.95 Hz

Fig. 9. FE model mode shapes of the Moholt building.

Table 5
Comparison between the FE model and experimental results.

Mode no.	Experimental f [Hz]	Numerical f [Hz]	MAC [%]
1	2.02	2.44	0.81
2	2.33	2.59	0.78
3	2.57	2.95	0.83

Structural elements with specified stiffness values are reinforced concrete floors and walls, and CLT floor panels and wall panels with openings. The non-structural mass on each floor of the building was estimated by documenting all relevant elements (e.g. concrete screed, facade, insulation, furniture, technical equipment, etc.). This non-structural mass was applied on each floor of the building as a uniform load of ~230 kg/m^2 smeared over the entire floor area.

A summary of FE natural frequencies and comparison with experimental results is shown in Table 5. As can be seen, the frequency values for the numerical model are higher than the experimental frequencies. The modal assurance criterion (MAC) values [39] are within the range of 80%. Fig. 9 shows the fundamental mode shapes of the building. All mode shapes have significant torsional components, which is similar to experimental mode shapes.

Based on the comparison of the natural frequencies in Table 5, the FE model has higher frequency values compared to the experimental ones. The modal properties of the building depend on the distribution of mass and stiffness in the building [40]. Therefore, the discrepancy between the FE model and the experiments might be caused by uncertainties in mass and/or stiffness properties and their distribution in the FE model. Updating both mass and stiffness properties might result in an undetermined system with infinite solutions [12]. In this study the best engineering judgement was made when estimating the mass properties of the building. On the other hand, the stiffness of the connections between the CLT panels is subject to significant uncertainty. Therefore, the stiffness properties of the connections were selected as uncertain parameters in this study. To further study the effect of uncertainty in the stiffness properties of the connections, the two modeling approaches of connections between the CLT panels were explored in the next section and their impact on the modal properties of the CLT buildings was investigated. The study on connections was conducted on a set of rectangular buildings for the sake of simplicity and to eliminate the effect of complex geometry, which is the case in the Moholt buildings.

Fig. 10. Aerial view of CLT Buildings in Tromsø [41].

3. Building set II: 10- and 13-storey CLT buildings in Tromsø

3.1. Buildings description

Dramsvegen Panorama is a student housing village consisting of multiple CLT buildings of different heights and is located in Tromsø, Norway (Fig. 10). In the current study, the two highest buildings were included in the field measurement campaign. Buildings of interest are shown in Fig. 10 and are 10-storeys and 13-storeys high. The total height of the 10-storey building is 30 m and the in-plane dimensions are 25.7 m by 13.9 m. The lower three floors are made of reinforced concrete, and the higher 7 floors are made of CLT panels. The highest building in Dramsvegen Panorama is 13-storeys tall with the height of the building being 39 m and a floor area of 25.3 m by 13.9 m. The two lowest floors are made of reinforced concrete, while the upper floors are made of CLT panels. The platform construction type was used in both buildings, where walls are interrupted at each floor level. Both 10-storey and 13-storey buildings have similar floor plans and vary only in the number of floors. Fig. 12 shows the typical floor plan in the buildings: 13 student rooms and the common living area in the middle. The timber floors are made of CLT panels with thicknesses varying between 120 mm (3 layers) and 160 mm (5 layers). In the 10-storey building, all CLT floors are made with 150 mm thick panels (5 layers). In the 13-storey building, CLT floors are made with 120 mm thick panels, except for the corridors, where 160 mm panels are used. The CLT wall panel thickness varies from 120 mm (3 layers) to 180 mm (7 layers). The floor composition is similar to the Moholt buildings and is presented in Appendix A. The CLT panels act as shear walls, which are kept in place with hold-down brackets. More detailed information on the layout and thickness of wall CLT panels in the building can be found in Appendix C. Similar to Moholt buildings, the properties of CLT panels were specified by Stora Enso and are listed in Table 1.

3.2. Field measurements

The measurement campaign on buildings in Tromsø was conducted in two stages. In the first stage, the ambient vibration measurement setup was installed on the 10-storey building and was recording measurements continuously for one month. Afterward, the setup was moved to the 13-storey building and was recording measurements for two months. The same experimental setup as the one described in the Moholt buildings testing was used: 4 triaxial accelerometers with a control box and connecting cables. Accelerometers were attached directly to CLT panels by using small screws as shown in Fig. 4(b). Fig. 11 shows the locations of accelerometers in the setup for 13-storey building. The accelerometers were installed at three different levels (13th, 12th, and 7th), to detect the relative floor movements. Two accelerometers were installed at the top floor of the building to detect any in-plane movements (Fig. 12). Similarly, in the 10-storey building accelerometers were installed on the 10th, 9th, and 4th levels.

3.3. Field measurement results

The ambient vibrations measurement data was processed using the same output-only Cov-SSI technique described in the previous section. Fig. 13 shows the stabilization diagram using 6-h long acceleration measurement recordings for 13-storey building with three stable frequencies- 1.30 Hz, 1.63 Hz, and 1.99 Hz. The power spectral densities are plotted on top of the stabilization diagram to verify the obtained frequencies. Based on the power spectral density peaks in Fig. 13 (solid and dashed lines indicate *x* and *y* sensor directions respectively), the first two modes are in orthogonal directions, the third mode has a strong component in the *y*-direction and a small component in the *x*-direction. Using acceleration data from sensors A1 and A2 the in-plane mode shapes were plotted as shown in Fig. 14. The first two modes (1.30 Hz and 1.63 Hz) are translational modes in y- and *x*-direction respectively. The third mode at 1.99 Hz is the torsional mode, but due to the lack of accelerometers, it was not possible to capture the exact shape of the
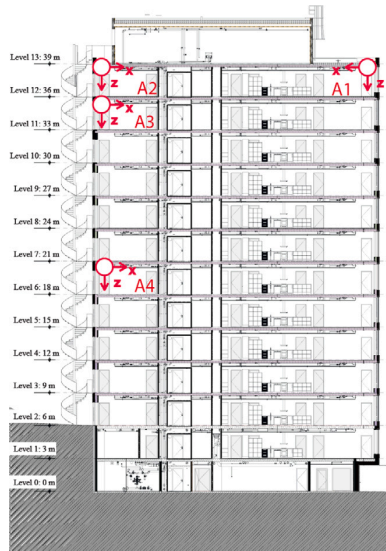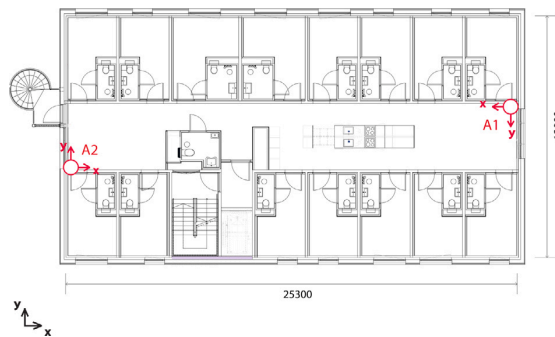
Fig. 11. Elevation view of the 13-storey building.

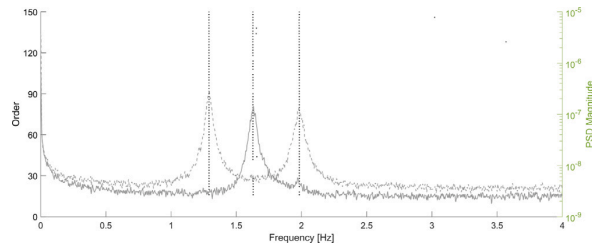**Fig. 12.** Typical floor plan of the 13-storey building.

Fig. 13. Stabilization diagram for the 13-storey building (vertically aligned dots) and power spectral densities in two in-plane directions (curves).

mode. Since 13-storey building and 10-storey building have almost identical in-plane geometry and vary only in the number of floors, resulting mode shapes and stabilization diagrams were quite similar, but frequency values were higher for the 10-storey building. The first two modes in 10-storey building are translational modes at 2.15 Hz and 2.45 Hz in y- and x-directions respectively, and the third mode is the torsional mode at 2.91 Hz.

Tables 6 and 7 show the result summary from processed acceleration measurements using 1-h increments for modal frequency and damping values along with standard deviations.
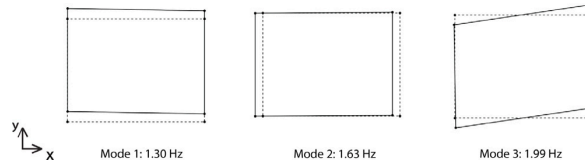
Fig. 14. Mode shapes for the 13-storey building.

Table 6
Frequency summary for the Tromsø buildings [Hz].

Building	f_1	σ_{f1}	f_2	σ_{f2}	f_3	σ_{f3}
13-storey	1.30	0.006	1.63	0.005	1.99	0.009
10-storey	2.15	0.006	2.45	0.010	2.91	0.010

Table 7
Damping summary for Tromsø buildings.

Building	ξ_1 [%]	$\sigma_{\xi1}$	ξ_2 [%]	$\sigma_{\xi2}$	ξ_3 [%]	$\sigma_{\xi3}$
13-storey	1.44	0.003	1.18	0.002	1.33	0.002
10-storey	1.37	0.003	1.57	0.001	1.55	0.002

3.4. Numerical modeling of connections

Two alternative approaches to model connections (e.g. shown in Fig. 3) in CLT buildings are presented:

- Modeling Type I (or "detailed" modeling): the connections between CLT panels are modeled as discrete connector elements with linear material properties (Fig. 15). Additionally, a detailed geometry of the building and actual CLT panel geometry was used in the "detailed" modeling approach. The discrete connector approach has been used extensively in seismic analysis-oriented research since it is convenient for non-linear analysis. However, the discrete connector approach with specified stiffness properties can be quite cumbersome for large building models and very time-consuming for structural engineers. The FE model assembly for modeling type I is shown in Fig. 16(a).
- Modeling Type II (or "simplified" modeling): connections are modeled as "connection-zone" elements- 2D shell elements with linear CLT material properties, but with reduced stiffness (Fig. 15). Additionally, the typical floor plan was used for each floor, as well as typical partitioning of the CLT panel geometry was used in the "simplified" modeling approach. This approach allows for estimating the stiffness contribution from the connections between CLT panels without explicitly modeling those connectors. The "connection-zone" approach has been successfully applied previously for the modeling of glue-laminated timber (glulam) frame buildings [42,43]. The FE model assembly for modeling type I is shown in Fig. 16(b).

In both modeling types, the finite element model of was developed in Abaqus CAE 2017 [37]. CLT panels were modeled with four-node shell elements with multi-layer material properties. For each layer, orthotropic material properties as given in Table 1 were assigned. The modeling of CLT panels, reinforced concrete floors, and foundation was similar to the numerical modeling of the Moholt building. The following paragraphs will on the two modeling approaches for connections between the CLT panels in greater detail.

Modeling type I

In modeling type I, connections between CLT panels are modeled with connector elements. These connector elements act as springs with specified stiffness properties, which are directly related to the stiffness values of connected CLT plates. This approach is more convenient instead of manipulating directly numerical values. Connectors have both axial and shear stiffness properties assigned separately as shown in Fig. 15. Expressions for axial and shear stiffness properties for the entire CLT plate are given in Eqs. (4) and (5) [44]:

$$D_{axial} = E_{0,mean} * h_\parallel \qquad (4)$$

$$D_{shear} = 0.75 * G_{0,mean} * h_{CLT} \qquad (5)$$

where $E_{0,mean}$ is the mean value of the modulus of elasticity timber in CLT, $G_{0,mean}$ is the mean value of the shear modulus for timber in CLT, $h_\parallel$ is the thickness of boards parallel to the grain, and h_{CLT} is the thickness of the CLT panel.

The axial (k_{axial}) and shear (k_{shear}) stiffness of connector elements between the two panels are directly related to the connected CLT panel properties and calculated as follows:

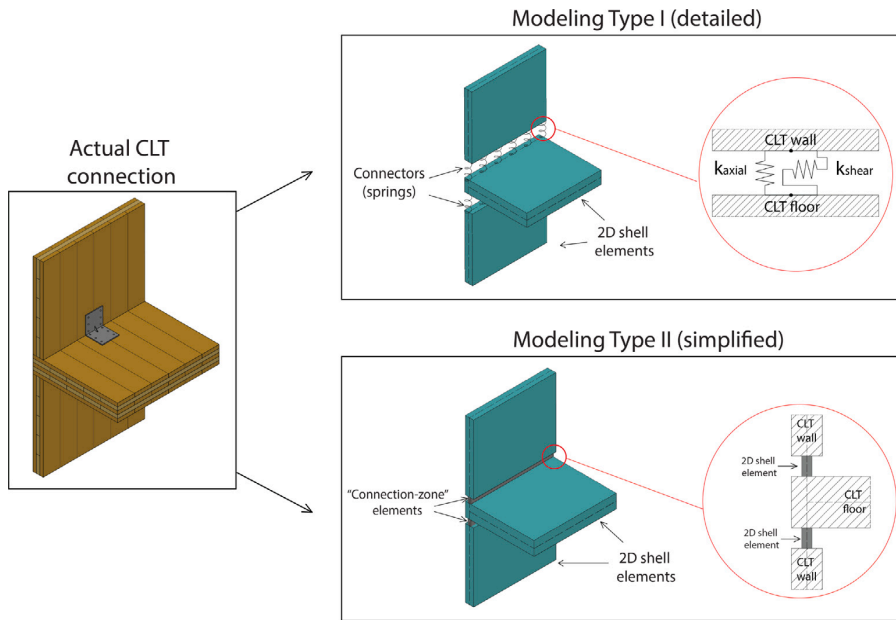$$k_{axial} = ASR * \frac{E_{0,mean} * L_{panel} * h_\parallel}{H_{panel} * n_{conn}} \qquad (6)$$

Fig. 15. CLT connection modeling approaches.

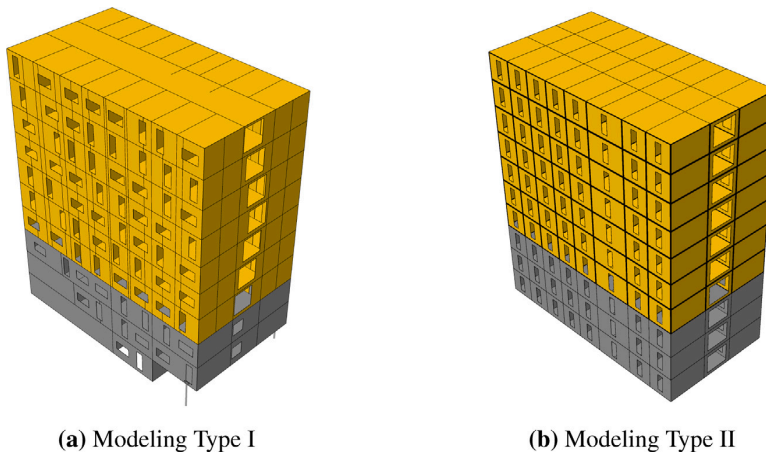**(a)** Modeling Type I   **(b)** Modeling Type II

Fig. 16. FE model assemblies comparison (gray color indicates reinforced concrete material, yellow color indicates CLT material).

$$k_{shear} = SSR * \frac{0.75 * G_{0,mean} * L_{panel} * h_{CLT}}{H_{panel} * n_{conn}} \tag{7}$$

where L_{panel} is the total length of the CLT panel along the joint, h_{CLT} is the total thickness of the panel, $h_{\parallel}$ is the thickness of lamellas parallel to the force, H_{panel} is the total height of the panel; n_{conn} is the number of connector elements between the two panels. The spacing of ≈300 mm was chosen because it is the largest spacing required to avoid stress concentration at the joints. Axial stiffness ratio (ASR) and shear stiffness ratio (SSR) are the axial and shear stiffness ratios of the connector respectively and these scaling ratios are used for further model updating to compare against the experimental results.

The storey height is 3 m, the largest width of the panel in the building is 2.5 m, and connector spacing is 300 mm. Assuming CLT properties from Table 1 and ASR = SSR = 1, the connector stiffness values for CLT sections of various thickness have estimated values as shown in Table 8, where $h_{\parallel}$ and $h_{\perp}$ are the thickness of the layers parallel and perpendicular to the load direction, respectively.

Table 8
Stiffness properties per connector element.

Thickness	$h_{\parallel}$ [mm]	$h_{\perp}$ [mm]	Wall/floor [kN/mm]		Wall/wall [kN/mm]	
			k_{axial}	k_{shear}	k_{axial}	k_{shear}
180 mm	120	60	122.2	8.6	72.0	10.1
160 mm	120	40	122.2	7.6	48.0	9.0
150 mm	110	40	112.0	7.1	48.0	8.4
140 mm	80	60	81.4	6.7	72.0	7.9
130 mm	100	30	101.8	6.2	36.0	6.7
120 mm	90	30	91.6	5.7	36.0	6.7

Table 9
Equivalent stiffness properties for "connection-zones".

Thickness	Wall/floor [kN/mm]		Wall/wall [kN/mm]	
	k_{axial}	k_{shear}	k_{axial}	k_{shear}
180 mm	3300.0	155.2	133.2	186.3
160 mm	2933.3	138.0	118.4	165.6
150 mm	2750.0	129.3	111.0	155.2
140 mm	256.6	120.7	103.6	144.9
130 mm	2383.3	112.1	96.2	134.5
120 mm	2200.0	103.5	88.8	124.2

Building geometry in modeling type I was made as detailed as possible as shown in Fig. 16(a): openings in walls and floors were placed at their exact locations, and secondary structural elements, such as steel columns were included in the model. The cutouts from the CLT panels were modeled according to the structural drawings.

Modeling type II

In modeling type II connections between CLT panels are modeled with "connection-zone" elements (Fig. 15). "Connection-zones" are 2D shell elements with orthotropic material properties of CLT panels and have varying thicknesses, which are related to the connected CLT panel thickness through the reduction factor, k_{red}. This reduction factor is equal to $t_{conn-zone}/t_{main}$, where t_{main} is the thickness of the CLT panel that is being connected. These "connection-zone" elements are tied at the endpoints to the adjacent main elements at centerlines as shown in Fig. 15. Assuming that the stiffness properties of the shell element are directly related to its thickness, the "connection-zone" stiffness can be varied from semi-rigid behavior ($k_{red} < 1$), to the rigid connection between the panels ($k_{red} = 1$). The modulus of elasticity of the "connection-zone" in the vertical direction and the shear modulus in the horizontal direction account for lateral deformation due to rocking and sliding of the CLT panel 15. The height of "connection-zone" is equal to the average height of the CLT panel, 150 mm. Unlike CLT panels, which are modeled with layered properties, "connection-zone" elements are modeled with homogeneous properties. Material orientation in the "connection-zones" is the same as the orientation of the outer layers of the CLT panels. Table 9 shows estimated equivalent axial and shear properties for "connection-zones" with $k_{red} = 0.1$ for the CLT panel with the height of 3 m and length of 2.5 m.

3.5. Model calibrating

Since the knowledge of the exact values of stiffness contribution from connections in CLT under ambient vibrations is limited, the model calibrating was performed using connection stiffness values as parameters. The output of interest in model calibrating is modal frequencies and modal assurance criterion (MAC) values [39] obtained from the experimental measurements. The objective function, measuring the difference between the numerical and experimental values was calculated as follows:

$$F_{obj} = \sum_{i=1}^{n} \gamma_i \left(\frac{f_{i,exp} - f_{i,num}}{f_{i,exp}} \right)^2 + \sum_{i=1}^{n} \lambda_i \left(1 - MAC_i \right)^2 \tag{8}$$

where F_{obj} is an objective function, $(*)_{i,exp}$ is the experimental output for mode i, $(*)_{i,num}$ is the numerical output for mode i, γ_i and λ_i are the weight factors, which are set to 1 for all values.

Before conducting the model calibrating, the two FE models were compared with rigid connections assigned. In modeling type II, a rigid connection is assumed when $t_{conn-zone} = t_{main}$. By comparing stiffness values from Tables 8 and 9, it can be seen that the stiffness factors in modeling type I have to be increased in order to represent rigid behavior similar to modeling type II. Based on calculations, a minimum factor ASR = SSR = 40 has been chosen to ensure rigid behavior. The results of the two models with rigid connections are shown in Tables 10 and 11. As can be seen, the two modeling types have slightly different values for frequencies. Since the geometry in modeling type I is more detailed and includes more panels and openings, and the bottom floor with the reduced area, it has lower stiffness compared to modeling type II, where simplified geometry and typical floor plan are used. The MAC values are quite similar and have high values, meaning they are similar to the experimental mode shapes. The frequency values in both modeling types are higher compared to the experimental frequencies, meaning that the rigid connection assumption is too stiff.

Table 10

Comparison of results for two modeling types with rigid connections for the 13-storey building.

Mode	Experimental f [Hz]	Modeling type I		Modeling type II	
		f [Hz]	MAC [%]	f [Hz]	MAC [%]
1	1.30	1.44	0.99	1.64	0.99
2	1.63	1.83	0.89	1.97	0.91
3	1.99	2.15	0.87	2.38	0.87

Table 11

Comparison of results for two modeling types with rigid connections for the 10-storey building.

Mode	Experimental f [Hz]	Modeling type I		Modeling type II	
		f [Hz]	MAC [%]	f [Hz]	MAC [%]
1	2.15	2.69	0.96	2.87	0.98
2	2.45	3.12	0.98	3.28	0.96
3	2.91	3.52	0.89	3.78	0.92

Table 12

Parameters for model updating.

Modeling Type	Parameter	Range
Type I	ASR	1–40
	SSR	1–40
Type II	$t_{wall/floor}$	0.01–1.00
	$t_{wall/wall}$	0.01–1.00

Table 13

Model updating results for the 13-storey building.

Mode	Experimental f [Hz]	Modeling type I		Modeling type II	
		f [Hz]	MAC [%]	f [Hz]	MAC [%]
1	1.30	1.30	0.99	1.39	0.99
2	1.63	1.66	0.89	1.58	0.92
3	1.99	1.95	0.87	1.94	0.87

Parameters for model updating are listed in Table 12. In both modeling types parameters are related to connection stiffness values. In modeling type I, ratios for axial and shear stiffness for connector elements, ASR and SSR respectively, are chosen as parameters for model updating. The values for parameters ASR and SSR range from 1 to 40, where the latter value represents rigid connection. In modeling type II, reduction factors for the thickness of the "connection-zones" are chosen as parameters for modeling updating. These parameters are divided into two types: reduction factor for the thickness of "connection-zone" between CLT wall and floor panels, $t_{wall/floor}$, and reduction factor for the thickness of "connection-zone" between CLT walls, $t_{wall/floor}$. The values for these parameters range from the smallest stiffness contribution ($t = 1\%$) to rigid connection ($t = 100\%$).

3.6. Model updating results

Since in both modeling types only two parameters were selected for model updating, the entire domain was investigated. Optimization was conducted by discretizing the entire parameter domain and calculating the corresponding objective functions. In modeling type I model updating was conducted by discretizing the domain with 0.1 step for parameters ASR and SSR. In modeling type II model updating was conducted by discretizing the domain with 0.01 step for parameters $t_{wall/floor}$ and $t_{wall/wall}$.

Table 13 shows model updating results of both modeling types in comparison with the experimental results for the 13-storey building and Fig. 17 shows the contour plot for objective function with 'X' indicating the location of the function minimum. Both modeling types have updated frequencies that are close to the experimental values, with modeling types I and II having final objective function values of 0.131 and 0.132 respectively. The updated values for connection parameters are shown in Table 13. The last 4 columns of Table 14 show the corresponding stiffness values for connections per CLT panel (with the thickness of 160 mm as an example). The final building mode shapes for both modeling types are shown in Figs. 18 and 19.

Table 15 shows the updated frequencies and MAC values of both modeling types in comparison with the experimental results for the 10-storey building. Both modeling types achieved values similar to the experimental results, with modeling types I and II having objective functions of 0.074 and 0.076 respectively. Fig. 20 shows the contour plot for the objective function with 'X' indicating the minimum of the function. Compared to the contour plot for the 13-storey building (Fig. 17), the contour plot for the 10-storey building has a more pronounced location of minimum, and the 10-storey building has smaller objective function values than 13-storey building (Fig. 20). The updated parameters with the corresponding stiffness values per CLT panel are shown in Table 16. The mode shapes of the 10-storey building after model updating are shown in Figs. 21 and 22.
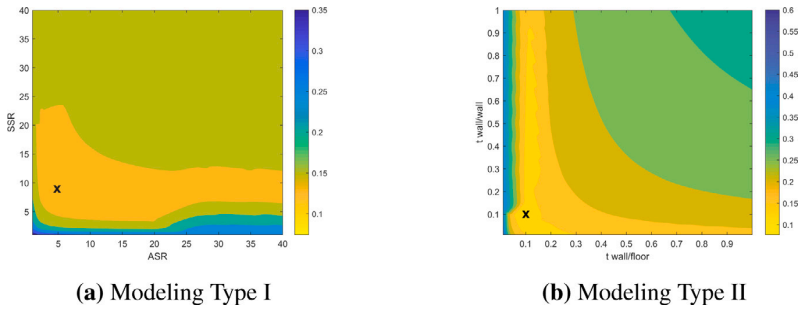
(a) Modeling Type I

(b) Modeling Type II

Fig. 17. Contour plots for the objective functions for the 13-storey building.
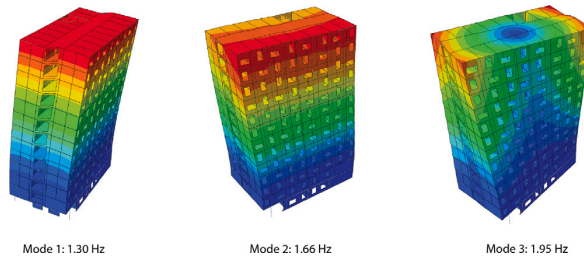
Mode 1: 1.30 Hz   Mode 2: 1.66 Hz   Mode 3: 1.95 Hz

Fig. 18. Modeling type I: mode shapes after model updating for the 13-storey building.

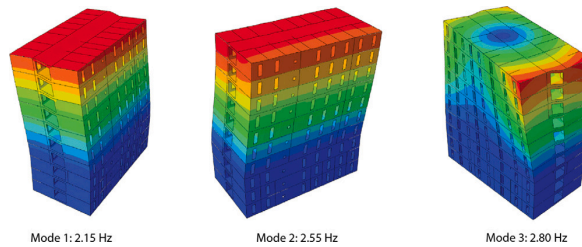Mode 1: 1.39 Hz   Mode 2: 1.58 Hz   Mode 3: 1.94 Hz
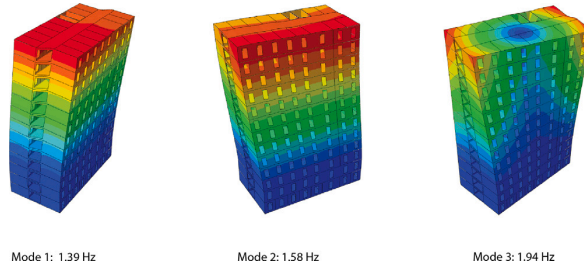
Fig. 19. Modeling type II: mode shapes after model updating for the 13-storey building.

Table 14
Parameters after model updating for the 13-storey building and corresponding connection stiffness values (per CLT panel).

Modeling type	Parameter	Value	Wall/floor [kN/mm]		Wall/wall [kN/mm]	
			k_{axial}	k_{shear}	k_{axial}	k_{shear}
Type I	ASR	4.8	5225	–	2508	–
	SSR	9.0	–	465.7	–	223.5
Type II	$t_{wall/floor}$	0.1	2933	138	–	–
	$t_{wall/wall}$	0.1	–	–	118	165

Table 15
Model updating results for the 10-storey building.

Mode	Experimental f [Hz]	Modeling type I		Modeling type II	
		f [Hz]	MAC [%]	f [Hz]	MAC [%]
1	2.15	2.16	0.96	2.21	0.99
2	2.45	2.52	0.98	2.44	0.97
3	2.91	2.80	0.93	2.81	0.92

(a) Modeling Type I   (b) Modeling Type II
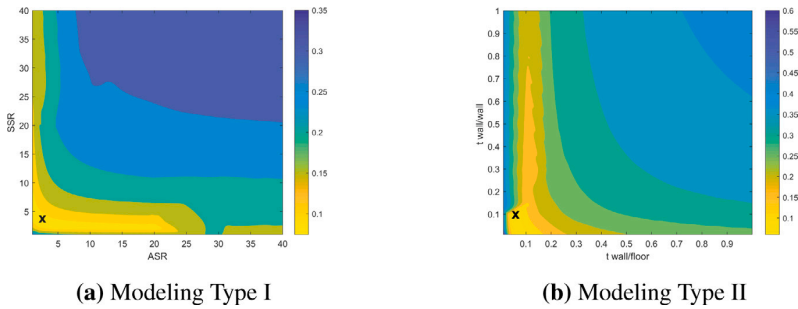
Fig. 20. Contour plots for the objective functions for the 10-storey building.
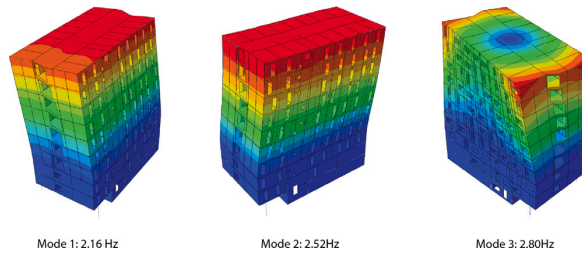
Mode 1: 2.16 Hz   Mode 2: 2.52 Hz   Mode 3: 2.80 Hz

Fig. 21. Modeling type I: mode shapes after model updating for the 10-storey building.

Mode 1: 2.15 Hz   Mode 2: 2.55 Hz   Mode 3: 2.80 Hz

Fig. 22. Modeling type II: mode shapes after model updating for the 10-storey building.

Table 16
Parameters after model updating for the 10-storey building and corresponding connection stiffness values (per CLT panel).

Modeling type	Parameter	Value	Wall/floor [kN/mm]		Wall/wall [kN/mm]	
			k_{axial}	k_{shear}	k_{axial}	k_{shear}
Type I	ASR	2.0	2200	–	1056	–
	SSR	3.5	–	181.1	–	86.9
Type II	$t_{wall/floor}$	0.06	1760	82.8	–	–
	$t_{wall/wall}$	0.1	–	–	71	99.3

Stiffness values for the two modeling types in Tables 14 and 16 differ significantly as they should due to different modeling approaches. In modeling type I the axial and shear stiffness are uncoupled and can be assigned independently, whereas, in modeling type II, the axial and shear properties are coupled and dependent on the CLT material properties.

Since the model updating for two buildings yielded different parameter values for both modeling types, an attempt was made to find common parameter values which would give close approximations for both buildings. Using the contour plots from Figs. 17(a) and 20(a) for modeling type I, the common values for parameters were found and the resulting objective functions were 0.159 for the 13-storey building and 0.102 for the 10-storey building, which is larger than the values for separate model updatings, but still gives a good approximation. Similarly, using contour plots from Figs. 17(b) and 20(b) for modeling type II, the common values for parameters were determined and the resulting objective functions were 0.137 and 0.098 for the 13-storey and 10-storey buildings

Table 17
Model updating results for the 13-storey building using common parameter values.

Mode	Experimental f [Hz]	Modeling type I		Modeling type II	
		f [Hz]	MAC [%]	f [Hz]	MAC [%]
1	1.30	1.24	0.99	1.35	0.99
2	1.63	1.54	0.89	1.52	0.92
3	1.99	1.79	0.87	1.86	0.87

Table 18
Model updating results for the 10-storey building using common parameter values.

Mode	Experimental f [Hz]	Modeling type I		Modeling type II	
		f [Hz]	MAC [%]	f [Hz]	MAC [%]
1	2.15	2.29	0.96	2.32	0.99
2	2.45	2.62	0.98	2.53	0.97
3	2.91	2.93	0.93	2.95	0.92

Table 19
Common parameter values for the two buildings after model updating (per CLT panel).

Modeling type	Parameter	Value	Wall/floor [kN/mm]		Wall/wall [kN/mm]	
			k_{axial}	k_{shear}	k_{axial}	k_{shear}
Type I	ASR	4.0	4400	–	2112	–
	SSR	4.0	–	207	–	99.3
Type II	$t_{wall/floor}$	0.08	2288	107.6	–	–
	$t_{wall/wall}$	0.08	–	–	92.3	129.1

respectively. The summary of the resulting frequencies and mode shapes are shown in Tables 17 and 18. The common parameter values and the corresponding stiffness values are given in Table 19.

It is important to note that the current modeling approach was designed for serviceability level conditions and seismic loading was not considered in this study. The FE models were developed with linear material properties and as-built mass values were applied.

4. Conclusions and recommendations

A study on the dynamic identification of multi-storey CLT buildings and the corresponding model calibrating of connection stiffness was presented. In building set I, experimental ambient vibration measurements were recorded for 5 similar 9-storey CLT buildings and compared against the simplified finite element model. In building set II, the two modeling approaches for connection stiffness between CLT panels were presented. The first approach is using the connector elements, which represent elastic springs in axial and shear directions. A second approach is a simplified approach, where shell elements with CLT material properties and reduced thickness are applied. Both approaches were applied to two multi-storey CLT buildings (10-storeys and 13-storeys) and model updating using connection stiffness properties as parameters was conducted and compared against the experimental results.

The following conclusions and recommendations are suggested after implementing the study:

- The experimental ambient vibrations measurements campaign achieved highly similar modal results for all 5 CLT buildings in Moholt showing the repeatability of the measurements.
- Damping values obtained for 7 CLT buildings ranged between 1.0%–2.0% based on output-only analysis for ambient-level vibrations. The range was similar for 9-storey buildings as well as for 13-storey building.
- Modeling approach with discrete connector elements and detailed geometry achieved close estimates after model updating. Though model updating achieved different parameters for different buildings, the common parameter values were found, which yielded close approximations for both buildings. The common parameter values are: 4.0 for both axial and shear stiffness ratio ($ASR = SSR = 4.0$).
- Modeling approach with "connection-zones" and simplified geometry was able to achieve close estimates of the building modal parameters. From the calibration study for both 10-storey and 13-storey building, it was shown that 0.08 is the value for both wall/floor and wall/wall connection thickness ($t_{wall/floor} = t_{wall/wall} = 0.08$), where close estimates were achieved for both buildings.

The resulting parameter values for connection stiffness in CLT panels can serve as useful references for practicing engineers in their prediction models for dynamic properties of multi-storey CLT buildings under serviceability level response. Specifically, the distributed connection modeling approach with simplified geometry can be used as a good time-saving predictive model. It should be mentioned that the modeling approach is not designed for seismic models where the nonlinear behavior of the connections takes place.

CRediT authorship contribution statement

Saule Tulebekova: Conceptualization, Methodology, Validation, Investigation, Formal analysis, Writing – original draft, Writing – review & editing, Visualization. **Kjell Arne Malo:** Conceptualization, Methodology, Writing – review & editing, Supervision, Funding acquisition. **Anders Rønnquist:** Writing – review & editing, Supervision.

Declaration of competing interest

The authors declare that they have no known competing financial interests or personal relationships that could have appeared to influence the work reported in this paper.

Data availability

Data will be made available on request.

Acknowledgments

Appendix A. Detailing of the structural elements in all CLT buildings

The detailing of the typical CLT floor/wall composition is presented below [mm]:
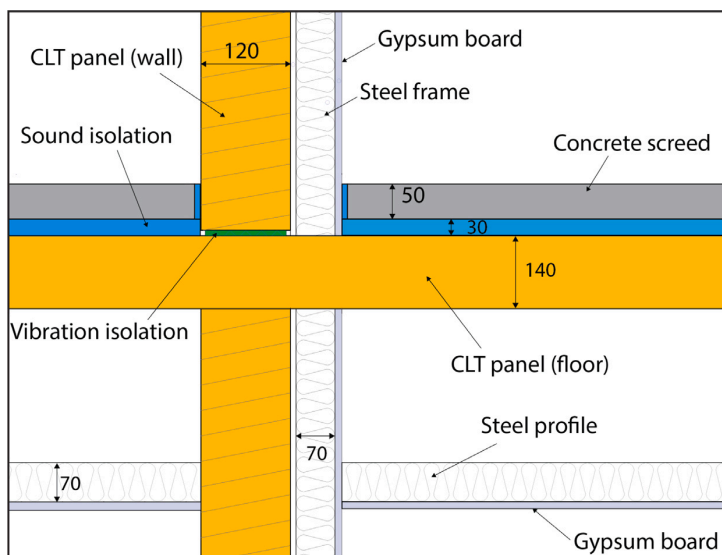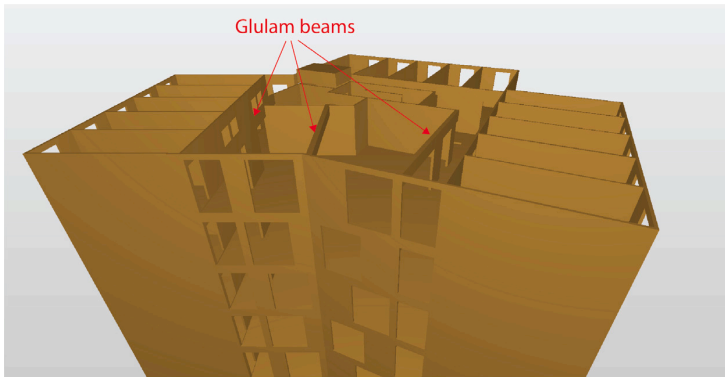

Typical floor/wall composition

Appendix B. Moholt building CLT panels layout

Typical layout of CLT panels in the Moholt buildings (the number after "CLT" indicates the thickness of the panel in [mm]):

CLT panels layout [mm]

	Floors			
	2-3	4-5	6-7	8-9
🟥	160	140	120	120
🟦	140	120	100	100
🟩	120	120	100	100
🟧	120	120	100	100
🟨	100	100	100	100
🟪	80	80	80	80

- - - - - - Glulam beam (GL30c) 200x500
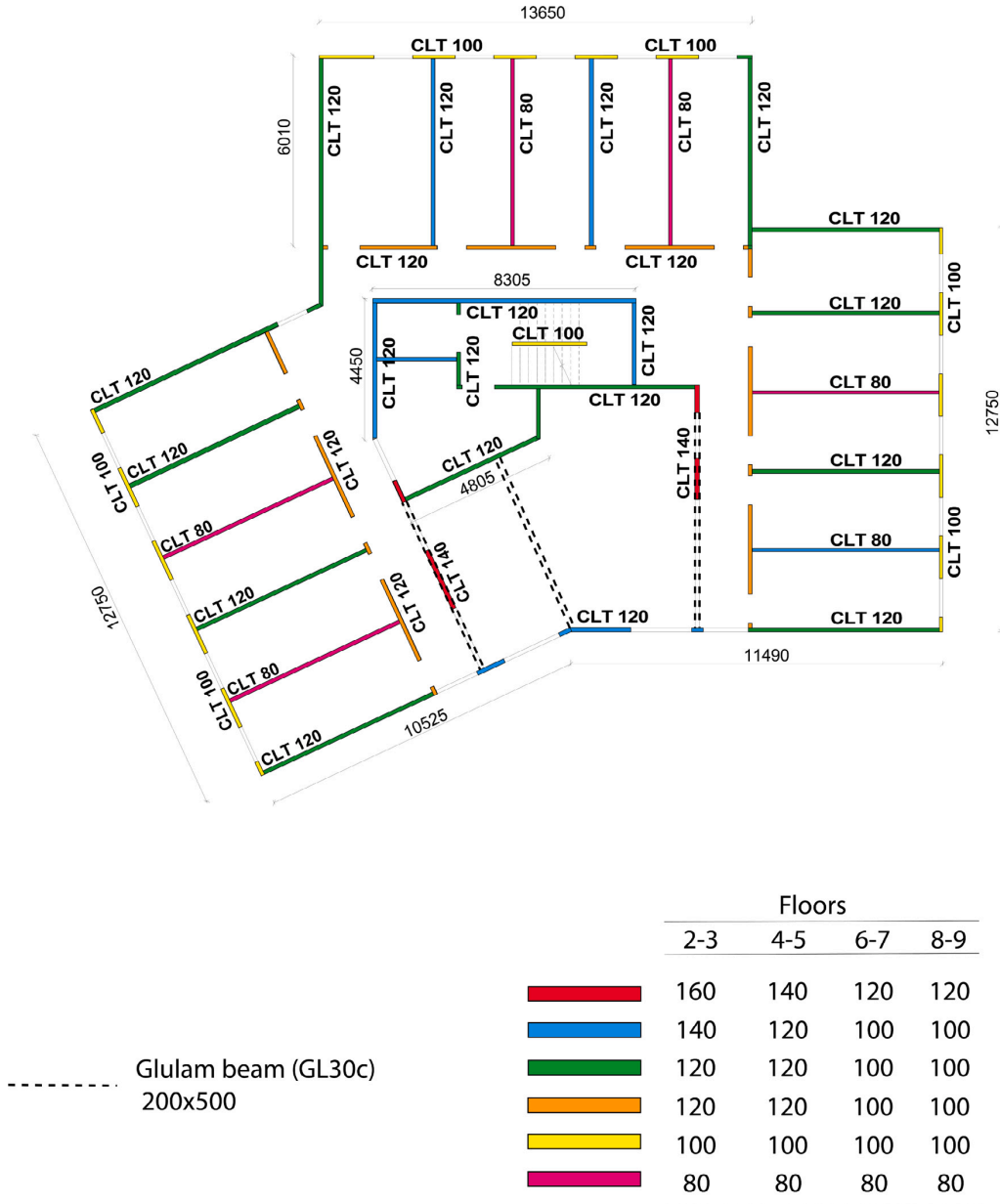
Location of glulam beams inside the Moholt building:

Glulam beams location

Appendix C. Tromso building CLT panels layout

Typical layout of wall CLT panels in the Tromsø buildings (the number after "CLT" indicates the thickness of the panel in [mm]).
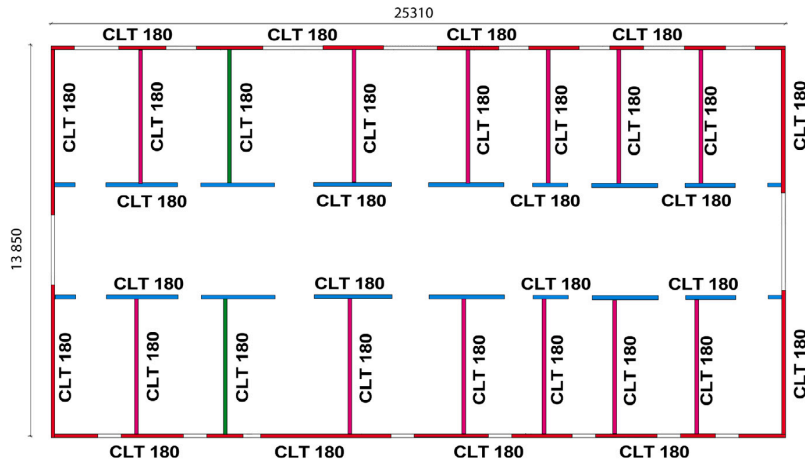
10-storey building:
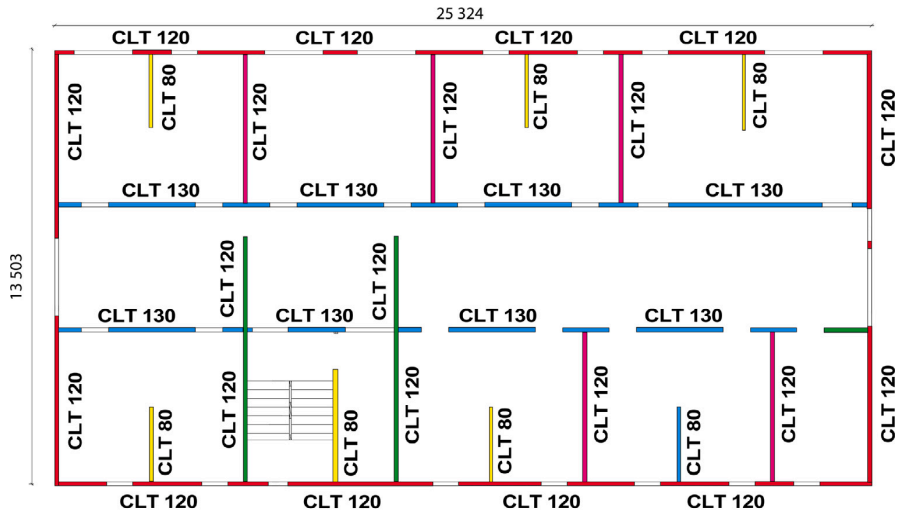
	Floors						
	4	5	6	7	8	9	10
	140	130	120	120	120	120	120
	140	140	140	130	130	120	120
	130	130	130	120	120	120	100
	140	140	130	130	120	120	100
	80	80	80	80	80	80	80

CLT panels layout [mm]

13-storey building:

|	Floors										
	3	4	5	6	7	8	9	10	11	12	13
▬ (red)	180	180	160	160	160	140	140	140	120	120	120
▬ (blue)	180	180	160	160	140	140	140	140	140	140	120
▬ (green)	180	180	180	180	180	180	160	140	140	140	120
▬ (magenta)	180	180	180	160	160	160	140	140	140	140	120

CLT panels layout [mm]

References

[1] R. Brandner, G. Flatscher, A. Ringhofer, G. Schickhofer, A. Thiel, Cross laminated timber (CLT: overview and development), Eur. J. Wood Wood Prod. (2017).
[2] J. Hildebrandt, N. Hagemann, D. Thran, The contribution of wood-based construction materials for leveraging a low carbon building sector in Europe, Sustainable Cities Soc. 34 (2017) 405–418.
[3] S. Pei, C. Lenon, G. Kingsley, P. Deng, Seismic design of cross-laminated timber platform buildings using a coupled shearwall concept, J. Archit. Eng. 23 (2017).
[4] N. Labonnote, A. Rønnquist, K. Malo, Modified hysteretic damping model applied to Timoshenko timber beams, Comput. Struct. 121 (2013) 22–31.
[5] M. Johansson, A. Linderholt, K. Jarnero, P. Landel, Tall timber buildings - A preliminary study of wind-induced vibrations of a 22-storey building, in: World Conference on Timber Engineering (WCTE) 2016, Vienna, Austria, 2016.
[6] I. Edskar, H. Lidelow, Wind-induced vibrations in timber buildings - parameter study of cross-laminated timber residential structures, Soil Dyn. Earthq. Eng. 128 (2020).
[7] X. Zhao, B. Zhang, T. Kilpatrick, I. Sanderson, D. Liu, Numerical analysis on global serviceability behaviours of tall glulam frame buildings to the eurocodes and UK national annexes, J. Civ. Eng. Constr. 10 (2021) 109–122.
[8] R. Abrahamsen, M. Bjertnaes, J. Bouillot, B. Brank, L. Cabaton, et al., Dynamic response of tall timber buildings under service loads - the dynaTTB research program, in: XI International Conference on Structural Dynamics Eurodyn 2020, Athens, Greece, 2020.
[9] T. Reynolds, R. Hariis, W. Chang, J. Bregulla, J. Bawcombe, Ambient vibrations tests of a cross-laminated timber building, Constr. Mater. 168 (2015) 121–131.
[10] T. Reynolds, D. Casagrande, R. Tomasi, Comparison of multi-story cross-laminated timber and timber frame buildings by in situ modal analysis, Constr. Build. Mater. 102 (2016) 1009–1017.
[11] I. Mugabo, A. Barbosa, M. Riggio, Dynamic characterization and vibration analysis of a four-story mass timber building, Front. Built Environ. 5 (2019).
[12] A. Aloisio, D. Pasca, R. Tomasi, M. Fragiacomo, Dynamic identification and model updating of an eight-story CLT building, Eng. Struct. 213 (2020).
[13] B. Kurent, B. Brank, W. Ao, Mode updating of seven-storey cross-laminated timber building designed on frequency-response-functions-based modal testing, Struct. Infrastruct. Eng. (2021).
[14] E. Karacabeyli, S. Gagnon, Canadian CLT Handbook, FPInnovations, Pointe-Claire, QC, Canada, 2019.

[15] R. Tomasi, I. Smith, Experimental characterization of monotonic and cyclic loading responses of CLT panel-to-foundation angle bracket connections, J. Mater. Civ. Eng. 27 (2015).

[16] T. Tannert, C. Loss, Contemporary and novel hold-down solutions for mass timber shear walls, Buildings 12 (2022).

[17] I. Gavric, M. Fragiacomo, A. Ceccotti, Cyclic behavior of typical screwed connections for cross-laminated (CLT) structures, Eur. J. Wood Wood Prod. 73 (2015) 179–191.

[18] T. Schmidt, H. Blas, Recent development in CLT connections part I: in-plane shear connection for CLT bracing elements under static loads, Wood Fiber Sci. (2018) 48–57.

[19] L. Pozza, A. Saetta, M. Savoia, D. Talledo, Coupled axial-shear numerical model for CLT connections, Constr. Build. Mater. (2017) 568–582.

[20] M. Popovski, I. Gavric, Performance of 2-story CLT house subjected to lateral loads, J. Struct. Eng. 4 (2015).

[21] V. Hristovski, B. Dujic, M. Stojmanovska, V. Mircevska, Full-scale shaking-table tests of xlam panel systems and numerical verification: specimen 1, J. Struct. Eng. 139 (2013).

[22] J. Huber, M. Ekevad, U. Girhammar, S. Berg, Finite element analysis of alternative load paths in a platform-framed CLT building, Struct. Build. 175 (2020) 379–390.

[23] G. Rinaldin, C. Amadio, M. Fragiacomo, A component approach for the hysteretic behaviour of connections in cross-laminated wooden structures, Earthq. Eng. Struct. Dyn. 42 (2013) 2023–2042.

[24] M. Yasumura, K. Kobayashi, M. Okabe, T. Miyake, K. Matsumoto, Full-scale tests and numerical analysis of low-rise CLT structures under lateral loading, J. Struct. Eng. 142 (2015).

[25] S. Rossi, D. Casagrande, R. Tomasi, M. Piazza, Seismic elastic analysis of light timber-frame multi-storey buildings: proposal of an iterative approach, Constr. Build. Mater. 102 (2016) 1154–1167.

[26] I. Christovasilis, L. Riparbelli, G. Rinaldin, G. Tamagnone, Methods for practice oriented linear analysis in seismic design of Cross Laminated Timber buildings, Soil Dyn. Earthq. Eng. 128 (2020).

[27] V. Rinaldi, D. Casagrande, C. Cimini, M. Follesa, M. Fragiacomo, And upgrade of existing practice-oriented FE design models for the seismic analysis of CLT buildings, Soil Dyn. Earthq. Eng. 149 (2021).

[28] CEN-EN 14080-2013: Timber Structures - Glue Laminated Timber and Glued Solid Timber - Requirements, European Committee for Standardization, Brussels, Belgium, 2013.

[29] NS-EN 338-2016: Structural Timber - Strength Classes, European Committee for Standardization, Brussels, Belgium, 2016.

[30] A.I. for Structural Engineering, Declaration of Performance CLT 2020/04, European Technical Assessment, Vienna, Austria, 2020.

[31] EN 10025-2:2019, Hot Rolled Products of Structural Steels. Part 2: Technical Delivery Conditions for Non-Alloy Structural Steels, organization=European Committee for Standardization, city = Brussels, Belgium,, 2019.

[32] P. Van Overschee, B. De Moor, Subspace Identification for Linear Systems: Theory, Implementation, Applications, Kluwer Academic Publishers, Leuven, Belgium, 1996.

[33] K. Kvåle, O. Øiseth, A. Rønnquist, Operational modal analysis of an end-supported pontoon bridge, Eng. Struct. (2017).

[34] B. Peeters, D. Roeck Guido, Reference-based stochastic subspace identification for output-only modal analysis, Mech. Syst. Signal Process. (1999).

[35] M. Valla, P. Gueguen, B. Augère, D. Goular, M. Perrault, Remote modal study of reinforced concrete buildings using a multipath lidar vibrometer, J. Struct. Eng. 141 (2014).

[36] P. Guéguen, A. Colombi, Experimental and numerical evidence of the clustering effect of structures on their response during an earthquake: A case study of three identical towers in the city of grenoble, france, Bull. Seismol. Soc. Am. 106 (2016).

[37] DassaultSystemes, ISight. Automated design exploration and optimization, 2014, https://www.3ds.com/fileadmin/PRODUCTS-SERVICES/SIMULIA.

[38] SwedishWood, The CLT Handbook: CLT Structures Facts and Planning, Brussels, Belgium, 2013.

[39] M. Pastor, M. Binda, T. Harcarik, Modal assurance criterion, Procedia Eng. 48 (2012) 543–548.

[40] Y. Zhou, Y. Zhou, W. Yi, T. Chen, D. Tan, S. Mi, Operational modal analysis and rational finite-element model for ten high-rise buildings based on on-site ambient vibration measurements, J. Perform. Constr. Facil. 31 (2017).

[41] Norges arktiske studentsamskipnad, Flotte, nye studentboliger naer campus er klare for innflytting!, 2021, https://samskipnaden.no/nyheter/2021-01-18-flotte-nye-studentboliger-naer-campus-er-klare-for-innflytting.

[42] S. Tulebekova, K. Malo, A. Rønnquist, P. Nåvik, Modeling stiffness of connections and non-structural elements for dynamic response of taller glulam timber frame buildings, Eng. Struct. (2022).

[43] K. Malo, R. Abrahamsen, M. Bjertnaes, Some structural design issues of the 14-storey timber framed building Treet in Norway, Eur. J. Wood Wood Prod. 74 (2016) 407–424.

[44] The CLT Handbook: CLT Structures - Facts and Planning, Swedish Wood, Stockholm, Sweden, 2019.

Paper II
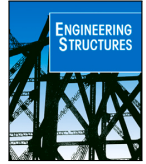
Modeling stiffness of connections and non-structural elements for dynamic response of taller glulam timber frame buildings

Saule Tulebekova [a,*], Kjell Arne Malo [a], Anders Rønnquist [a], Petter Nåvik [a,b]

[a] *Department of Structural Engineering, Norwegian University of Science and Technology (NTNU), Richard Birkelands vei 1A, Trondheim, 7491, Norway*
[b] *SWECO Norge AS, Drammensveien 260, Oslo, 0212, Norway*

ARTICLE INFO

ABSTRACT

Currently, there is limited knowledge of the dynamic response of taller glue laminated (glulam) timber buildings due to ambient vibrations. Based on previous studies, glulam frame connections, as well as non-structural elements (external timber walls and internal plasterboard partitions) can have a significant impact on the global stiffness properties, and there is a lack of knowledge in modeling and investigation of their impact on the serviceability level building dynamics. In this paper, a numerical modeling approach with the use of "connection-zones" suitable for analyzing the taller glulam timber frame buildings serviceability level response is presented. The "connection-zones" are generalized beam and shell elements, whose geometry and properties depend on the structural elements that are being connected. By introducing "connection-zones", the stiffness in the connections can be estimated as modified stiffness with respect to the connected structural elements. This approach allows for the assessment of the impact of both glulam connection stiffness and non-structural element stiffness on the dynamic building response due to service loading. The results of ambient vibration measurements of an 18-storey glulam timber frame building, currently the tallest timber building in the world, are reported and used for validation of the developed numerical model with "connection-zones". Based on model updating, the stiffness values for glulam connections are presented and the impact of non-structural elements is assessed. The updating procedure showed that the axial stiffness of diagonal connections is the governing parameter, while the rotational stiffness of the beam connections does not have a considerable impact on the dynamic response of the glulam frame type of building. Based on modal updating, connections exhibit a semi-rigid behavior. The impact of non-structural elements on the mode shapes of the building is observed. The obtained values can serve as a practical reference for engineers in their prediction models of taller glulam timber frame buildings serviceability level response.

1. Introduction

Rising awareness of the importance of sustainability in the general public has led professionals in structural engineering to incorporate the use of environmentally friendly materials in their design. Therefore, the focus on timber, which is known for its natural origin and negligible carbon footprint compared to widely used steel and concrete, is understandable. Currently, timber as a structural material is being extensively utilized in the construction of buildings [1].

In general, the lateral loading on taller glulam timber frame buildings is governed by wind-induced vibrations [2]. The intrinsic properties of wood, including low density and stiffness, make taller timber buildings susceptible to horizontal excitation under wind loading [3].

The stiffness, mass, and damping properties and their distributions in buildings are the factors that affect the vibration response of taller glulam timber frame buildings. Estimation of stiffness in glulam timber frame buildings can be challenging and depends on the structural system used [4]. Experimental results from ambient vibration measurements show that the eigenfrequencies obtained from the numerical modeling can be systematically underestimated due to the assumption of pinned connections in glulam timber frames [5,6].

The past studies on taller glulam timber frame buildings emphasize the fundamental importance of connections in timber structures under serviceability level dynamic loading [7]. In glulam timber frame buildings, the dowel-type connections make a considerable contribution to

the structure stiffness [8]. The estimation of such connection stiffness can, however, be challenging. In a number of studies, it has been shown that the static dowel connection stiffness, which is calculated in accordance with Eurocode 5 [9], is different from the stiffness calculated from the in-service cyclic tests [8,10]. The common practice in modeling the dynamic response of glulam timber frame buildings is to assign pinned conditions to the connections between glulam elements, [5,6,11,12].

The impact of non-structural elements on the serviceability level response of tall buildings has been acknowledged in both steel and reinforced concrete buildings [13]. The previous studies on ambient vibration measurements of timber buildings suggested that contribution from the stiffness of non-structural elements, such as internal plasterboard partition walls and exterior wall cladding (brickwork, glass, and timber), affects the serviceability level dynamic response of the building [14,15]. One study where operational modal testing was performed, showed that the addition of internal plasterboards had considerably stiffened the whole building in the translational directions [16]. These studies indicate the importance of assessment of the effect of non-structural elements on the dynamic response of buildings.

The main objective of this paper is to present an alternative numerical modeling approach for connections and non-structural elements (internal plasterboard partition walls and external timber walls), which can be used for the investigation of the serviceability level dynamic response of taller glulam buildings. The information at hand for structural engineering of serviceability dynamics of buildings is basically mean values of stiffness and mass of the individual components constituting the building. The structural interactions of the components are dependent on the layout and are usually much more uncertain than the properties of the components. The current practice is to either design the connections as pin elements or to assign a specified stiffness value. The latter can be a cumbersome process since the stiffness estimates depend on the connection layout, which may vary from floor to floor. The "connection-zones" directly relate the stiffness of connection to the stiffness of the glulam timber element that is being connected. This approach allows for an automated numerical investigation of the timber connections under ambient vibrations and a better interpretation of the estimated connection stiffness. The paper is written in the following order. First, the experimental results based on ambient vibration measurements of an 18-storey glulam timber frame building (Mjøstårnet, Norway) are presented. Then, in the numerical modeling section, the "connection-zones" approach for modeling connections in glulam and non-structural elements is presented, and overall numerical modeling of the Mjøstårnet building is described. After that, a parametric study is conducted to explore the effect of stiffness of connections and non-structural elements on the dynamic response of the building. Finally, a model updating study is conducted to obtain the values for parameters of interest. The goal of this study is to present values for stiffness of connections and non-structural elements (internal plasterboard partitions and external timber walls) for practitioners to use as a reference when developing numerical models of taller glulam buildings for serviceability level vibration response prediction.

2. Ambient vibrations testing

2.1. Building description

The test building is named Mjøstårnet (the Mjosa Tower, Fig. 1) and is located in Brumunddal, Norway. The total architectural height of the building (including the truss work on the top) is 85.4 m and the total height including the spire is 88.8 m. The plan dimensions are 36.3 m by 15.7 m, see also Fig. 5(b). The summary of the structural system of the building is shown in Fig. 2. The load-carrying system of the building consists entirely of timber: glue laminated timber (glulam) beams, columns and diagonals. The strength grade for glulam is

GL30c in accordance with EN 14080:2013 [17]. The average beam cross-section is 400 mm by 500 mm, the corner column cross-section is 600 mm by 1500 mm, and the average diagonal cross-section is 600 mm by 750 mm. The glulam truss members are interconnected with combinations of 10 mm slotted-in steel plates and 12 mm diameter dowels [18]. The steel grade for plates is S355 in accordance with EN 10025-2, which corresponds to 355 MPa yield strength [19]. The steel grade for dowels is EN 1.4418 in accordance with EN 10088, and has a measured yield strength of 755 MPa [20]. Cross-laminated timber (CLT) is used in the elevator and staircase shafts, but is not designed to be part of the horizontal load carrying system. The average thickness of CLT panels is 200 mm. The CLT panels consist of 5 layers of C24 spruce boards in accordance with EN 338 [21]. The first ten floors are made of "Trä8" system — prefabricated timber decks, which were developed by Moelven [22]. "Trä8" system is composed of Kerto-Q® structural laminated veneer lumber (Kerto-Q LVL [23]) beams and a top flange, which is topped with 36-mm thick acoustic panel and 50-mm thick concrete screed (Fig. 3). Stiffening elements made of Kerto-S® structural laminated veneer lumber (Kerto-S LVL [23]) were used for stiffening in the perpendicular to span direction. The bottom flanges are made of glulam timber. The wooden decks average span is 7.5 m, average width is 2.6 m and total thickness is 360 mm. The upper six floors are made of 300 mm thick concrete slabs to increase the self-weight of the structure in order to meet the serviceability requirements. The facade of the building is comprised of prefabricated wooden panels. The truss-type glulam pergola is built on top of the structure for architectural appearance. All structural timber elements have been provided by Moelven, a Scandinavian producer of structural timber. The summary of material properties for structural timber are shown in Table 1.

The building foundation consists of a set of circular steel piles which are approximately 30 m long, have a diameter of 400 mm and thickness of 12.5 mm. The pile head is a 2000-mm thick concrete slab at the base of the building. The piles are in contact with the bedrock at an approximate depth of 30 m. Above, the soil consists of sand, clay, and moraine. Based on foundation conditions, the boundary conditions as pinned supports under the column ends above the concrete foundation were chosen for modeling.

Wind loading was determined to be the dominating load in the design combinations. The calculated wind speed was 22 m/s corresponding to the static wind pressure of 1.12 kN/m2 in accordance with EN 1991-1-4 [9].

2.2. Experimental setup

Experimental dynamic characterization of the Mjøstårnet building was performed using ambient vibration measurements. Two different setups have been used: setup on the roof and setup inside the building. In both setups, a set of 3 triaxial accelerometers along with a data acquisition system were used for experimental testing. In setup on the roof, the accelerometers have been mounted on the pergola truss at the top of the building as shown in Fig. 4. This setup allowed for capturing the eigenfrequencies and in-plane movement, but did not allow for determining the mode shapes along the height of the building. Therefore, the setup has been moved inside the building and the accelerometers have been placed at the different levels. In the second setup, accelerometers were placed on 3 different floors, 10th, 16th, and 18th, aligned vertically in order to capture higher translational vibration modes (Fig. 5(a)). The locations of the accelerometers were based on modal analysis results from the numerical model of the building. The accelerometers were attached with a magnet to a metal plate, which was mounted directly on the glulam beam by screws (Fig. 5(c)). Since the experimental setup is being used for long-term measurements, the placement of accelerometers was limited to locations that are not obstructing the service of the building and are not accessible to the public and residents. The building is in a fully operational mode, which

(a) Building front view
("Long direction")

(b) Building side view
("Short direction")

Fig. 1. Mjøstårnet building (dimensions in m).

Glulam frame   Floors   CLT shafts   External walls   Internal partitions
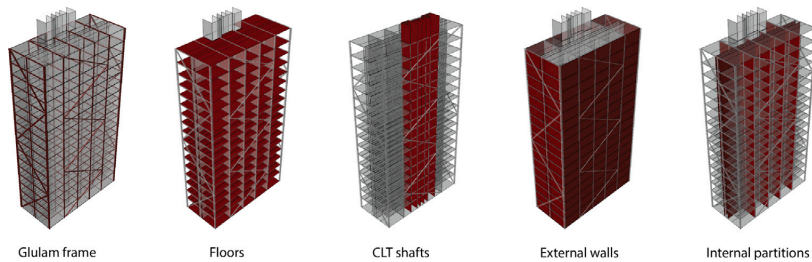
Fig. 2. Building structural system.

Table 1
Orthotropic material properties.

Material	ρ [kg/m^3]	E_1 [MPa]	E_2 [MPa]	E_3 [MPa]	G_{12} [MPa]	G_{13} [MPa]	G_{23} [MPa]
Glulam GL30c	430	13 000	300	300	650	650	91.5
CLT, 5 layers	420	6 960	4 650	300	650	650	650
Kerto-Q® LVL	510	10 500	2 200	130	820	430	22
Kerto-S® LVL	510	13 800	450	130	600	600	11

limited the options for placement of the setup significantly. As seen from the building plan (Fig. 5(b)), the corners of the building, which have the highest displacement, were not accessible to the general public and the setup could not be installed there. After discussion with the building maintenance company, the staircase for the fire escape, which is used only for emergency cases, was chosen for mounting the setup.

Since the fire safety system requires that the space be isolated from the rest of the building, it was not possible to extend the wiring system to other locations on the same floor. The location of the accelerometers in the fire staircase is shown on the plan view of the building (Fig. 5(b)). The triaxial accelerometers have high sensitivity of 2000 mV/g and a lower frequency range between 0 Hz and 1000 Hz [25]. The sampling
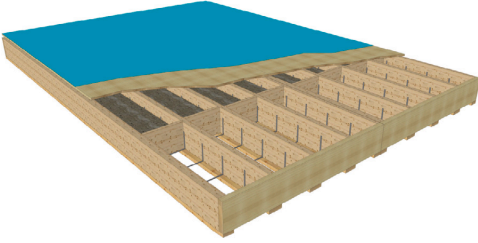
Fig. 3. Graphical illustration of Trä8 floor system [24].
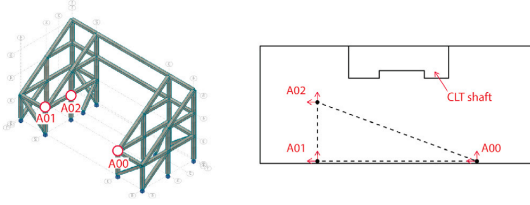

Fig. 4. Accelerometer setup on the roof.

rate for data was 400 Hz. The recorded data was resampled to 20 Hz using an antialiasing filter in Matlab 2020b [26]. This experimental setup has been running continuously since December 15, 2020, and recording the measurements to a server (as of February 2022). Based on the wind data from the nearest weather station, a 3 hr acceleration time series from 5th April 2021 with a mean wind speed of 9.8 m/s were chosen for further analysis.

2.3. Theoretical background

The data was analyzed using the operational modal analysis (OMA) technique. The family of stochastic subspace identification (SSI) techniques is a common approach to deal with output-only measurements and is explained in detail in the literature [27]. In the SSI techniques, a mathematical model with certain parameters adjusted to fit the raw acceleration time series data is developed and calibrated. In this study, the data-driven stochastic subspace identification technique (DD-SSI) approach was used to obtain the modal frequencies, mode shapes, and damping ratios [27,28]. In DD-SSI, the technique is performed directly on the measured response data, without pre-processing it. In SSI techniques, the dynamic system is assumed to be described by the discrete stochastic state–space model as shown below:

$$\{z_{k+1}\} = [A]\{z_k\} + \{w_k\} \tag{1}$$

$$\{y_k\} = [C]\{z_k\} + \{v_k\} \tag{2}$$

where $\{z_{k+1}\}$ is a state–space vector, which holds the current state of the system, $\{y_k\}$ is a measured output at a specified sampling rate, $\{w_k\}$ and $\{v_k\}$ are system noise and measurement noise respectively, k is a discrete time step, $[A]$ is a state matrix and $[C]$ is an output matrix. The modal parameters are then extracted from the identified matrices $[A]$ and $[C]$ [29]. The important task is to properly identify the model with a reasonable number of parameters. This is performed in the state–space model by choosing the model order, i.e. the dimension of the A-matrix [28]. The state–space model of order i is then used to identify the eigenvalue μ_i, from which the corresponding pole λ_i can be obtained at a sampling period t_s. Hence, the modal frequency and damping ratios, f_i and ζ_i, can be calculated for each pole as follows:

$$\lambda_i = \frac{ln(\mu_i)}{t_s} \qquad f_i = \frac{Im(|\lambda_i|)}{2\pi} \qquad \zeta_i = \frac{Im(|\lambda_i|)}{|\lambda_i|} \tag{3}$$

The calculated poles are then plotted on the stabilization diagram which allows distinguishing between the spurious poles and true poles. Spurious poles usually appear due to inaccuracies in measurements, non-stationarity of data, etc. The procedure for determining the true poles, i.e. the poles containing the eigenfrequency and eigenvalue of the physical system, is through assigning the tolerance to the frequency and damping results. The true poles then appear on the stabilization diagram as the aligned poles which are constant along the specific frequency. The DD-SSI method has been applied successfully on various civil engineering structures [29–31].

2.4. Results

In this study, the stability criteria for frequency and damping were 1% and 5% respectively and the chosen order number was 100. Fig. 6 shows the stabilization diagram of the combined signals from the accelerometers in the setup inside the building. The aligned vertical dots show the identified stable frequencies (6 in total). In addition, the power spectral densities in two orthogonal in-plane directions were plotted as gray curves. The left vertical axis represents the model order and the right vertical axis represents the magnitude of the power spectral density. The stabilization diagram from the accelerometer data on the roof showed similar identified frequencies to the ones presented in Fig. 6. The mode shapes from both setups can be seen in Fig. 7 and Fig. 8. The first two modes are translational modes in two orthogonal directions: 1st translational mode at 0.493 Hz in the short direction (Fig. 1(b)), 2nd translational mode at 0.529 Hz in the long direction (Fig. 1(a)). The third mode is the torsional mode at 0.813 Hz as seen from Fig. 8. Mode 4 is the second bending mode at 1.918 Hz in the long direction, and mode 5 is the second bending mode at 2.146 Hz in the short direction. The 6th stable frequency at 2.215 Hz is captured in a long direction, but the mode shape is not possible to determine due to its higher-order and lack of accelerometers. Damping factor values for modes 1–6 are 1.5%, 2.3%, 2.2%, 1.2%, 1.7% and 2.0% respectively.

3. Numerical modeling

A numerical model of the building was developed in Abaqus CAE 2017 [32]. Fig. 9 shows the developed FE model of the building with the mesh geometry. The sensitivity study on the mesh size showed an insignificant impact on the output natural frequencies. Therefore, a larger mesh size was chosen to reduce the computational time and facilitate the optimization process. In Fig. 9(a) the entire assembly mesh is shown, which includes external walls, glulam frame members, CLT shafts, floor elements, and internal partitions. Fig. 9(b) shows the glulam frame model without the external walls and internal partitions. "Connection-zones" are added as generalized beam elements to represent connections between the glulam frame elements. "Connection-zones" are added as shell elements to represent connections between non-structural elements/CLT shaft and glulam frame, as well as connections between floor elements. The chart showing the stages adding "connection-zones" in glulam timber frame elements and non-structural elements is shown in Fig. 10. In the following sections, each part of the numerical model of the building is described in detail.

3.1. Structural elements modeling

The glulam frame elements were modeled with one-dimensional Timoshenko elastic beam elements with an orthotropic material model. Concrete floors were modeled as 4-node shell elements with the linear elastic isotropic model. Architectural truss work, (Fig. 1), at the top of the roof was modeled as added distributed mass on the roof slab. The balconies at levels 12–17 were modeled as added masses on glulam beams at the locations of balconies.

The prefabricated timber deck Trä8 is a composite structure and due to its complexity, a single shell element representing the global deformation model of the floor was chosen for analysis. For this purpose, a
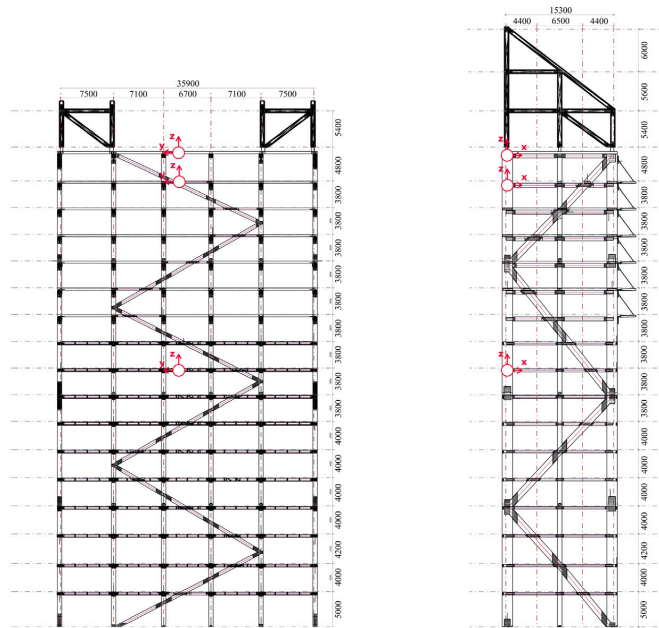
(a) Building frame view with accelerometer positions in long and short directions respectively (measures in mm)

(b) Building frame view with accelerometer positions

(c) Testing equipment including the control box and accelerometer mounted on the glulam beam
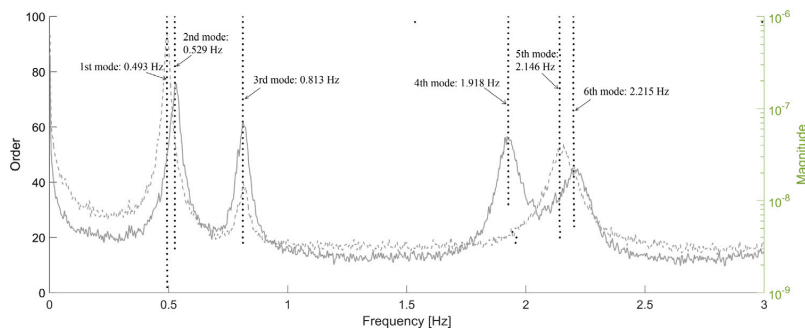
Fig. 5. Experimental setup.

Fig. 6. Stabilization diagram of the combined signals (vertically aligned dots) and power spectral densities in two orthogonal in-plane directions (gray lines).

Table 2
Simplified timber deck model properties after optimization.

Model	E_1 [MPa]	E_2 [MPa]	E_3 [MPa]	G_{12} [MPa]	G_{13} [MPa]	G_{23} [MPa]	Objective function
Initial	1300	300	300	600	600	50	7.47e−6
Optimized	4800	120	990	600	600	50	5.71e−9

Fig. 7. Identified mode shapes from merged accelerometer data sets.

Fig. 8. Mode shapes from setup on the roof.

Table 3
Live load estimates.

Occupational type	Actual load [kN/m²]	Code (SLS) [kN/m²]
Office	0.16	0.9
Hotel	0.21	0.6
Apartment	0.33	0.6
Rooftop deck	0.16	1.2

in Table 3. The actual live load estimates were applied to the building model.

3.3. Glulam frame connections

In engineering practice, it is common to assume a pinned connection between timber elements due to a lack of accurate information about the connection [34]. In reality, the connection between the timber elements is neither pinned, nor rigid, but rather semi-rigid, i.e. it partially transfers the action. Therefore, it is convenient to directly relate the stiffness properties of the connection to the main timber elements. Manually calculating and assigning stiffness properties to the connections and conducting sensitivity study on them can be a cumbersome task due to the large scale of the model and large variety of cross-sections. Keeping that in mind, modeling of connections in this study was performed by introducing the so-called "connection-zones". The stiffness properties of these "connection-zones" are directly related to the connected glulam elements, which facilitates the parametric modeling process. These zones are separate elements with generalized properties which allow to arbitrarily assign cross-sectional area and moment of inertia. The approach of representing the axial stiffness of the connection with "connection-zones" was previously described in the study by [4]. In this study, the axial and rotational stiffness are assumed to be linearly dependent on cross-sectional area and the second moment of inertia respectively. Thus, reduction factors can be introduced, which account for the reduced cross-sectional area and reduced moment of inertia in the connections. A dimensionless reduction factor equals the ratio between the reduced property of the "connection-zone" and the connected element, e.g. $k_{red,A} = A_{red}/A_{main}$ or $k_{red,I} = I_{red}/I_{main}$.

The glulam frame in the current study consists of a set of beams, columns, and diagonals, which are connected to each other with dowels and slotted-in steel plates (Fig. 12(a)). The "connection-zones" were assigned at the endpoints of beams and diagonals, (Fig. 12(b)). The ends of "connection-zones" are tied to the connected elements at their centerlines. The "main" element in this context is either the glulam beam element which is connected to the column with the dowel connection or the glulam diagonal element, which is connected to the glulam column, and beam elements with the dowel connection. The length of "connection-zones" is assumed to be equal to the height of the main element (beam or diagonal). The cross-sectional area and moment of inertia are related to the connected structural element through the reduction factor k_{red}. Material properties of the connected glulam section are assigned to the "connection-zone" element and the density is modified according to the change in geometry to keep the mass unaltered.

3.4. Non-structural elements

External walls and internal partitions were modeled for the purpose of investigating their contribution to the global dynamic behavior of the building. External walls in the building of interest are composite and
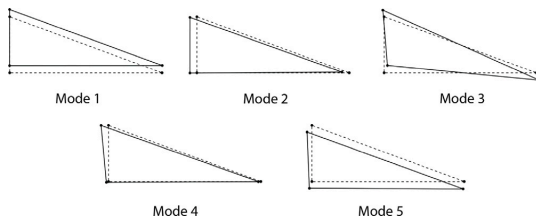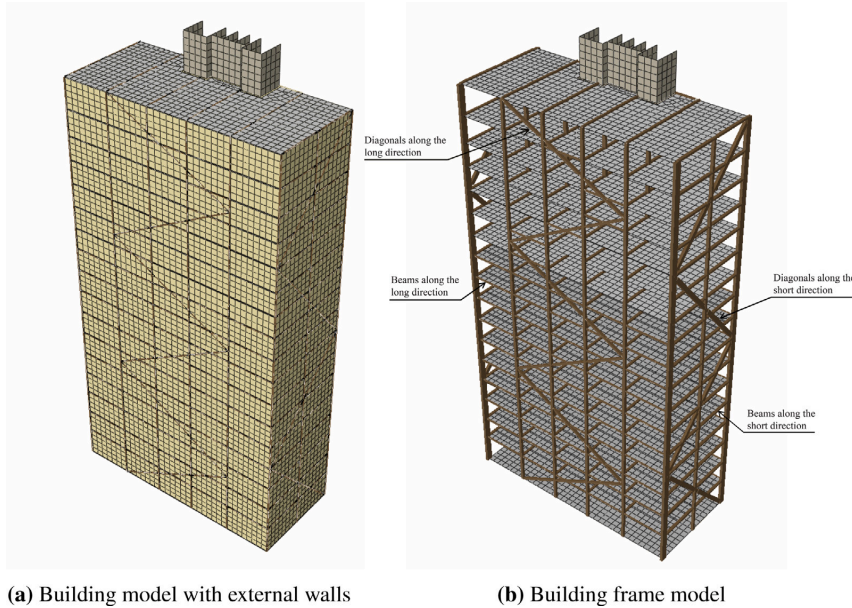
detailed model of the composite timber deck was developed in Abaqus as shown in Fig. 11. The pressure load was applied in three orthogonal directions and the resulting deflections were then used as objective functions to optimize the elastic constants of an orthotropic shell element, shear properties were kept the same. This shell element was then used as a simplified model of the composite deck in the building model to reduce computational time and facilitate model updating. The resulting material properties after optimization are shown in Table 2 and the thickness of the shell element was 240 mm.

The material properties used for wooden elements in the numerical modeling are given in Table 1. The concrete with a density of 2400 kg/m³, an elastic modulus of 34 GPa, and a Poisson ratio of 0.2 was used for modeling.

3.2. Modeling mass

Building structural system consists mainly of prefabricated timber elements with known material and geometric properties. Thus, it is assumed that it is possible to estimate the dead load distribution accurately. Estimates of added mass, which include the mass of non-structural elements and live load contribution were made. The added mass was applied as a uniformly distributed load on the floor elements. The mass estimates of external walls and internal partitions were taken from the technical report of the Norwegian research organization [33]. The weight of the external wall is 1 kN/m² and the weight of internal partitions is 0.5 kN/m². According to the Eurocode 1 [9], the specified live load values shall be based on the occupation type of the floor and a fraction of this live load shall be assigned as structural load for serviceability limit state (SLS) (Table 3). However, these values significantly overestimate the actual live load in the current building. Based on the architectural layout of different occupational floors, the actual live loads were investigated and calculated and results are shown

(a) Building model with external walls   **(b)** Building frame model

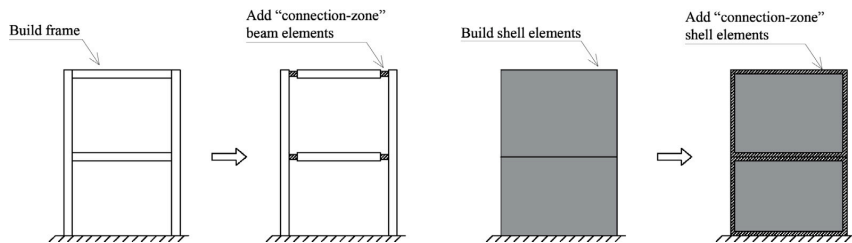**Fig. 9.** Numerical model of the building with mesh geometry.

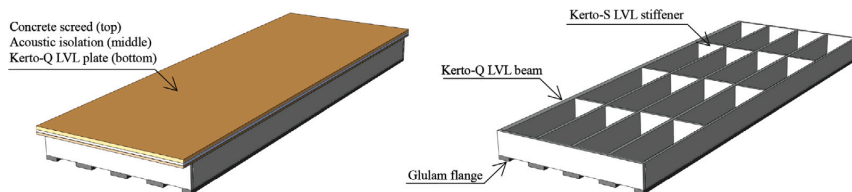**Fig. 10.** Sequence of adding "connection-zones" to the building model.

Fig. 11. Model of the composite timber deck.

consist of several layers. The inner layer starts with the 13-mm gypsum plasterboard, followed by the 198-mm isolation made of mineral wool and 13-mm wind barrier made of gypsum plasterboard. The outer layer consists of the external timber cladding followed by timber framing work with 73-mm air gap. The external wall is attached to the Kerto-Q timber panel with screws and angles. The Kerto-Q panel is in turn supported by the composite timber floor which transfers the load to the load-carrying glulam beams.

External walls were modeled as simplified 4-node elastic shell elements in order to investigate their stiffness contribution to the dynamics of the whole structure. Similar to the "connection-zones" in glulam frames described earlier in this chapter, separate shell elements were assigned also between the external wall and the glulam element to represent the "connection-zone" (Fig. 13). The in-plane stiffness of the connection represented by the shell element is assumed to be directly related to its thickness. The variation of stiffness in the shell connection is performed by introducing the reduction factor, k_{red}, which represents
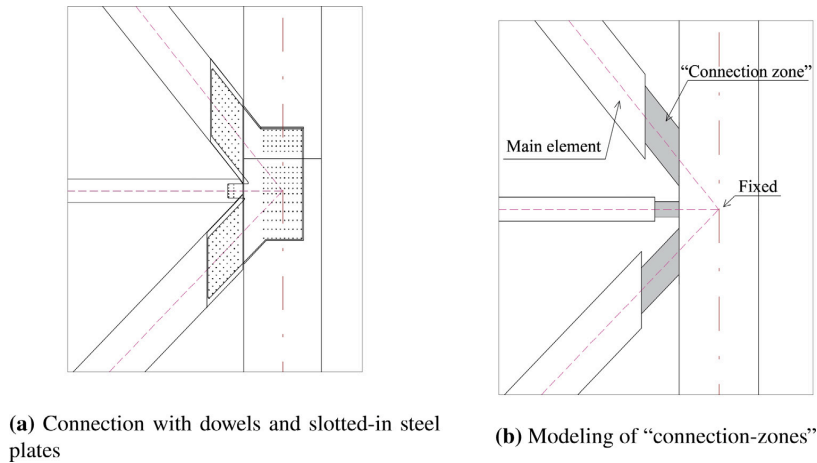
(a) Connection with dowels and slotted-in steel plates

(b) Modeling of "connection-zones"

Fig. 12. Modeling of glulam frame with "connection-zone" beam elements.

reduction in thickness of the "connection-zone" element with respect to the main shell element, t_{red}/t_{main}. In this context, the "main shell" element is an external wall element (or a partition wall element described later in the section), which is connected to the adjacent structural timber elements such as glulam frame and floors. The length of the shell "connection-zone" element is assigned to be equal to the thickness of the external wall element. The "connection-zone" elements are tied to the adjacent elements at the centerlines (Fig. 13).

Based on the composition of the external wall, only gypsum plasterboard can be considered as a material with stiffness contribution. However, the numerical implementation of such small "connection-zone" elements in comparison to their length is not feasible, since it requires much finer mesh, which in turn leads to significantly increased computational time. Thus, the lowest value for plasterboard thickness in the numerical implementation was limited to 100 mm, which is around 10 times higher than the actual single gypsum plasterboard thickness. Since the thickness of the gypsum plasterboard in the numerical model increased in comparison to actual thickness, the values for the stiffness should be reduced accordingly to represent the actual panel behavior. Therefore, FEM models of the external wall consisting of double-layer 13-mm gypsum plasterboard and 100-mm plasterboard were developed and an optimization study with a deflection as objective function was conducted. The elastic modulus of a single 13-mm gypsum plasterboard was taken from the literature and is equal to 140 MPa [35], the shear modulus was taken as 70 MPa. Then, the optimization study was conducted on the 100-mm plasterboard to determine the stiffness properties of the panel with the objective function being shear deflection values. Gypsum plasterboards were modeled with 4-node elastic isotropic shell elements. The resulting elastic and shear moduli of the 100-mm plasterboard corresponding to the double layer gypsum plasterboard from the external wall after optimization were 36.4 MPa and 18.2 MPa respectively.

Internal partition walls in the building are made of two layers of 13-mm gypsum plasterboards on each side of the wall, separated by a 100-mm gap for steel framing studs. Internal partitions are structurally connected to the floors elements. Similar to the external walls, the in-plane stiffness contribution is assumed to come from the gypsum plasterboards. Therefore, the modeling approach described in the previous paragraph was applied. The "connection-zone" elements were introduced at the top and bottom of the partition wall elements at the location where they are attached to the floor elements. The lower limit
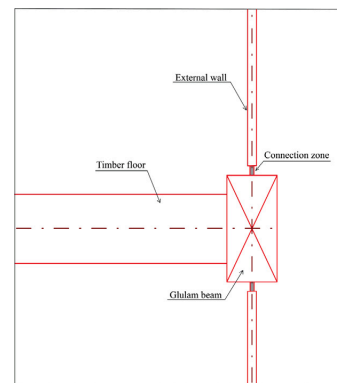

Fig. 13. Modeling of the external wall with "connection-zone" shell elements.

for modeling the thickness of internal partition elements was 100 mm, which is around 2 times higher than the actual gypsum plasterboard thickness. Thus, a similar optimization technique to the one used for external walls was implemented. The resulting values of elastic and shear moduli after optimization were 72.8 MPa and 36.4 MPa for an isotropic model of the 100-mm gypsum plasterboard.

The elevator and staircase shafts in the building are made of CLT panels stacked on top of each other. The shafts are not intended to carry any lateral load and were not considered as part of the load-carrying system during the design process. The CLT panels are connected to the floors at each level by means of steel brackets and screws. "Connection-zone" shell elements have been added between the CLT shaft elements and a sensitivity study has been conducted, where the thickness of the "connection-zone" element was varied in the range 0.1–1.0 while keeping all other parameters fixed. The change in the outputs of interest, i.e. eigenfrequencies and MAC values (explained in the further sections) was negligible, with maximum change reaching 0.4%. Thus, the study on the impact of the stiffness contribution from CLT shafts was not included in the present parametric study. The fixed value for the thickness of the "connection-zone" between the CLT shafts and floor elements ($t_{CLT} = 0.5$) was used.

4. Model updating

Sensitivity-based model updating based on ambient vibration data has been proven to be effective in their application on real structures in structural engineering [36]. The numerical model of the building presented in this study was scripted in Python [37], and the properties of interest were parametrized in order to investigate their sensitivity and conduct model updating using the results from the experimental setup.

4.1. Parameter selection

The dynamic modal response of the numerical model of the building depends on both mass and stiffness properties. Optimization of both mass and stiffness can lead to an underdetermined problem with an infinite number of solutions as mentioned in [38]. The mass properties are not investigated in the current study since it is assumed that density and geometric properties of the prefabricated elements can be well estimated in comparison to the connection stiffness properties. The glulam bending modulus of elasticity (MOE) and density (ρ) have a coefficient of variance values (COV) of 0.13 and 0.1 respectively [39]. In addition, the actual live load estimates were calculated based on the architectural drawings and site visits, and these values are applied to the numerical model. The stiffness properties in the numerical model include the stiffness of main load-carrying elements (glulam frame and slabs), connections between those elements, and potentially non-structural elements. The stiffness parameters of the timber structural elements, such as Young's modulus, are taken from the specification of the manufacturer and the highly layered composition of the glulam elements ensures the mean value properties of the wooden elements. On the other hand, the stiffness of connections in timber lacks accurate representation. The current practices on the prediction of connection stiffness do not give accurate values for the stiffness of the connection. Additionally, the effect of non-structural elements is generally excluded but might contribute significantly in low-level dynamics. Therefore, stiffness of connections in the glulam frame as well as connections in the non-structural elements were chosen for parametric analysis.

Based on the results from the ambient vibration measurements, it can be seen that the first two bending mode frequencies, as well as the two second bending mode frequencies, are very close to each other. This might be due to the fact that the span of diagonals, which are part of the lateral load resisting system, is similar in both directions (Fig. 5(a)). Therefore, the connection stiffness was studied separately in two directions of the building plane in order to investigate their effect on the dynamic response of the building. Table 4 shows the list of parameters of interest. Each of those parameters is a "connection-zone" element in the numerical model. "Long" and "short" subscripts stand for "connection-zone" elements in the long and short direction of the building respectively (Fig. 9(b)). I_{short} and I_{long} are moments of inertia of the "connection-zone" elements at the end of a beam element, where it is connected to the column. The range in values for I_{short} and I_{long} is given as a percentage of the main element and is representative of reduction in the rotational stiffness of "connection-zone" elements, k_{red}. The range of values for A_{long} and A_{short} is given as a percentage of the connected element and give the reduction in axial stiffness of "connection-zone" elements, k_{red}. Similarly, A_{long} and A_{short} represent the "connection-zone" in the truss diagonals at the points where they are connected to the beams and columns (Fig. 9(b)). A preliminary parameter study showed that the moment of inertia in diagonals and axial stiffness of the beams have no significant effect on the eigenfrequencies of the building. This is consistent with the truss-type structural system of the building, where diagonals were designed to carry the horizontal loads, which leads to insignificant axial stiffness contribution from beams. Therefore, only moments of inertia of beam connections and areas of the diagonal connections are studied in the glulam frame.

The connections between the non-structural elements and the main structure are given in terms of the thickness of the connection (Table 4). $t_{external}$ is the thickness of "connection-zone" elements which are located at the top and bottom ends of the external wall panels where they are connected to glulam beams. The range of values for $t_{external}$ is given as a percentage of the thickness of the external wall and represents a reduction in the in-plane stiffness of the "connection-zone" elements. $t_{partition}$ is the thickness of the "connection-zone" elements which are located at the top and bottom ends of the partition wall elements, where they are connected to the floor elements. The range of values for $t_{partition}$ is given as a percentage of the thickness of the internal partition walls and represents a reduction in the in-plane stiffness of the "connection-zone" elements. Both $t_{external}$ and $t_{partition}$ represent the reduction in stiffness contribution to the main structure.

4.2. Sensitivity analysis

Sensitivity analysis was performed to assess the effect of the parameters of interest on eigenfrequencies and modal assurance criterion (MAC, explained below) values. The range for each parameter was set as a percentage value of the property of the main element, Table 4. The lowest value represents the negligible stiffness transfer, whereas the highest value represents the full stiffness transfer, i.e. rigid connection. MAC is the measure of the correlation between the two sets of modes and is calculated as shown below [40]:

$$MAC(r,q) = \frac{\left| \{\varphi_A\}_r^T \{\varphi_X\}_q \right|^2}{\left(\{\varphi_A\}_r^T \{\varphi_A\}_r \right) \left(\{\varphi_X\}_q^T \{\varphi_X\}_q \right)} \tag{4}$$

where $\{\varphi_X\}_q$ is the experiment modal vector for mode q, $\{\varphi_A\}_r$ is the analytical modal vector for mode r. MAC takes values between 0 (no similarity between modes) and 1 (high similarity between modes). When several modes are compared, the result is a MAC matrix where diagonal elements have values of 1 in ideal situation.

The Latin Hypercube Sampling (LHS) method was adopted for the current sensitivity study. LHS is a Monte-Carlo type technique, which allows for exploring the entire parameter range with minimized computational demand [41]. In LHS, the parameter design space is uniformly divided with the same number of divisions N for all factors. The parameter levels are then randomly combined to create a Latin Hypercube design matrix with N points. In this study, the sensitivity analysis with LHS was performed using the Design of Experiments (DOE) component of ISight, a tool for automated simulations which can be integrated into Abaqus CAE [42]. The number of samples, $N=100$ was selected for analysis and a uniform distribution was chosen for each parameter, K. The $N \times K$ matrix is generated from the randomly sampled values and based on this matrix simulations explore the sensitivities of the input parameters and evaluate their significance by calculating the partial rank correlation coefficients ($PRCC$). $PRCC$ is the measure of the linear relationship between the parameter of interest and the output.

Sensitivity analysis was performed on a total of 6 input parameters with respect to 9 outputs (5 natural frequencies and 4 MAC values). The summary of the sensitivity study is shown in Fig. 14. For better representations, the absolute values of partial rank correlation coefficients of each parameter were plotted both against eigenfrequencies and MAC values. Based on the sensitivity ranks for eigenfrequencies, parameters A_{long} and A_{short} have the largest contributions to most frequencies (Fig. 14(a)). Parameter I_{short} has a significant effect on natural frequencies as well. Natural frequencies from mode 2, 4 and 5 have some contribution from I_{long}, $t_{partition}$ and $t_{external}$. Most of the MAC values, Fig. 14(b), have the dominant contribution from A_{short}. The first two MAC values are affected by A_{long}, whereas the last two MAC values are affected by A_{short} and I_{short}. Most of the MAC values have minor contributions from I_{long}, $t_{external}$ and $t_{partition}$. Mode 4 is affected considerably by $t_{external}$. Based on the results of the sensitivity analysis, all 6 parameters from Table 4 were chosen for model updating.

Table 4
Parameters for sensitivity analysis and model updating.

"Connection-zone" parameter	Description	Range of k_{red} [% of main element]
I_{short}	Moment of inertia of beams in long direction	1–100
I_{long}	Moment of inertia of beams in short direction	1–100
A_{short}	Cross-sectional area of diagonals in short direction	1–100
A_{long}	Cross-sectional area of diagonals in long direction	1–100
$t_{external}$	Thickness of connection between external wall and beam	1–100
$t_{partition}$	Thickness of connection between internal partition and floors	1–100

(a) Absolute ranks for eigenfrequencies
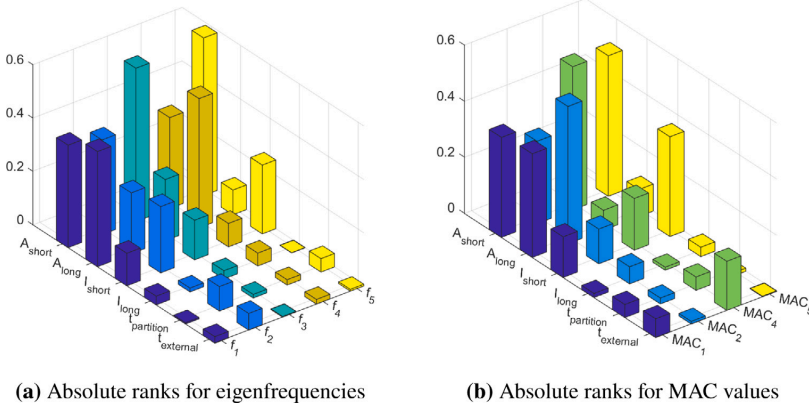
(b) Absolute ranks for MAC values

Fig. 14. Absolute partial rank correlation coefficients.

4.3. Model updating

The purpose of the model updating is to minimize the difference between the numerical model and the experimental modal response. The objective function for model updating included the modal parameters: 5 lowermost eigenfrequencies ($f_1 - f_5$) and MAC values for the 1st and 2nd bending modes in two translational directions ($MAC_1, MAC_2, MAC_4, MAC_5$). MAC value for torsional mode (MAC_3) was not included in model updating due to the lack of sensors to accurately estimate the mode shape. The objective functions used in the model updating are given as follows:

$$F_{freq} = \sum_{i=1}^{n} \gamma_i \left(\frac{f_{i,exp} - f_{i,num}}{f_{i,exp}} \right)^2 \tag{5}$$

$$F_{MAC} = \sum_{i=1}^{n} \gamma_i \left(1 - diag(MAC(\phi_{i,exp}, \phi_{i,num})) \right) \tag{6}$$

where F is an objective function, $(*)_{i,exp}$ is the experimental output of mode i, $(*)_{i,num}$ is the numerical output of mode i, ϕ is the mode shape vector, γ_i is the weight factor, which was set to 1 for $f_1 - f_3$ and $MAC_1 - MAC_2$ values, the higher modes weight factors were set to 0.5. The higher weight factor was used for lower modes due to the fact, that they are better identified in the OMA analysis and the mode shapes have the simple cantilever form, while higher modes have a higher level of uncertainty.

Model updating was performed using the ISight tool which can be integrated into the Abaqus CAE, where the numerical model of the building was created. The Multi-Island Genetic Algorithm was chosen for optimization [43]. Genetic Algorithms (GAs) are optimization algorithms based on natural selection and genetics concepts. GAs work on the population of possible solutions, where each individual solution is assessed based on the quality of the result (how far it is from the target values). The mating pool is then generated from the high-quality individual solutions, and parent combinations are selected from this

pool to produce an even higher quality offspring. In Multi-Island GA, there are several mating pools in which high-quality individual solutions are generated, and periodically these pools exchange a portion of their population in a process called migration. In this study the number of islands (mating pools) was set to 10, the sub-population size and the number of generations were set to 10, the rate of migration was set to 0.01.

4.4. Model updating results

Model updating has been performed using four different sets of parameters. In Set 1, all of the parameters from Table 4 were used for model updating. In Set 2, parameters I_{short} and I_{long} were combined into one parameter I_{beam}, and parameters A_{short} and A_{long} were combined into one parameter $A_{diagonal}$. Parameters $t_{external}$ and $t_{partition}$ were included into the second set as well. The purpose of generalizing stiffness parameters into I_{beam} and $A_{diagonal}$ is to compare with the results of the first set updating and observe whether the generalized axial and rotational stiffness parameters will be able to predict the building dynamic response. Set 3 includes parameters I_{short} and I_{long} for beam rotational stiffness and parameters A_{short} and A_{long} for diagonal axial stiffness. Parameters $t_{external}$ and $t_{partition}$ are excluded from model updating in Set 3. Set 4 includes only two parameters: I_{beam} and $A_{diagonal}$. Parameters $t_{external}$ and $t_{partition}$ were kept constant and were excluded from model updating in Set 4.

The results of the FE model updating with Set 1 parameters are shown in Tables 5 and 6. The range for parameters in model updating was chosen the same as in the sensitivity analysis, confer Table 4. Approximately 1000 iterations were performed in model updating to explore the entire design space. The initial values in Table 6 were chosen to represent the starting assumption of pinned connections in the glulam frame and negligible stiffness contribution from non-structural elements. Table 5 shows the natural frequencies and MAC

Table 5

Comparison between experimental and numerical modal properties (Set 1).

Mode	Initial model			Updated model (Set 1)			Experimental
	f [Hz]	Difference	MAC	f [Hz]	Difference	MAC	f [Hz]
1	0.506	2.64%	0.82	0.511	3.65%	0.93	0.493
2	0.509	−3.78%	0.88	0.518	−2.08%	0.97	0.529
3	0.820	0.86%	–	0.817	0.49%	–	0.813
4	1.915	−0.16%	0.25	1.954	1.88%	0.85	1.918
5	1.957	−8.81%	0.38	1.972	−8.11%	0.97	2.146

Table 6

k_{red} values for Set 1 after model updating.

Parameter	Initial	Updated
I_{short}	1%	65.3%
I_{long}	1%	92.7%
A_{short}	100%	33.5%
A_{long}	100%	68.3%
$t_{external}$	1%	94.1%
$t_{partition}$	1%	45.8%

values after model updating along with the initial model results and experimental natural frequencies. It can be seen that while there is a slight improvement in natural frequencies, MAC values have improved significantly after model updating. In particular, considerable improvement in mode shape prediction is observed for modes 1 and 2. The total objective function improved from 0.647 to 0.071 after model updating, resulting in an 89% decrease. The numerical mode shapes after model updating are shown in Fig. 15.

The updated values of I_{short} and I_{long} increased considerably compared to the initial values (Table 5). This means that the glulam connections have considerable rotational stiffness contribution which is different from the pin-condition assumption that was selected initially. The value of I_{long} updated to 92.7% of the main element, while the updated value for I_{short} is 65.3%. The values of A_{short} and A_{long} were reduced in comparison with the initial values, which means that the initial assumption of full axial load transfer in the connection was not sufficient. Similarly to the moments of inertia, updated A_{long} value is larger than the updated A_{short}, 68.3% and 33.5% respectively (Table 6). The parameters $t_{external}$ and $t_{partition}$, which represent the non-structural elements contribution, increased significantly from their initial value. Tables 7 and 8 show the summary of the model updating for Sets 1–4. In comparison with the Initial Set, the objective function for Sets 1–4 was lower after model updating. However, the objective function for Sets 2–4 was higher than for Set 1, which had an objective function value of 0.071. As seen from Table 7, the eigenfrequencies achieved after model updating with Sets 1–4 were in good accordance with the experimental results. Model updating with Sets 1–3 achieved acceptable MAC values.

5. Discussion

The discussion of the model updating results in this section is based on the assumption that the structural masses, live loads, and structural material stiffness properties were estimated with an acceptable level of uncertainty. While the authors have used their best engineering judgment in the calculation of structural masses and live loads, the uncertainty related to these estimations can still be considerable. The presented numerical modeling approach of the glulam building using "connection-zones" helps to generalize the connection properties making it easier for practicing engineers to use the obtained results as a reference for their prediction models.

5.1. Glulam connections

Dowelled glulam connections exhibit a nonlinear behavior even at low excitation levels due to several factors including an initial slip of dowels inside the drilled holes and inherent cracks and imperfections

of the applied timber material [4]. Therefore, the structural behavior of the dowelled connections is subject to uncertainty. Several sensitivity studies have been done to explore the effect of both axial and rotational stiffness of glulam frame connections on the vibration response of the building [4,6]. The studies on the sensitivity of the rotational stiffness showed a negligible difference between the pinned connections and connections with stiffness values based on Eurocode 5 calculations [6]. The Eurocode 5 calculations, however, lack the accurate representation of the connection stiffness and underestimate the actual value based on the sub-assembly experimental results [10]. On the other hand, the rigid connection scenario in the study by [6], showed a considerable increase in fundamental frequencies of the building.

Model updating of parameters I_{long} and I_{short} in this study showed that the rotational stiffness in glulam connections is neither negligible, nor rigid, but rather exhibits a semi-rigid behavior. Similarly, the axial stiffness parameters A_{long} and A_{short} have updated values which are less than the initial value of 100% of the main elements, meaning that connection is semi-rigid in the axial direction as well. The sensitivity study by [4] showed that variation of axial stiffness in glulam truss has an effect on the eigenfrequencies of the structure, which is consistent with the findings in this paper. As seen from Table 6, both A_{long} and I_{long} have updated values, which are consistently higher than the values of A_{short} and I_{short} respectively. The model updating of glulam timber frame connections implies that there exists significant variation in the stiffness, which should be investigated further. The geometry of the building might have a considerable impact on the updated stiffness of the connections since it can be seen that the model updating with separate elements for long and short directions achieves better results in comparison with other sets.

5.2. Non-structural elements

The study explored the effect of the external wall and internal partition stiffness on the dynamic response of the building. By modifying the connection thickness parameters, $t_{external}$ and $t_{partition}$, the contribution of non-structural member stiffness was varied from negligible, $t_* = 1\%$, to a full stiffness transfer, $t_* = 100\%$. Based on the sensitivity study, the external partition stiffness contribution to the natural frequencies was insignificant since the load-bearing contribution consisted only of two 13-mm thick gypsum plasterboards and low stiffness. However, there was a noticeable effect on the MAC values (Fig. 14(b)) for modes 1 and 4 (Fig. 15). After Set 1 model updating the value of $t_{external}$ was 94.1% of the main shell element, whereas after Set 2 model updating the value of $t_{external}$ was 88.6%. The actual connection between the external wall and main structure is, however, not very rigid based on the detailing drawings. On the other hand, the stiffness contribution from non-structural elements might be considerable at low-level vibrations and further investigation is required on the topic. The internal partitions have a slightly higher stiffness contribution compared to external walls since they consist of the 2-ply double-sided gypsum plasterboard with a steel frame. Therefore, non-structural element parameters $t_{external}$ and $t_{partition}$ have contributions to mode shapes of the structure and should be accounted for when performing modal analysis of the building. The results of the model updating showed that under ambient vibrations, the non-structural members have a considerable impact on the MAC values in the dynamic response of the timber building, which is consistent with the previous studies [14,15].
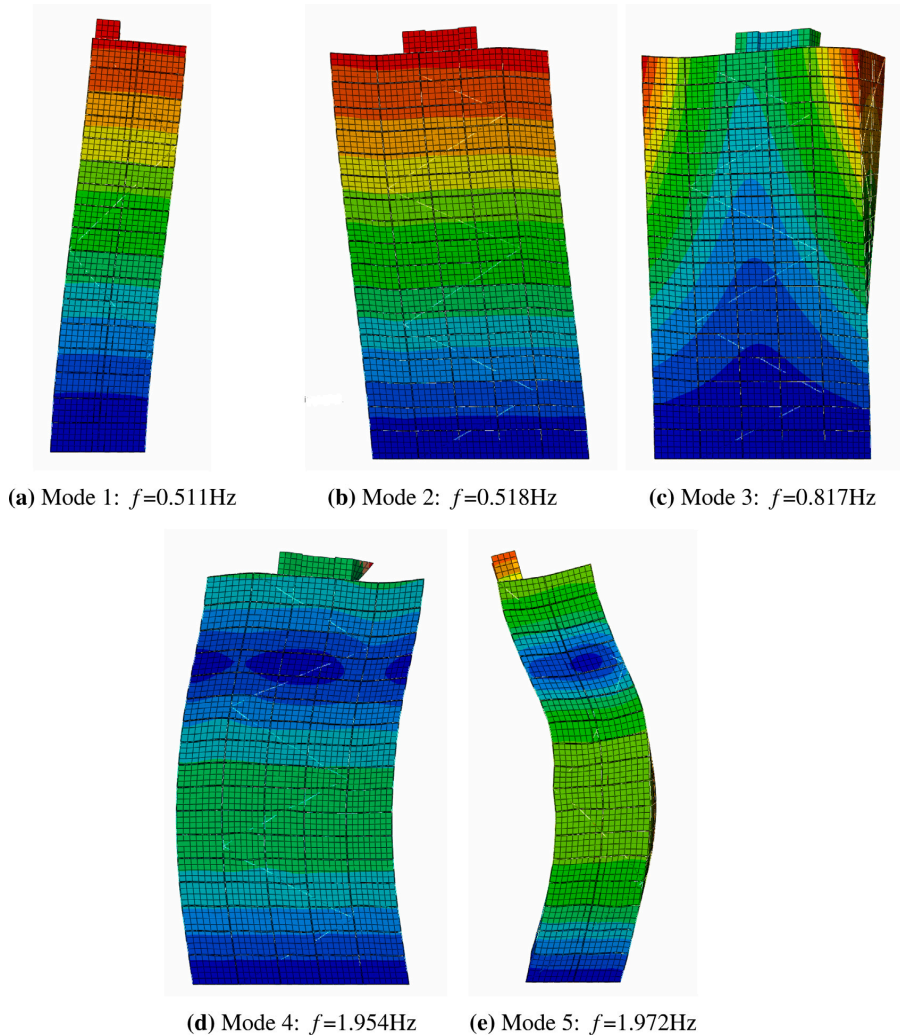
(a) Mode 1: f=0.511Hz **(b)** Mode 2: f=0.518Hz **(c)** Mode 3: f=0.817Hz

(d) Mode 4: f=1.954Hz **(e)** Mode 5: f=1.972Hz

Fig. 15. Numerical mode shapes after model updating with the first set.

Table 7
Comparison between experimental and numerical modal properties for all sets.

Mode	Set 1			Set 2			Set 3			Set 4			Experim.
	f [Hz]	Change [%]	MAC	f [Hz]	Change [%]	MAC	f [Hz]	Change [%]	MAC	f [Hz]	Change [%]	MAC	f [Hz]
1	0.511	3.6	0.93	0.510	3.4	0.88	0.513	4.0	0.93	0.507	2.8	0.73	0.493
2	0.518	−2.0	0.97	0.513	−3.0	0.93	0.519	−1.89	0.97	0.509	−3.7	0.79	0.529
3	0.817	0.4	–	0.826	1.6	–	0.817	0.4	–	0.821	0.98	–	0.813
4	1.954	1.8	0.85	1.961	2.24	0.81	1.966	2.5	0.84	1.954	1.88	0.70	1.918
5	1.972	−8.1	0.97	1.970	−8.2	0.93	1.979	−7.7	0.96	1.959	−8.71	0.85	2.146

6. Conclusions

This paper presents an approach to model connections in glulam frame buildings. "Connection-zones" are introduced in the model and represent the rotational and axial stiffness, in this case, of doweled connections. This approach allows for the implementation of modeling of the connection stiffness influence on the dynamic response of building in a parametrized manner. The dynamic properties of the glulam timber frame building have been achieved successfully using the proposed approach for connections modeling. An ambient vibration procedure and subsequent system identification of an instrumented 18-storey glulam building identified 5 vibrational modes, which were used for model validation and model updating. In summary, the axial stiffness parameter has the largest impact on both fundamental frequencies and

Table 8

k_{red} values for all sets after model updating.

Parameter	Initial	Set 1	Set2	Set 3	Set 4
I_{short}	1%	65.3%	3.4%	83.1%	1.0%
I_{long}	1%	92.7%	3.4%	51.0%	1.0%
A_{short}	100%	33.5%	88.1%	34.0%	97.0%
A_{long}	100%	68.3%	88.1%	94.9%	97.0%
$t_{external}$	1%	94.1%	88.6%	–	–
$t_{partition}$	1%	45.8%	82.6%	–	–
$Obj.function$	0.647	0.071	0.119	0.075	0.360

MAC values, whereas the rotational stiffness parameter has the least impact. The non-structural parameters accounting for external walls and internal partitions have a considerable effect on the MAC values of the structure. The assumption of an accurately predicted mass was adopted, which is the main limitation in the current study since there is some uncertainty in relation to the mass estimates. A future study will include the long-term monitoring of the building in order to evaluate the dependence of the amplitude of the wind-induced vibrations. The authors believe that the stiffness ratios for "connection-zones" in this study can serve as a useful reference for practitioners designing glulam timber frame buildings.

CRediT authorship contribution statement

Saule Tulebekova: Conceptualization, Methodology, Validation, Investigation, Formal analysis, Writing – original draft, Writing – review & editing, Visualization. **Kjell Arne Malo:** Conceptualization, Methodology, Writing – review & editing, Supervision, Project administration, Funding acquisition. **Anders Rønnquist:** Conceptualization, Methodology, Writing – review & editing, Supervision. **Petter Nåvik:** Investigation, Writing – review & editing.

Declaration of competing interest

The authors declare that they have no known competing financial interests or personal relationships that could have appeared to influence the work reported in this paper.

Acknowledgments

References

[1] Zubizarreta M, Cuadrado J, Orbe A, Garcia H. Modeling the environmental sustainability of timber structures: A case study. Environ Impact Assess Rev 2019;78.

[2] Zhao X, Zhang B, Kilpatrick T, Sanderson I, Liu D. Numerical analysis on global serviceability behaviours of tall glulam frame buildings to the eurocodes and UK national annexes. J Civ Eng Const 2021;10:109–22.

[3] Ramage M, Burridge H, Busse-Wicher M, Fereday G, Reynolds T, Shah D, et al. The use of timber in construction. Renew Sustain Energy Rev 2017;68:333–59.

[4] Malo K, Abrahamsen R, Bjertnæs M. Some structural design issues of the 14-storey timber framed building treet in Norway. Eur J Wood Prod 2016;74:407–24.

[5] Bjertnaes M, Malo K. Wind-induced motions of "Treet" - A 14-storey timber residential building in Norway. In: World conference on timber engineering. Quebec City, Canada; 2014.

[6] Lazzarini E, Frison G, Trutalli D, Marchi L, Scotta R. Comfort assessment of high-rise timber buildings exposed to wind induced vibrations. Struct Design Tall Spec Build 2021.

[7] Foster R, Reynolds T, Ramage M. Proposal for defining a tall timber building. J Struct Eng 2016;142.

[8] Reynolds T, Harris R, Chang W. Stiffness of dowel-type timber connections under pre-yield oscillating loads. Eng Struct 2014;65:21–9.

[9] CEN1991-1-1. Eurocode 1: Actions on structures. Part 1-1: General actions. Brussels, Belgium: European Committee for Standardization; 2002.

[10] Solarino F, Giresini L, Chang W, Huang H. Experimental tests on a dowel-type timber connection and validation of numerical models. Buildings 2017;7.

[11] Johansson M, Linderholt A, Jarnero K, Landel P. Tall timber buildings - A preliminary study of wind-induced vibrations of a 22-storey building. In: World conference on timber engineering. Vienna, Austria; 2016.

[12] Edskar I, Lidelow H. Dynamic properties of cross-laminated timber and timber truss-building systems. Eng Struct 2019;186:525–35.

[13] Li B, Hutchinson G, Duffield C. Contribution of typical non-structural components to the performance of high-rise buildings based on field reconnaissance. J Buil Apprais 2010;6:129–51.

[14] Mugabo I, Barbosa A, Riggio M. Dynamic characterization and vibration analysis of a four-story mass timber building. Front Built Environ 2019;5.

[15] Worth M, Omenzetter P, Morris H. Ambient and forced vibration testing and finite element model updating of a full-scale post-tensioned laminated veneer lumber building. In: 2012 new zealand society for earthquake engineering (NZSEE) annual conference. 2012.

[16] Ellis B, Bougard A. Dynamic testing and stiffness evaluation of a six-storey timber framed building during construction. Eng Struct 2001;23:1232–42.

[17] 14080 C. EN 14080-2013: Timber structures - glue laminated timber and glued solid timber - Requirements.. Brussels, Belgium: European Committee for Standardization; 2013.

[18] Abrahamsen R. Mjøstårnet - construction of an 81 m tall timber building. In: 23rd inernational holzbau-forum IHF 2017. 2018.

[19] 103 CE. NS-EN 10025-2. Hot rolled products of structural steels. Part 2: Technical delivery conditions for non-alloy structural steels. Brussels, Belgium: European Committee for Standardization; 2019.

[20] 10088 C. EN 10088-3-2014: Stainless steels. Part 3: Technical delivery conditions for semi-finished products, bars, rods, wire, sections and bright products of corrosion resisting steels for general purposes.. Brussels, Belgium: European Committee for Standardization; 2014.

[21] 338 C. EN 338-2016: Structural timber - strength classes. Brussels, Belgium: European Committee for Standardization; 2016.

[22] Moelven. Flervåningshus Trä8, https://www.moelven.com/se/produkter-och-tjanster/allt-om-limtra/flervaningshus-tra8/.

[23] MetsäWood. Mechanical properties. Kerto LVL. 2021, https://www.metsawood.com/global/Tools/MaterialArchive/MaterialArchive/Kerto-manual-lvl-mechanical-properties.pdf.

[24] Liven H. Treet i Bergen og Mjøstårnet i Brumunddal. Høyhus i tre - Utfordringer. 2017, https://www.treteknisk.no/resources/filer/aktuelt/brd-foredrag/Mjostarnet-og-andre-hoge-bygg.pdf.

[25] Kistler. MEMS capacitive triaxial accelerometer for low frequency applications, K-beam: Type 8396a2d0. 2021, https://www.kistler.com/en/product/type-8396a/.

[26] The Math Works I. MATLAB (R2020b). Natick, Massachusetts: The MathWorks Inc.; 2019.

[27] Van Overschee P, De Moor B. Subspace identification for linear systems: theory, implementation, applications. Leuven, Belgium: Kluwer Academic Publishers; 1996.

[28] Rainieri C, Fabbrocino G. Operational modal analysis of civil engineering structures: an introduction and guide for applications. New York, USA: Springer; 2014.

[29] Kvåle K, Øiseth O, Rønnquist A. Operational modal analysis of an end-supported pontoon bridge. Eng Struct 2017;148:410–23.

[30] Zhou X, Cao L, Khan I, Li Q. Data inspecting and denoising method for data-driven stochastic subspace identification. Shock Vib 2018;2018.

[31] Øiseth O, Rønnquist A, Kvåle K, Sigbjörnsson R. Monitoring wind velocities and dynamic response of the hardanger bridge. Springer, Cham; 2014, Dynamics of Civil Structures, Volume 2. Conference Proceedings of the Society for Experimental Mechanics Series.

[32] Simulia. Abaqus FEA software. Dassault systèmes; 2017.

[33] SintefByggforsk. Egenlaster for bygningsmaterialer, byggevarer og bygningsdeler. Byggforskserien 471.031, Trondheim, Norway: SINTEF; 2013.

[34] Shu Z, Li Z, Yu X, Zhang J, He M. Rotational performance of glulam bolted joints: Experimental investigation and analytical approach. Constr Build Mater 2019;213:675–95.

[35] Telue Y, Mahendran M. Behaviour and design of cold-formed steel wall frames lined with plasterboard on both sides. Eng Struct 2004;26:567–79.

[36] Kodikara K, Chan T, Nguyen T, Thambiratnam D. Model updating of real structures with ambient vibration data. J Civ Struct Health Monit 2016;6:329–41.

[37] Reed D, Wiig L. Parametric study of tall timber buildings. Trondheim, Norway: Norwegian University of Science and Technology; 2020.

[38] Aloisio A, Pasca D, Tomasi R, Fragiacomo M. Dynamic identification and model updating of an eight-story CLT building. Eng Struct 2020;213.

[39] JCSS. JCSS probabilistic model code. Part 3: Resistance models. Section 3.5. properties of timber. Joint Committee on Structural Safety; 2006.

[40] Pastor M, Binda M, Harcarik T. Modal assurance criterion. Procedia Eng 2012;48:543–8.

[41] Gomero B. Latin hypercube sampling and partial rank correlation coefficient analysis applied to an optimal control problem. Knoxville, Tennessee, USA: University of Tennessee; 2012.

[42] DassaultSystemes. Isight. Automated design exploration and optimization. 2014, https://www.3ds.com/fileadmin/PRODUCTS-SERVICES/SIMULIA.

[43] Chen H, Ooka R, Kato S. Study on optimum design method for pleasant outdoor thermal environment using genetic algorithms and coupled simulation of convection, radiation and conduction. Build Environ 2006;43:65–71.

Paper III

Tulebekova, Saule ; Ao, Wai Kei; Pavic, Aleksandar ; Malo, Kjell Arne ; Rønnquist, Anders.
Identification of modal properties of a tall glue-laminated timber frame building under long-term ambient vibrations and forced vibrations.

This paper is submitted for publication and is therefore not included.

Paper IV

INVESTIGATION OF LONG-TERM MODAL PROPERTIES OF A TALL GLUE-LAMINATED TIMBER FRAME BUILDING UNDER ENVIRONMENTAL VARIATIONS

Saule Tulebekova[1], Kjell Arne Malo[2], Anders Rønnquist[3], Petter Nåvik[4]

ABSTRACT: Evaluation of long-term modal properties, such as natural frequencies and damping ratios, is important for tall timber buildings, which can be prone to environmental variations. However, in long-term operational modal analysis, the estimation of modal properties, especially damping ratios can be subject to significant uncertainty due to requirement of stationarity of the input data. Therefore, a combined variational mode analysis and data-driven stochastic subspace identification method was used for modal identification to reduce the potential errors related to the input data. The method was employed to investigate the long-term modal properties of an 18-story glulam frame building using ambient vibration data of 18 months. The observed natural frequencies exhibit seasonal behaviour with an average variation of ±0.02 Hz. Damping ratios do not show a seasonal relationship as opposed to the natural frequencies. The identified natural frequencies tend to have an inverse relationship with the mean temperature, while a positive correlation between the natural frequencies and the relative humidity is observed.

KEYWORDS: dynamic identification, ambient vibrations, tall timber building, VMD, SSI, modal properties.

1 INTRODUCTION

Tall timber buildings are relatively new in the construction industry, and as a result, there is still much research being conducted to understand their dynamic response under different loads, including service loads [1]. In general, tall timber buildings tend to have a lower natural frequency compared to traditional steel and concrete buildings due to inherently low stiffness and mass properties. This means that they are more susceptible to vibrations caused by external forces such as wind or human activities, and this can affect their performance and occupant comfort [2]. Excessive vibrations during strong winds might lead to discomfort for building occupants, particularly on the higher floors, if the design is incorrect.

Modal identification is a process used to determine the natural frequencies, damping ratios, and mode shapes of a structure. It is an important step in evaluating the dynamic response of a structure, as it provides information about the behaviour of the structure under different loading conditions.

Different techniques and methods can be used for modal identification of structures. For example, the operational modal analysis (OMA) method, which relies on ambient vibrations induced by natural events, can be used to identify the dynamic properties of the structure under real-life operating conditions. Other techniques such as impact testing or shaking table tests can also be used to identify the dynamic properties, but they require significant planning and labour and can be quite costly. In comparison to other techniques, OMA is a cost-effective and relatively easy method, which is suitable for long-term measurements.

Data-driven stochastic subspace identification (SSI-DATA) is an OMA technique used to extract dynamic models from ambient vibration data. SSI techniques involve constructing a mathematical model of the structure using the measured response data. This model can then be used to estimate the properties of the structural system. One of the limitations of ambient vibration techniques for modal identification, such as SSI, is the assumption of stationarity. This assumption requires that the ambient vibration signals remain constant over time, which is not always the case in practice. Non-stationarity can occur due to changes in the ambient conditions, such as wind or temperature, or due to changes in the dynamic behaviour of the structure itself. To overcome this issue, the variational mode decomposition (VMD) can be used, which decomposes the initial signal into a set of oscillatory components containing the modes of the structure.

The modal identification of timber buildings presents some additional challenges that are unique to this type of construction. For example, timber structures are more susceptible to environmental factors such as temperature

and humidity, which can cause changes in their material properties over time. In addition, timber buildings tend to have a more complex and variable behaviour compared to traditional steel and concrete structures, which can make their modal identification more challenging.

Several studies investigating the effects of environmental variations on the dynamic properties of timber buildings are available [3,4]. However, no previous studies on the relation between the environmental factors and the dynamic response of tall glulam frame building were conducted.

Considering these challenges, this paper investigates the modal properties of a tall glue-laminated timber (glulam) frame building under long-term ambient and operational variations using combined VMD/SSI technique. The effect of the variational environmental conditions on the identified dynamic properties is investigated using the meteorological data from the nearby weather station.

2 FIELD MEASUREMENTS SETUP

2.1 BUILDING DESCRIPTION

Mjøstårnet is an 18-storey tall glulam (glue-laminated timber) frame building located in Brumunddal, Norway (Fig.1). As of March 2023, Mjøstårnet is considered the tallest residential timber building in the world [5]. The load-bearing system of the building consists entirely of structural timber elements. The building height is 88.8 meters and the structural system consists of glulam trusses connected with slotted-in steel plates [6]. Cross-laminated timber (CLT) is used in the elevator and staircase shafts and the floors are made of prefabricated timber decks (floors 1-10) and concrete decks (floors 11-18). The concrete decks are added purely as additional mass due to occupational serviceability requirements. The pergola truss is mounted at the top of the building for architectural appearance.

(a) Building location   (b) The Mjøstårnet building view
Fig.1. The Mjøstårnet building

2.2 EXPERIMENTAL SETUP

A long-term ambient vibration monitoring system was installed inside the building (Figs.2-4). The hardware in the system consists of three Kistler K-Beam® accelerometers, model 8395A2D0 [7], one CompactRIO controller by National Instruments, and connecting wires and cables. The accelerometers have sensitivity of 2000 mV/g and the sampling rate for data was 400 Hz. The building has been in full operational condition, therefore, the placement options for the long-term monitoring setup were quite limited. After the discussion with the building manager, the setup was installed in the emergency staircase shaft. This staircase could only be accessed in emergency cases only, therefore, it was not obstructing the normal operations of the building. Prior to the current accelerometer setup, the accelerometers were installed at the roof of the building. Therefore, to ensure that the captured modes from the current setup were representative of the global structural behaviour, the identified modes were compared against their counterparts from the setup on the roof. More details regarding the comparison of the two setups can be found in [8].
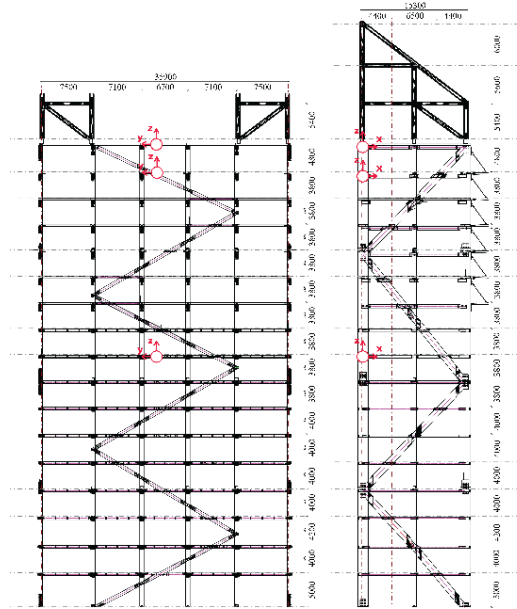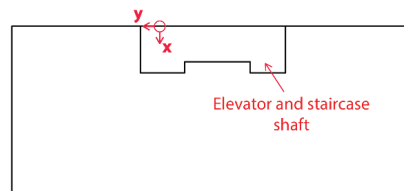

Fig.2. Accelerometer setup inside the building.

Fig.3. Plan view of accelerometer setup.

Fig.4. Long-term monitoring setup with the control box.

3   METHODOLOGY

The combined VMD and SSI-DATA methodology is outlined in the Fig.5. First, the initial ambient vibration data is decomposed into a set of modal components using the VMD technique. These identified modal components are then evaluated using the spectral analysis and the modes containing the structural behaviour are selected for further analysis. Then, the SSI-DATA technique is applied separately on each structural mode and the corresponding natural frequencies and damping ratios are identified. The following sections present the methodology in more detail.
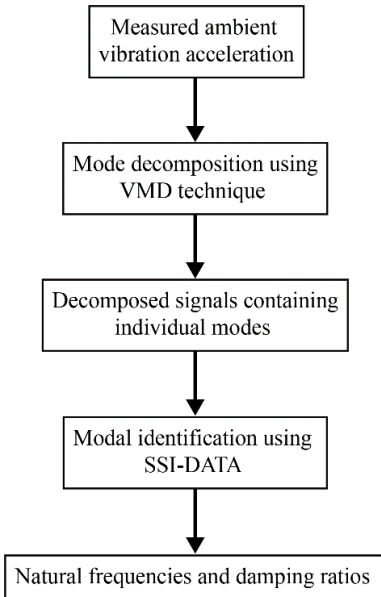
Fig.5. Combined VMD/SSI-DATA methodology.

3.1   VARIATIONAL MODE DECOMPOSITION (VMD)

VMD is a signal decomposition method that aims to decompose a complex signal into a set of intrinsic mode functions (IMFs) or oscillatory components [9]. Each IMF represents a distinct oscillation mode in the signal, which is characterized by a particular frequency and amplitude modulation. The VMD algorithm is based on an optimization problem that seeks to minimize the total power of the signal subject to a set of constraints. The constraints ensure that the extracted IMFs are spatially and temporally localized and are well-separated in the frequency domain. A more detailed description of the technique can be found in [9]. The VMD algorithm can be briefly described as follows:

- Obtain frequency spectrum of each mode by applying the Hilbert transform.
- Shift the frequency spectrum of the mode to the estimated centre frequency using the exponential tune.
- Solve the following minimisation problem to estimate the bandwidth of each mode using the Gaussian smoothness of the demodulated signal:

$$\min_{\{u_k\},\{\omega_k\}} = \left\{ \sum_k \left\| \partial_t \left[\left(\delta(t) + \frac{j}{\pi t} \right) * u_k(t) \right] e^{-j\omega_k t} \right\|_2^2 \right\}$$

$$s.t. \quad x(t) = \sum_{k=1}^{K} u_k(t)$$

where $u_k(t)$ are the decomposed modes, ω_k are the corresponding central frequencies, $\|.\|_2$ is the L2 norm, ∂_t is the derivative with respect to time, $\delta(t)$ is the Dirac delta function, $x(t)$ is the original signal.

After application of the VMD the initial signal is decomposed into a set of modes compacted around the central frequency. The signals containing structural modes are then selected for further analysis.

3.2   STOCHASTIC SUBSPACE IDENTIFICATION (SSI)

Once the signals containing structural modes were identified, thee data-driven stochastic subspace identification (SSI-DATA) technique is applied on each signal separately. The procedure for the SSI-DATA method is explained in detail in [10-12], and a brief description of the method is presented here. In SSI-DATA, the dynamic system is assumed to be described by the discrete state-space model:

$$\mathbf{x}_{k+1} = \mathbf{A}\mathbf{x}_k + \mathbf{w}_k \qquad (1)$$

$$\mathbf{y}_k = \mathbf{C}\mathbf{x}_k + \mathbf{v}_k \qquad (2)$$

where x is a state space vector, which holds the current state of the system at time instant t, y is a measured output at a specified sampling rate, w and v are system noise and measurement noise, respectively, A is a state matrix, and C is an output matrix.

The state-space model of order i is used to identify the eigenvalue μ_i, from which the corresponding pole λ_i can

be obtained at a sampling period t_s. Then, the frequency and damping values, ω_i and ξ_i, can be calculated for each pole. The expressions for the calculation process of the values mentioned above are as follows:

$$\lambda_i = \ln(\mu_i)/t_s \qquad (3)$$

$$\omega_i = Im(|\lambda_i|) \qquad (4)$$

$$\xi_i = -Re(\lambda_i)/|\lambda_i| \qquad (5)$$

Stabilization diagram is then plotted with the stability criteria for natural frequency and damping ratio of 1% and 5% respectively, and the vertically aligned poles on the stabilization diagram indicate a stable frequency.

4   RESULTS

4.1   MODAL DECOMPOSITION

The acceleration time series were processed separately in the x- and y-direction (see Fig.3 for coordinate reference). Acceleration time series were resampled to 8 Hz sampling rate and the band-pass filter between 0.2 Hz - 1.0 Hz was applied to remove the noise and response outside the range of interest. In total three fundamental frequencies were identified: mode 1 at 0.5 Hz (first bending in the x-direction), mode 2 at 0.54 Hz (first bending in the y-direction), and mode 3 at 0.84 Hz (torsion). Fig.6(top) shows the original acceleration time series containing noisy data in the x-direction with the corresponding Fourier spectrum, where the peaks at 0.5 Hz (mode 1, bending) and 0.84 Hz (mode 3, torsion) can be seen.

Below the original data series are the two decomposed signals, which are called the intrinsic mode functions (IMFs) using VMD method, which show only one peak at their respective frequencies, indicating that the signals containing fundamental modes have been successfully separated. Similarly, Fig.7 shows the original acceleration time series containing noisy data in the y-direction (top) and its decomposed IMFs containing the fundamental modes along with the Fourier spectra indicating the fundamental frequencies in y-direction: mode 2 (bending) and mode 3 (torsion). These intrinsic mode functions containing the modes of interest were further processed using the SSI-DATA technique to identify the natural frequencies, damping ratios and mode shapes. Each mode-containing signal was processed separately. The methodology was applied continuously over the entire monitoring period (Jan.2021-Jun.2022) on 1-hr data segments to investigate the variation of the identified modal properties with time.
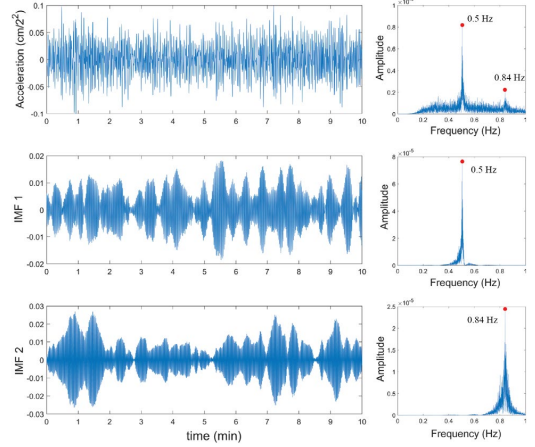

Fig.6. Input signal in x-direction (top) and its decomposed intrinsic mode functions (IMFs) with the corresponding Fourier spectra.
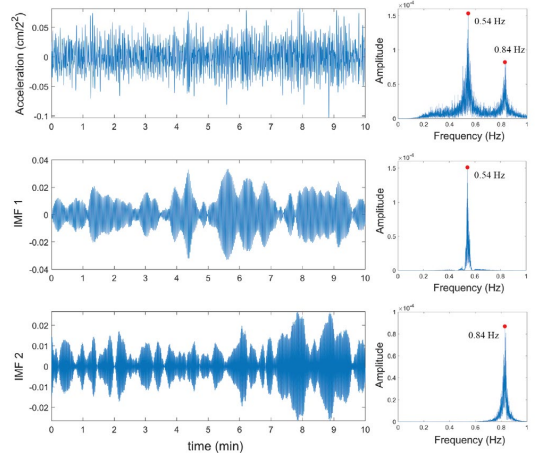

Fig.7. Input signal in y-direction (top) and its decomposed intrinsic mode functions (IMFs) with the corresponding Fourier spectra.

4.2   LONG-TERM MODAL PROPERTIES

The long-term monitoring records of the total of 18 months (Jan.2021-Jun.2022) were processed using the combined VMD/SSI-DATA methodology. Fig.8 shows the variation of the identified natural frequencies with time and the corresponding statistical distributions using 1-hour increments of the acceleration response for the first three modes of vibration. The torsional mode is plotted in both x- and y-direction. From observation, a seasonal pattern of natural frequencies can be observed. The highest values for natural frequencies are observed in the late winter (January-March), while the lowest values are observed in the late summer (July-September). The total natural frequency variation is ±0.015 Hz for mode 1, ±0.02 Hz for mode 2, ±0.03 Hz for mode 3. A larger scatter of identified values can be observed for mode 3 in

the x-direction compared to the y-direction which might be due to the accelerometer placement: location of accelerometers close to the centreline might not allow for a proper identification of the torsional mode in the x-direction.

Fig.9 shows the variation of the identified damping ratios with time and the corresponding statistical distribution using 1-hour increments of the acceleration response for the first 3 modes. Similarly, a larger scatter is observed for mode 3 in the x-direction compared to the y-direction. Unlike natural frequencies, no seasonal variation of damping ratios can be observed. The mean values for the identified damping ratios seem to be quite stable at values around 1% except for mode 3 in the x-direction, where a larger variation is observed.

From Figs.8 and 9, it can be seen that the natural frequencies and damping ratios can be identified quite stably indicating the effectiveness of the combined VMD/SSI-DATA technique for extraction of long-term modal properties from ambient vibration data.

4.3 EFFECT OF ENVIRONMENTAL CONDITIONS

The meteorological data from the closest weather station was used to investigate the effect of the environmental conditions on the identified dynamic properties. The location of the weather station is approximately 10 km away from the building and the weather statistics for the monitoring period was obtained from the Norwegian Climate Service Centre [13]. The following environmental properties were selected for further analysis: mean air temperature (°C) and mean relative humidity (%).

The building in this study is located in a region with humid continental climate with cold and dry winters and comfortably warm summers. The warmest month of the year is July with mean daily temperature of 17°C and the coldest month of the year is December with daily mean temperature of -4.5°C.

Fig.10 shows the mean daily natural frequencies for the first 3 modes plotted together with the mean daily air temperature. The smoothed variations using 1-month averaging window are plotted to represent the trend of the parameters with time. From observation, for all natural frequencies the variation occurs in a similar seasonal manner. The highest frequencies are observed in the late winter and the lowest frequencies are observed in the late summer, with an exception of the first frequency, where the additional peak can be observed in the early summer period. For modes 2 and 3 (x- and y-direction) an inverse relationship is observed between the natural frequencies and the air temperature. The inverse relationship might be caused by the delay between the variational changes and the structural response. For mode 1, the inverse seasonal relationship can be observed in the winter, however, in summer the frequencies seem to have an increasing trend with increase of temperature.
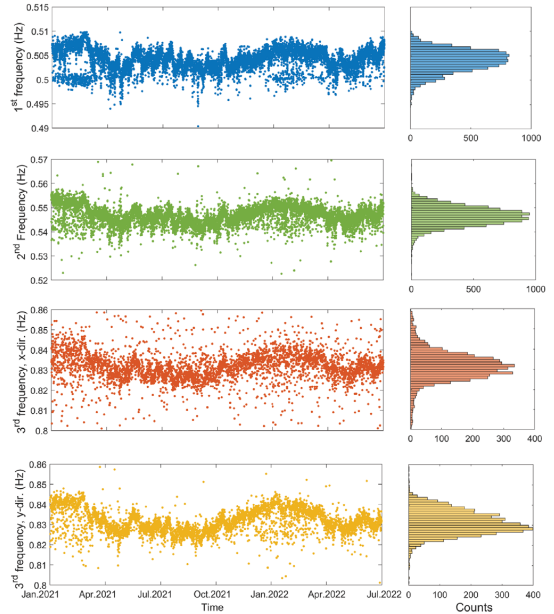

Fig.8. Variation of identified frequencies from 1-hour data segments over time (left) and the corresponding statistical distributions (right) for the first 3 modes of vibration.
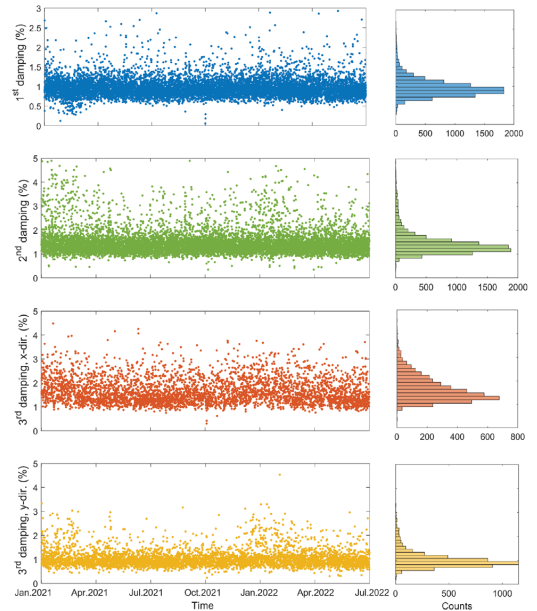

Fig.9. Variation of identified damping ratios from 1-hour data segments over time (left) and the corresponding statistical distributions (right) for the first 3 modes of vibration.
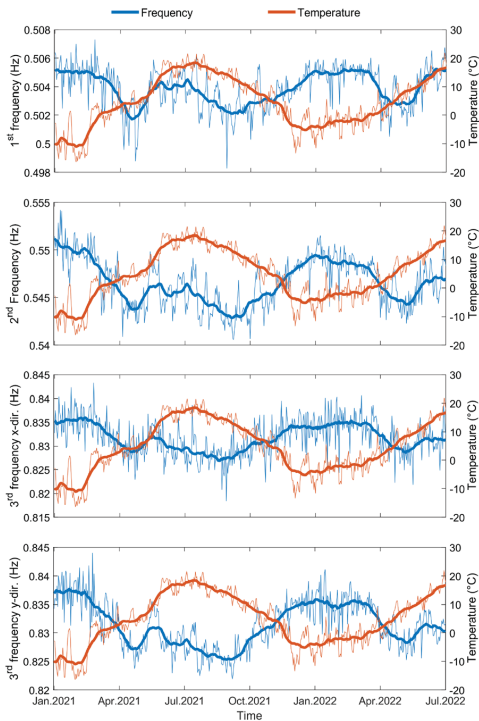
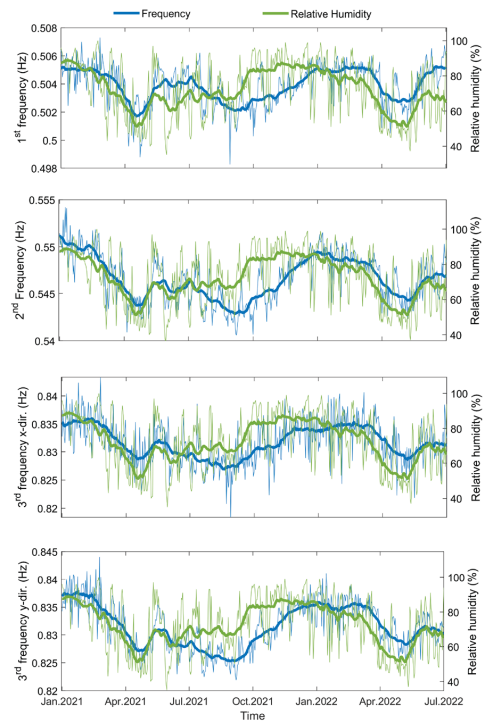**Fig.10.** Variation of identified frequencies (1-day mean) and temperature.

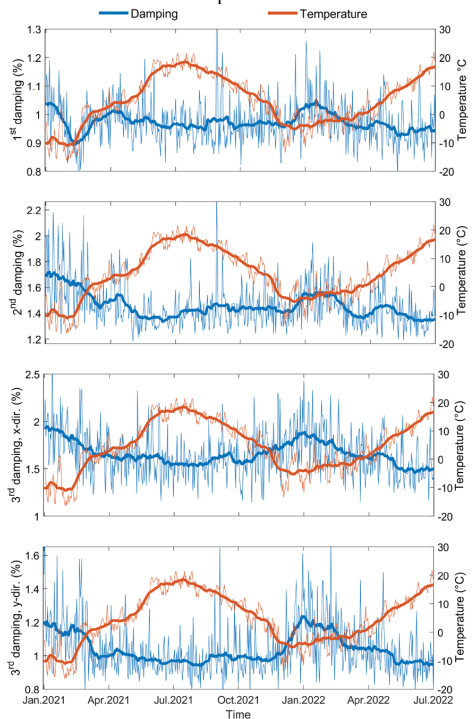**Fig.12.** Variation of identified frequencies (1-day mean) and relative humidity.

Fig.11. Variation of identified damping ratios (1-day mean) and temperature.
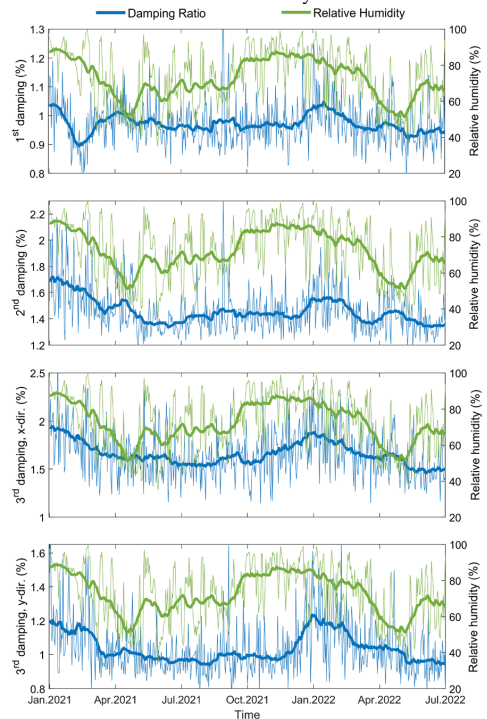

Fig.12. Variation of identified frequencies (1-day mean) and relative humidity.

The variation of mean daily damping ratios is plotted together with the mean daily air temperature as shown in Fig.11. The 1-month smoothed plots are plotted on top of the variations to indicate the trend of parameters with time. No clear relationship is observed between the damping ratios and the seasonal temperature for all three modes of vibration. However, it can be observed that damping ratios are higher in the January-February period compared to the other months for all modes.

Fig.12 shows the variation of the mean daily natural frequencies plotted together with the mean daily relative humidity. The thick smoothed plots (1- month averaging) indicate the trend of the parameters with time. All of the natural frequencies exhibit a positive trend with the relative humidity: with increase of mean relative humidity the natural frequencies increase as well. However, a small delay is observed, indicating that it takes time for the structural properties to respond to the change in relative humidity.

Mean daily damping ratios are co-plotted together with the mean daily relative humidity in Fig.12. From observation no evident effect of the relative humidity on the damping ratios is observed.

For a closer investigation of the effect of environmental conditions on the natural frequencies, 1-month variations of the parameters were co-plotted as shown in Fig.13 for July 2021. Each dot on the figure represents a 1-hour mean value of the parameter. From observation, the relationship between the natural frequency and temperature is not fully clear. A positive relationship between the natural frequency and the relative humidity is observed: increase in the relative humidity results in the gradual increase of the natural frequency with a delay. A similar positive trend between the 1st natural frequency and the relative humidity in Fig.13 was observed for the other two frequencies as well.
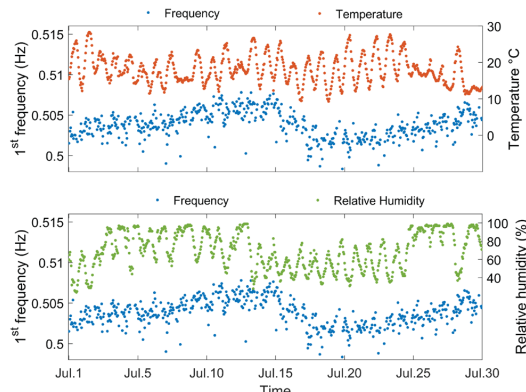

Fig.13. 1-month period (July 2021) variation of identified frequencies co-plotted with mean temperature and mean relative humidity (each dot represents 1-hr segment).

5 CONCLUSIONS

This paper investigated identification of the long-term modal properties under variable environmental conditions of an 18-story glulam frame building in Norway. The combined VMD/SSI-DATA scheme was applied to the measured ambient vibration response. First, the original signal was decomposed with VMD technique into intrinsic mode functions containing the modes; then, the SSI-DATA technique was applied separately on each mode-containing signal to obtain natural frequencies and damping ratios. The identified modal properties were quite stable indicating that the combined methodology can be effectively used for dynamic properties extraction from the ambient vibration data of the tall glulam frame building. The identified natural frequencies for most modes exhibit a similar seasonal behaviour, where highest values for natural frequency are observed in the late winter and the lowest values are observed in the late summer. The identified damping ratios for all modes did not exhibit seasonal variations and have quite stable mean values. From co-plotting the identified frequencies and mean air temperatures, the inverse relationship can be observed for most modes. From co-plotting the natural frequencies and mean relative humidity, a clear positive trend is observed, where the increase in the relative humidity is followed by the increase of the natural frequency for all modes. A delay in response might be caused by the time required for the structural properties of timber to be affected by the environmental conditions. Thus, both temperature and relative humidity impact the natural frequencies: high delay (around 6 months) is observed for temperature variations and a low delay (1-2 months) is observed for the relative humidity.

It is important to note, that in this study analysis of the effect of environmental conditions on the natural frequencies and damping ratios has certain limitations. A longer period of observation is needed to establish a clearer relationship between the seasonal variations and the natural frequencies. Additionally, an on-site weather station measuring both the indoor and outdoor environmental conditions should be installed for a more accurate investigation of the effect of environmental conditions on the dynamic properties of the building.

ACKNOWLEDGEMENT

REFERENCES

[1] Johansson, M., Linderholt, A., Bolmsvik, Å., Jarnerö, K., Olsson, J., and Reynolds, T. Building Higher with Light-weight Timber Structures – the Effect of Wind induced Vibrations. *Proc. Internoise*, San Francisco, 2015.
[2] Heiduschke, A., Kasal, B., and Haller, P. Performance and Drift Levels of Tall Timber Frame Buildings under Seismic and Wind Loads. *Structural Engineering International: Journal of the International Association for Bridge and Structural Engineering (IABSE),* 18(2): 2008.
[3] Leyder, C., Chatzi, E., and Frangi, A. House of natural resources – modal vibration tests and long-term monitoring.

ETH Zurich, Structural Engineering – Timber structures. 2021.

[4] Larsson, C., Abdeljaber, O., Bolmsvik, Å., and Dorn, M. Long-term analysis of the environmental effects on the global dynamic properties of a hybrid timber-concrete building. Engineering Structures, 268 (2022).

[5] The Council on Tall Buildings and Urban Habitat (CTBUH), *CTBUH Ratifies "World's Tallest Timber Building" Following Height Criteria Update*, in *GLOBAL TALL BUILDING NEWS*. 2019.

[6] Abrahamsen, R. Moelven Limtre AS. *Mjøstårnet-Construction of an 81 m tall timber building*. in *International House Forum*. 2017.

[7] Kistler Instrument Corp., *Vehicle Acceleration Measurement*. 2014: 75 John Glenn Drive Amherst, NY14228 USA.

[8] Tulebekova, S., Malo, K.A., Rønnquist, A., and Nåvik, P. *Modeling stiffness of connections and non-structural elements for dynamic response of taller glulam frame buildings*. Engineering Structures, 261 (2022).

[9] Dragomiretksiy, K. and Zosso, D. *Variational mode decomposition*. IEEE Transactions on signal processing 62 (2014).

[10] Van Overschee, P. and B. De Moor, *Subspace identification for linear systems: Theory—Implementation—Applications*. 2012: Springer Science & Business Media.

[11] Kvåle, K.A., Øiseth, O. and Rønnquist, A. *Operational Modal Analysis of an end-supported pontoon bridge*. Engineering Structures, 148:410-423, 2017.

[12] Kvåle, K.A. Operational Modal Analysis toolboxes for Matlab. Available at: https://github.com/knutankv/koma/tree/v.1.0.7.

[13] Norsk Klimaservicesenter (Norwegian Climate Service Centre). Observations and weather statistics. Meterological Institute (MET). Available at: https://seklima.met.no/.

NTNU
Norwegian University of
Science and Technology